Doctoral Dissertation
Doctoral Program in Mechanical Engineering (34th Cycle)

Design, prototype and experimental validation of innovative manual wheelchairs for everyday life and sport

By

Paride Cavallone

******

Supervisor:
Prof. G. Quaglia

Doctoral Examination Committee:
Prof. L. Bruzzone, Referee, Università di Genova
Prof. G. Reina, Referee, Politecnico di Bari

Politecnico di Torino
2022

Declaration

I hereby declare that the contents and organization of this dissertation constitute my own original work and does not compromise in any way the rights of third parties, including those relating to the security of personal data.

Paride Cavallone

2022

* This dissertation is presented in partial fulfillment of the requirements for **Ph.D. degree** in the Graduate School of Politecnico di Torino (ScuDo).

Abstract

The thesis concerns the complete develop, from the concept to the experimental test, of manual wheelchairs both for everyday and sport use with an innovative system of propulsion. Starting from the state of the art, an innovative system of propulsion has been developed to solve some critical aspects about the standard system of propulsion as to increase of the efficiency, to reduce the pain on the upper limb and to increase the mobility and the independence of the users. The functional and the executive design have been developed for both the wheelchair for everyday life, Handhweelchair.q, and sport, Handwheelchair.q racing. Then, in the prototyping phase, the functionality of each subsystem has been verified and optimised. In 2019, we started a collaboration with the doctors, physiatrists and physiotherapists of the U.S.U. (Unità Spinale Unipolare) in Turin, in order to conduct the experimental activity with spinal cord injury patients. The pandemic has interrupted the collaboration. The test have been conducted on able-bodied subjects with the main goal to define the methodology and the experimental apparatus to test the innovative wheelchair. Different tests have been conducted: test to analyse the efficiency of the prototype from a mechanical point of view, test to analyse the force of the user applied on the wheelchair in different condition of external load, test to evaluate the prototype in different configurations, test to compare the standard and innovative wheelchair from electromyography activities.

Contents

List of Figures

List of Tables

Chapter 1

Introduction

1.1 Wheelchair users

The report written by the WHO, World Health Organization, in 2018 [1] shows as 1% of the global population requires a wheelchair for daily mobility. The wheelchair, manual [2] or electric [3], is a device to facilitate mobility in persons with a limited function of one or both lower limbs. The causes of the reduced function of the lower limb are different and can be due to a birth defect or as a result of a traumatic or non-traumatic event. The main disorders are: spinal cord injury [4], spina bifida [5], traumatic brain injury [6], lower limb injury and amputees [7] [8]. The persons affected by these disorders have a relevant impact on the economic and social points of view. For example, the estimated spinal cord injury, SCI, traumatic and non-traumatic, incidence is 40-80 new cases per million population per year [9]. This means that every year, between 250.000 and 500.000 people suffer a spinal cord injury. An Australian report [10] reveals that the lifetime cost per incident case of spinal cord injury is estimated to be 5 million dollars per case of paraplegia and 9.5 million per case of quadriplegia. Spinal cord injuries affect a large fraction of the world population, severely impairing the activities of daily living. Notwithstanding the marginal (0.2%) decrease in SCI occurrences from 1990 to 2016, the incidence of SCI was still markedly high in 2016, amounting to roughly 0.93 million of new cases worldwide [11]. The consequences of SCI span a broad spectrum, from the emergence of disorders typically associated with physical inactivity [12] [13] to mental health problems [14]. The constitution of the WHO defines health as "…a state of physical, mental, and social well-being and

not merely the absence of disease or infirmity" [15] and good health is a prerequisite for participation in a wide range of activities including education and employment [16] .[17] reveals as "…the more physical activity was associated with a lower scale value of depression and anxiety and a higher scale value in perceived social support". Different studies [18][19] show that the daily wheelchair use is insufficient to maintain or improve physical capacity and consequently is insufficient to avoid secondary health conditions such as obesity and cardiovascular diseases [20]–[22]. In conclusion, sport or physical activity is an important tool of rehabilitation from a physical and psychological point of view. However, if on the one hand sport and physical activity are important, on the other hand, there are negative consequences related to the overload of the upper extremity, discussed in the next section.

The Sustainable Development Goals, SDGs, are defined as "the actions to end poverty, protect the planet and improve the lives and prospects of everyone, everywhere. The 17 goals were adopted by all United Nations Member State in 2015, as part of the 2030 Agenda for Sustainable Development which set out a 15-years plan to achieve the goals" [23]. In particular, the Sustainable Development Goal 3, SDG 4, is related to "Good health and well-being" and the official wording is "To ensure healthy lives and promote well-being for all at all ages". In this scenario is important to develop technologies in order to guarantee a good quality of life for all disabled people.

1.2 Shoulder joint and shoulder pain in manual wheelchair users

Of our particular interest is the loading of upper limb muscles during wheelchair propulsion. Locomotion of subjects with limited function of one or both lower limbs is ensured through the use of wheeled mobility equipment, with the most popular examples being manual wheelchairs, power wheelchairs, and scooters [24]. Manual wheelchairs are the most employed means of mobility in the SCI population: among the 3.6 million users in North America, nearly 90% use a manual wheelchair [25].

The arm is connected to the body by the shoulder that is a complex system of joints: glenohumeral, acromioclavicular and sternoclavicular joints and the scapulothoracic gliding plane. The interaction of these joints allows to have a wide range of motion (mobility) of the shoulder joint and the arm covers about 65% of a

sphere [26]. In order to obtain a large mobility, it is important to maintain the kinematic pairs in contact (stability) [27]. Both mobility and stability are the main characteristics of the shoulder joint. These characteristics and the complex structure of the shoulder joint makes it susceptible to injuries. The upper limb is the most commonly affected site in manual wheelchair users. Indeed, different studies have reported that over 70% of manual wheelchair users suffer from shoulder pain [28]–[30]. Moreover, repetitive stress injury has been often observed in SCI subjects [31], likely because of the overt necessity of using the upper limbs for locomotion. In addition to hindering the mobility of SCI subjects, these injuries impact on whichever activity demands the use of the shoulder joint. With the goal of preventing or minimising the consequences of these musculoskeletal injuries, wheelchairs based on different systems of propulsion have been designed in the last years. For instance, recent studies have reported a diminished excitation of the shoulder muscles when subjects were asked to reproduce the movement necessary to move a wheelchair using reverse propulsion [32] and lever system [33] approaches than when relying on the standard handrim propulsion system. While these results are encouraging, the efficiency of the movement with these innovative systems remains an issue, at least in paraplegia. In addition to alleviating the muscle demand, these systems should ensure the same extent of mobility as that experienced with the conventional wheelchair. Moreover, the percentage of shoulder pain is higher in wheelchair users who practice wheelchair sports [34], [35]. In addition to the wheelchair propulsion, different daily activities cause shoulder pain such as transfers and weight lifting in general, especially from the seated position [36]. The repetition of these activities leads to overuse injuries.

1.3 A brief history of wheelchair and wheelchair racing

The history of the wheelchair is related to the history of the invention of the wheel. Since the invention of the wheel, the main application was the transport of “things” and not only inanimate things, but also people. Several paintings, from different ancient cultures, represents the transport of people for several reasons, for example in Figure 1.1a is reported Ramesses II at the Battle of Kadesh, 1275 BC [37]. At the beginning, the transport of things and people was possible by the use of draft animals because the efficiency of the wheels was very low and they were very heavy. The metal ages were fundamental for the development of the wheel, especially for the kinematic pairs. Probably, one of the first wheelchairs represented come from a decoration on a Greek ancient vase [38] Figure 1.1b, which represents a person who pushes a chair with two rear wheels and a person seated on it.

a) b)

Figure 1.1: a) Mural painting in ancient Egypt and b) painting on ancient Greek vase.

One of the first representations, Figure 1.2, of the first self-propelling vehicle for disabled people is the tricycle designed and prototyped by a Swiss watchmaker, Stephan Farffler, in the seventeenth century [39].

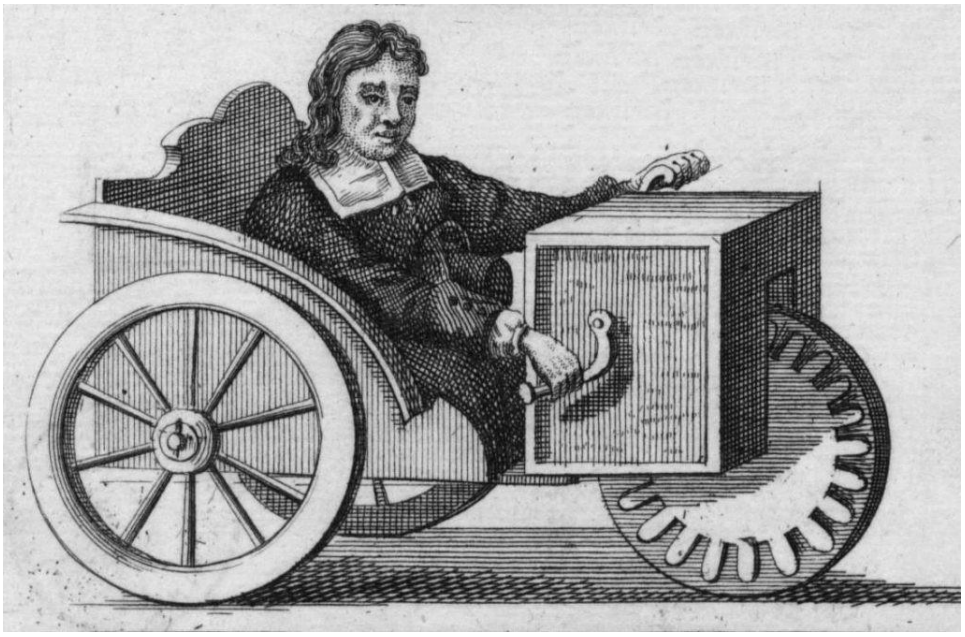

Figure 1.2: Representation of the first self-propelling vehicle for disabled

The figure shows a three-wheeled vehicle in which the front wheel is propelled by cranks.

A fundamental stage concerns the first patent about the first self-propelled wheelchair “Invalid chair”, 16 Febrauary 1869, by Blunt & J.S. Smith [40], Figure 1.3. There are different interesting aspects: the two rear wheels enable the self-propulsion, two castor front wheels, the folding backrest and the folding footrest. In addition, the chair is connected to the rear wheels with a spring.

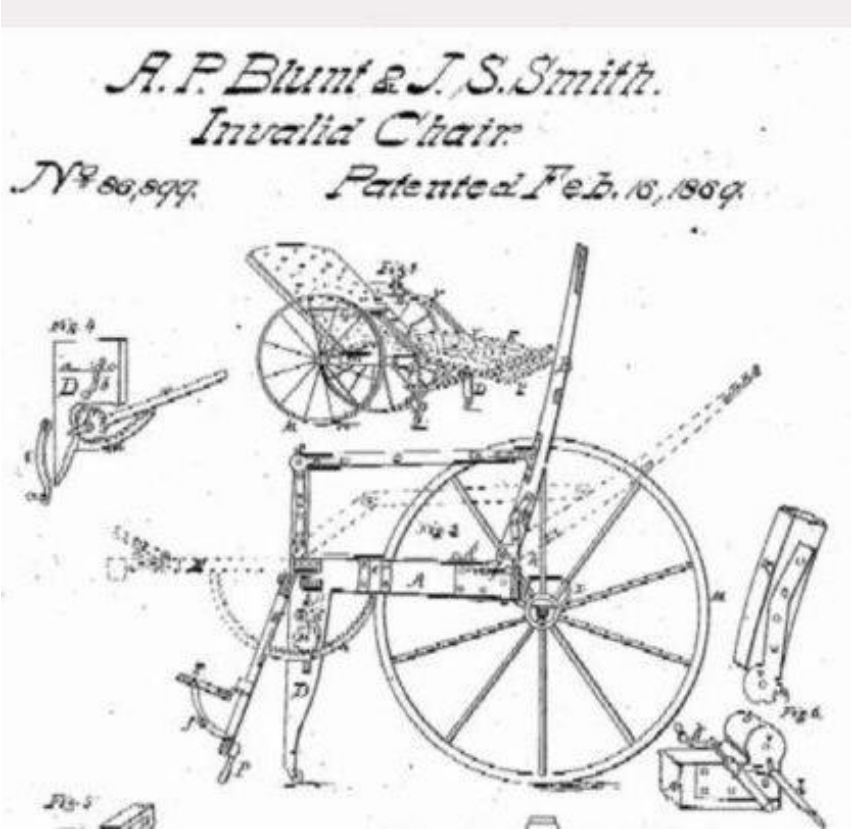

Figure 1.3: Patent of the first self-propelled wheelchair named “Invalid chair”

The history of racing wheelchairs is closely related to two aspects: the evolution of the wheelchair, previously described, and the sport activities practiced on the wheelchair. In 1944, the neurologist Ludwing Guttmann started to work at the “Stoke Mandeville Hospital” [41], in England, in the first research centre for Spinal Cord Injury, SCI. The first meeting of Guttmann with the injured spinal cord was in 1916 at the Konigshutte Compensation Hospital, in Silesia, in which he was a volunteer. In this hospital worked Wilheim Wagner that wrote a book “*Die verletzungen der wirkelsule und des ruckenmarks*” (*Injuries of the spine and spinal cord*) [42]. At the Stoke Mandeville Hospital, at that time, most of the patients were injured soldiers of the second world war. Although, despite the injuries, the soliders were generally in good health, such that Guttman proposed rehabilitation practices

based on sport activities. In fact, the paper [43] reports that "…*Guttmann is credited with the aspiration to improve the dismal prospects of post-war spina injury patients, and the inspiration of using sports as rehabilitative practices*.", and also that "*Guttman is regarded by many as the founder of the modern treatment of spinal injuries*.". The 29 July 1948, at the same time of the opening ceremony of the XIV Olympic Games, the first edition of "Stoke Mandeville Games" was held. In 1952, the "Stoke Mandeville Games" become the "1st International Stoke Mandeville Games".

Figure 1.4: Wheelchair athletes at the Stoke Mandeville Games in the 1950s

In 1960, thanks to the collaboration between Guttmann and the Italian doctor Antonio Maglio, the "1st Paralympic Games" was held in Rome at the same time of the "XVII Olimpic Games" [44]. In the Paralympic Games in Tokyo in 1964, the 60 m race for men and women was added and it represents the first wheelchair race at the Paralympic Games. In the next edition in Tel Aviv in 1968, the 100 m race was added and in 1972 in Heidelberg, the slalom race was introduced, Figure 1.5a. The wheelchairs employed in these three editions of the Paralympic games were wheelchairs for every-day life, as Figure 1.5 shows. Figure 1.5b shows the start of the men Paralympic race of 1964 in Tokyo. In this photo there are two types of wheelchairs: the first type is the wheelchair with two rear wheels with the handrim and two small front pivoting wheels. The second type is instead a wheelchair with 2 front wheels without the handrim and a rear small pivoting wheel. Both were everyday-life wheelchair models in those years.

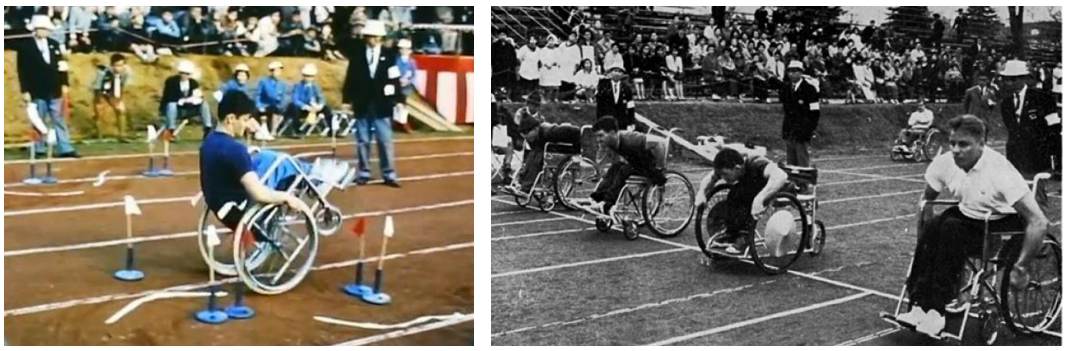

a) b)

Figure 1.5: a) Slalom race and b) start the men Paralympic race of 1964 in Tokyo

Until 1975, the racing wheelchairs had many characteristics of the everyday life wheelchairs, as shown the Figure 1.6a. At the time of the Paralympics Games in 1976, even the clothes, the training, and the diet were not specialised even if new races were introduced: 200 m, 400 m, 800 m and 1500 m. Only during the Paralympics Games in 1984 in Los Angles, the racing wheelchair had a considerable development and the differences with conventional wheelchairs were remarkable, as shown in Figure 1.6b.

a) b)

Figure 1.6: a) Wheelchair race at the Paralympics Games in 1976 and b) in 1984

Figure 1.6b is very interesting because shows two different racing wheelchairs in the same race. The first two wheelchairs in the pictures have the rear wheels with a camber angle and have 2 front pivoting wheels as shown in Figure 1.7a. The wheelchair in the third position is a different model, reported in Figure 1.7b, in which the two front pivoting wheels were controlled by a mechanism. In 1975, Bob Hall was the first wheelchair athlete to compete officially in a marathon [45].

He finished the race in 2h and 58'. Since the mid '70s the first specialised racing wheelchair started to appear. Bob Hall was one of the innovators about the evolution of the racing wheelchair [46]. In fact, in 1978, Hall founded the company "*Hall's wheels*" and he designed his first wheelchair that weighed around 7 kg.

a) b)

Figure 1.7: Different models of racing wheelchair at the beginning of the '80s

At the end of the '80s, the racing wheelchair become more efficient, the speed increased and the stability and the control of the wheelchair become a problem. In this scenario, two solutions were adopted. The first concerned the camber angle of the rear wheel. The second was about the introduction of a steering system and a crown compensation. About the latter topic, in 1989, Rory A. Cooper wrote a paper about three different systems of crown compensation [47]. In the second half of the '80s, Jackson Cycles designed and prototyped the first three-wheeled racing wheelchair, Figure 1.8a used by Paul Cartwright [48]. The main innovative characteristic concerns the front wheel. The front wheel has a diameter greater than usual front wheels, the pivoting axis is vertical and there is an offset between the axis and the hub, practically a castor front wheel. In the second prototype, Figure 1.8b, used by Chris Hallem, the steering axis is not vertical [49]. From that time on, wheelchair athletes started to prefer the three-wheeled wheelchair with the steering. This architecture is examined in detail in paragraph 2.3.

Before 1988, the Paralympic Games were named "International games for the disabled", only then they have been renamed "Paralympic Games" starting from the game held in Rome in 1960. In 1988 there was officially the first edition of the "Paralympic Games". For this event, the rules and regulations were rewritten less restrictively in order to allow the use of the three wheeled racing wheelchair. Since the Paralympic Games in Barcelona, in 1992, Figure 1.9a, the racing wheelchairs had the same characteristics of the present racing wheelchair about the functional

design: two rear cambered wheels with the hand rim, a large castor front wheel with a brake, steering system and a compensator steering mecahnism. In the following years, the main evolution has concerned the material composition and the weight of the frame, going from steel to titanium and then aluminium to the carbon, the efficiency and the material of the components as the hub, roll bearings, wheels, the biomechanical, the nutrition, the training, and the aerodynamic, Figure 1.9b.

a) b)

Figure 1.8: Racing wheelchair with a) a front pivoting wheel and b) front steering wheel

a) b)

Figure1.9: a) Rainer Kuschall at the Paralympic Games in Barcellona, 1992 and b) Tatyana McFadden at the Paralympic Games in Rio de Janeiro.

1.5 Wheelchair classification

The wheelchair market is composed of two main categories: manual wheelchairs and electric power wheelchairs. A manual wheelchair is propelled by the user's muscular force while a electric wheelchair is propelled by electric motors.

Manual wheelchairs can be classified by the usage and by the propulsion system. The two main uses are for every-day use and for sport, while the main propulsion systems are handrim, lever and handbike.

Table 1.1: Classification of manual wheelchairs

	Wheelchair for everyday life with the handrim system [50]
	Wheelchair for everyday life with the lever system [51]–[53]

	Handbike for everyday life [54]
	Handbike for sport [55]–[58]
	Racing wheelchair for sport with the handrim system [59]–[64]
	Wheelchair for sport as basketball and tennis with the handrim system [65]–[67]

The systems of propulsion can be analysed in different ways: The trajectory of the hand, the transmission ratio and the biomechanical movement. All manual wheelchairs have a common characteristic: the trajectory of the propulsion motion is fixed. The trajectory of the pushrim system is an arc of circumference centred on the rear wheel. The trajectory of the lever system is an arc of circumference centred on the joint of the lever that, in some cases, coincides with the centre of the rear wheel. At last, the trajectory of the handbike is a circumference centred on the joint of the cranks. The transmission ratio, for each transmission system, is defined as the ratio between the output displacement of the wheelchair, x_w, and the input displacement of the user's motion, x_u, Eq. (1.1).

$$\tau = \frac{x_w}{x_u} \tag{1.1}$$

For the pushrim system, Figure 1.10, the transmission ratio, τ_p, is defined by Eq. (1.2), where r_{rw} is the radius of the rear wheel, r_h is the radius of the handrim and θ_{rw} is the angular displacement of the rear wheel.

$$\tau_p = \frac{x_w}{x_u} = \frac{\theta_w r_w}{\theta_w r_h} = \frac{r_{rw}}{r_h} \tag{1.2}$$

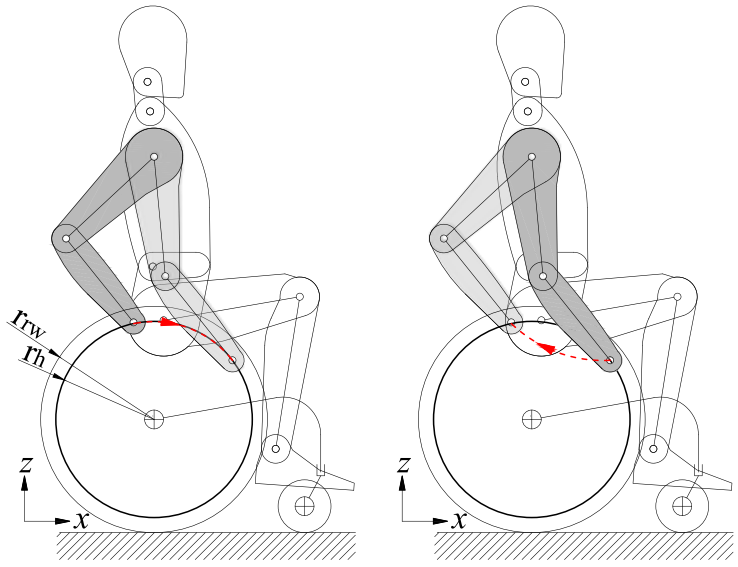

Figure 1.10: Wheelchair with the handrim system

This transmission ratio depends on the usage of the wheelchair. For every-day life wheelchairs, the ratio is about 1 due to ergonomic reasons. Whereas for racing wheelchairs, it is greater than 1 and it depends on the type of race, the speed and the physical characteristics of the user. For sports such as basketball, tennis the transmission ratio is around 1.

For lever-based propulsion systems, Figure 1.11, the transmission ratio is defined by the Eq. (1.3), where r_2 is the chainring radius, r_1 is the sprocket radius, l is the lever length and θ_2 is the angular displacement of the lever. In some models, the radius of the chainring is variable as in bicycles, while in other models is fixed, but there also other models where the chainring is not present and the lever is integral with the sprocket.

$$\tau_l = \frac{x_w}{x_u} = \frac{\theta_w r_w}{\theta_2 l} = \frac{\theta_w r_w r_2}{\theta_w l r_1} = \frac{r_{rw}}{r_1}\frac{r_2}{l} \tag{1.3}$$

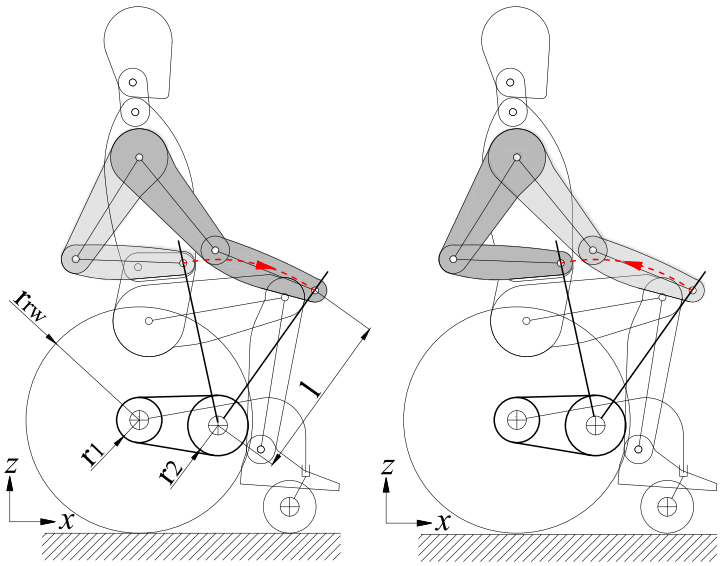

Figure 1.11: Wheelchair with a lever system

For handbikes, Figure 1.12, the transmission ratio is defined by Eq. (1.4) where r_{fw} is the radius of the front wheel, r_2 is the chainring radius, r_1 is the sprocket radius, c is the crank length and θ_2 is the angular displacement of the crank.

$$\tau_h = \frac{x_w}{x_u} = \frac{\theta_w r_w}{\theta_2 c} = \frac{\theta_w r_w r_2}{\theta_w c r_1} = \frac{r_{fw}}{r_1}\frac{r_2}{c} \tag{1.4}$$

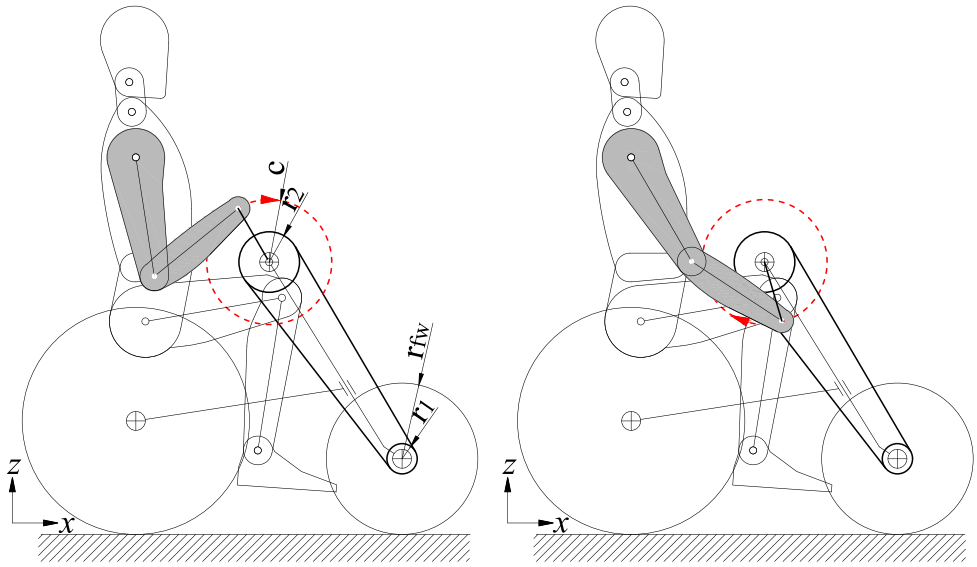

Figure 1.12: Handbike

The value of the transmission ratio of handbikes depends on the usage and in general it is variable as in a bicycle.

In general, the systems of propulsion are composed of an active and recovery phase [68], with the exception of the handbike in which there is no recovery phase [69]. The active phase is when the user propels the wheelchair, while in the recovery phase the user comes back in the initial position.

This was indeed one of the reasons motivating the design of a wheelchair propelled through a pulley-cable system [70]–[75].

1.6 Indices

In literature, there are different indices for different applications to the world of the wheelchair.

The WUSPI [76], [77], Wheelchair User's Shoulder Pain Index, is an index to detect difficulties in performing daily activities due to shoulder pain in wheelchair users, in other words, the index WUSPI is an index to measure shoulder pain in individuals using wheelchairs. The SPADI [78], Shoulder Pain and Disability Index, is developed to measure the pain and disability associated with shoulder pathology. The WICI [79], Weighted Integrated Comfort Index, is a indices to measure the comfort of the wheelchair evaluating the contact of the user and the wheelchair. Another interesting index, related to comfort, is the Stability Index [80]

that “can give objective information to find the most appropriate wheelchair setting both for daily and sport use”.

The indices IPI [81], Index Pitch Instability, and Iroll [82], Index Rolling resistance, are two indices that help the user to choose the wheelchair and to modify the wheelchair characteristics in order to optimize the efficiency of the wheelchair and the comfort for the user. These indices are important to evaluate the system composed of wheelchair and user.

The indeces FEF, Fraction Effective Force, and MEF, Mechanical Effective Force, [83]–[85] are two indices to evaluate the efficiency of the propulsion system. In particular, the FEF and MEF have been defined to evaluate the handrim system. The indices MEF and FEF differently compare the useful force for the transmission of motion and the total force of the user applied on the handrim. The index FEF can be used for different systems of propulsion, such as lever system and handbike.

Chapter 2

Mechanical design

2.1 Concept

The idea of the innovative system of propulsion is to propel a wheelchair with a gesture inspired by a rowing motion, without the use of the lower limb, employing a pulley-cable system. From a biomechanical point of view, in the sagittal plane, the motion concerns the shoulder extension-flexion and elbow flexion-extension. As in the rowing motion, the gesture is composed of two phases: an active phase in which the user provides power to the wheelchair and a recovery phase in which the user goes back to the initial position. The use of a cable system is an important characteristic because the kinematic of the gesture is not fixed. In Figure 2.1 the concept of the innovative wheelchair for everyday-life is depicted, and its mechanical design is reported in detail in section 2.2. The same idea can be applied to the racing wheelchair that is reported in detail in paragraph 2.3.

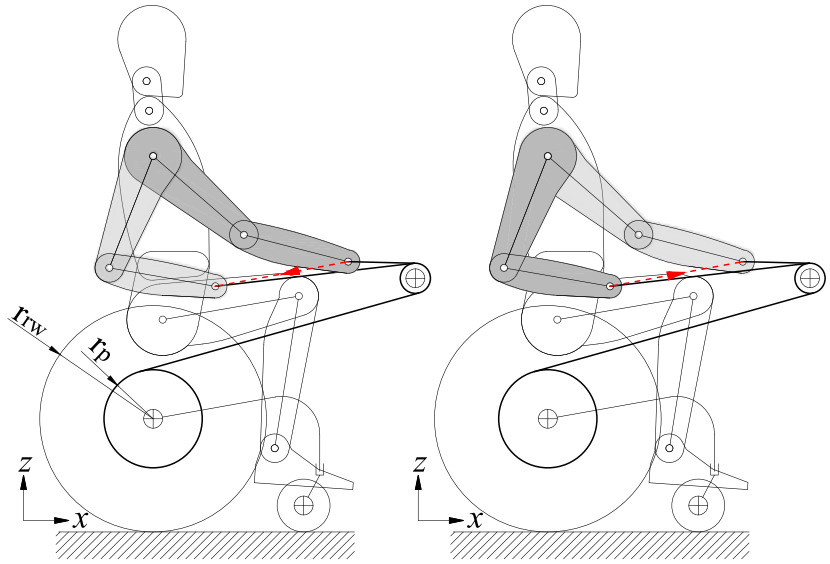

Figure 2.1: Concept of the innovative manual wheelchair named Handwheelchair.Q

2.2 Handwheelchair.q every-day life

Handwheelchair.q is a prototype of a manual wheelchair with a double system to propel it. The first system is the handrim in which the user pushes two rims integral with the rear wheels, right and left, for indoor use. This is the most popular system. In addition, there is the second system which is the pulley-cable system described in the previously, for outdoor use. The prototype is based on a standard wheelchair with the handrim system in which the pulley-cable system is added. The subsystems that must be added to the prototype are the return pulleys with the supporting rods, the handles, and the mechanism for the transmission of motion. These subsystems will be described in detail in the next paragraphs from the requirements, to the functional design, and up to the executive design.

2.2.1 Requirements

It is important that the footprint dimensions respect the main rules that came from the legislation to avoid restricting the mobility of the wheelchair in public spaces, such as offices, hospitals, sidewalks, and transport public, because, in principle, all public space should be designed barrier-free. The most important size that must be respected is the width, Figure 2.2a. All manual wheelchairs for independent use must let users transfer from the wheelchair to the car/bedroom/chair/toilette. Therefore, the lateral-front side of the seat must be barrier-free as shown in Figure 2.2b.

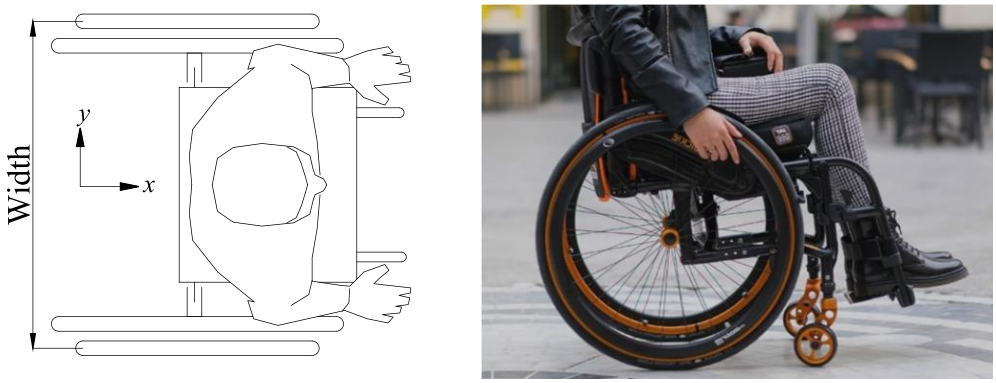

a) b)

Figure 2.2: a) Top and b) lateral view of a wheelchair

Secondly, the switching from handrims to the pulley-cable system must be easy and efficient. The pulley-cable system should not interfere with the handrim system and vice versa.

In addition, appropriate systems to guarantee the safety of the user have to be defined considering that the standard wheelchairs do not have a brake system, but the users brake with the friction of the hands on the handrims. This brake system could be dangerous and is not safe, especially on a descent.

As previously said, one of the fundamental subsystems of the prototype is the mechanism for the transmission of motion from the user to the wheelchair through the pulley-cable system. Such a mechanism must guarantee four operating modes: the first two modes concern the active and the recovery phase, respectively. The third mode is the freewheel phase, that is when the user is not propelling the wheelchair but the wheels rotate, for example, during a descent,. The last one is in the reverse phase, which occurs when the user pushes the handrim in the opposite direction.

In the active phase, the mechanism enables the power transfer from the user to the wheel. In this phase, the mechanism works as a simple pulley integral with the rear wheel in which the angular speed of the pulley, $\dot{\theta}_P$, and the angular speed of the rear wheel, $\dot{\theta}_{rw}$, are the same, defining Condition 1.

$$\dot{\theta}_P > 0 \ \wedge \ \dot{\theta}_{rw} = \dot{\theta}_P \qquad \text{Condition 1}$$

During the recovery phase, the cable has to be rewound around the pulley. In this phase the mechanism has to decouple the motions of the pulley and the rear wheel, since the pulley angular speed is negative whereas the wheel angular speed is positive.

$$\dot{\theta}_P < 0 \ \wedge \ \dot{\theta}_{rw} > 0 \qquad \text{Condition 2}$$

In the freewheel phase, the user does not push the handrim, but the wheel rotates. In this phase, the mechanism must decouple the motion of the pulley from the wheel one.

$$\dot{\theta}_P = 0 \ \wedge \ \dot{\theta}_{rw} > 0 \qquad \text{Condition 3}$$

In the reverse phase, the angular speed of the wheel is negative and the angular speed of the pulley is zero.

$$\dot{\theta}_{rw} < 0 \;\&\; \dot{\theta}_P = 0 \qquad \text{Condition 4}$$

In Figure 2.3 the kinematic phases of the mechanism are reported.

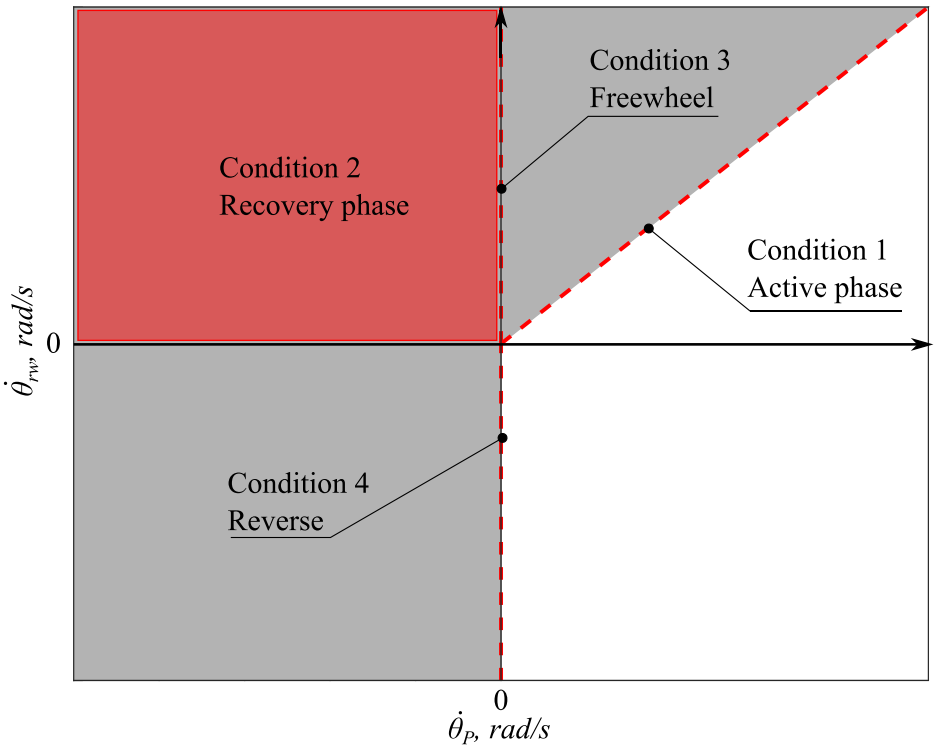

Figure 2.3: Kinematic phases of the mechanism.

As last requirement, from a psychological point of view, is important that the prototype has a "light" design in order to reduce the visual impact.

2.2.2 Functional design

In Figure 2.4, the general functional design of the prototype Handwheelchair.q is shown. The prototype is composed of different subsystems: the mechanism for the transmission of motion with the pulley, the rear wheels, the handrim, the return pulley, the telescopic rod, the front wheels, the seat, the frame, the handle with a brake lever, and the brake. The prototype is based on a standard wheelchair and so the frame, the seat and the rear wheel are not discussed here in detail.

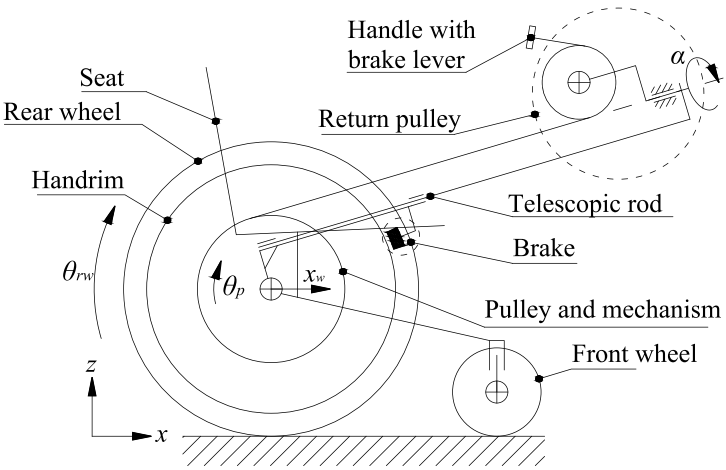

Figure 2.4: Functional design of Handwheelchair.q

The main idea of the functional design is to define a complete subsystem composed of the rear wheel with the mechanism for the transmission of motion, the pulley, the telescopic rod and the return pulley. This subsystem is mounted on the standard wheelchair through the shaft of the rear wheel. The rotation of the telescopic rod, around the axis of the rear wheel, is limited by a flange specifically designed for each wheelchair frame . This idea enables to have subsystems independent from the wheelchair and a single component, the flange, for each frame.

First of all, the telescopic rods enable to position the return pulleys in order to be able to perform the gesture inspired by the rowing motion. The position of the return pulley can be regulated based on its user in order to optimise the gesture. For this reason, the angular position and the length of the telescopic rod must be variable. In Figure 2.5, Area 1 represents the ideal area in which the return pulley has to be positioned so that the user is able to perform the gesture. The definition of this area takes into account the different users heights and different shoulder angles on the sagittal plane. Area 2 signifies the area that can be used for the position of the telescopic rod and the return pulley when the wheelchair is used in standard configuration and to facilitate getting in and out of the wheelchair. Area 3 represents the possible positions of the return pulley with a telescopic rod. In the minimum extension the return pulleys do not obstruct the getting in and out of the wheelchair and the ideal Area 1 is partially covered by Area 3. The correct position of the return pulley has to be defined

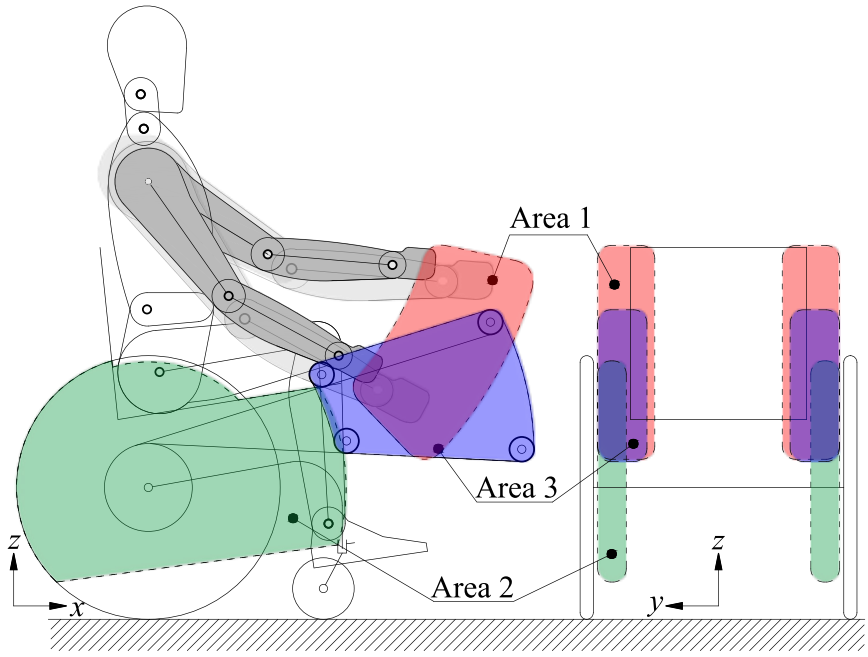

Figure 2.5: Position of the return pulleys

Secondly, the return pulleys have two passive degrees of freedom. The first is the rotation around its axes. The second is the pivot around the axis of the cable that connects the pulley and the return pulley, as shown in Figure 2.6. The pivot degree of freedom limits the friction of the cable on the throat of the return pulley. This degree of freedom enables to keep constant the axis of the cable that connects the return pulley and the pulley.

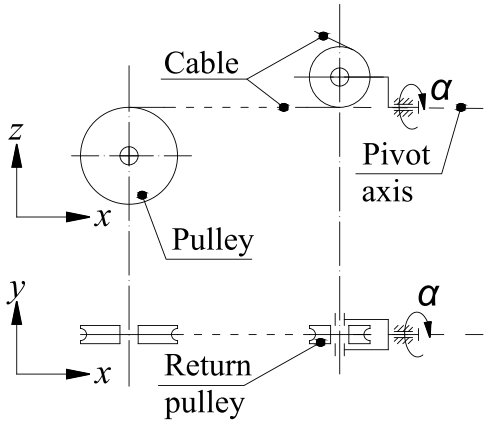

Figure 2.6: Functional design of the return pulley

The longitudinal position of the return pulley, x_{rp}, is variable, thanks to the telescopic rod onto which is mounted, and the lateral offset, y_{rp}, is defined by a specific flange, as shown in Figure 2.7. The figure depicts the brake system also positioned on the telescopic rod. The longitudinal position of the brake, x_b, is defined by the radius of the rear wheel and a brake flange enables to correct the lateral offset, y_b, between the telescopic rod and the rear wheel. The brake lever is mounted on the handle.

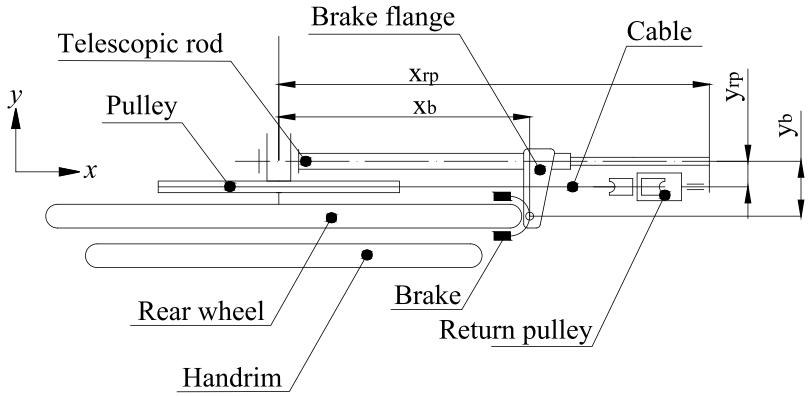

Figure 2.7: Functional design of the telescopic rod

A possible linear functional design of the mechanism for the transmission of motion is reported in Figure 2.8. The mechanism is composed of different subsystems. The first subsystem is the pulley with the power spring. The second subsystem is the mechanism composed of the pulley ratchet, the pawl ratchet and the rocker. The last two subsystems are the rear wheel and the fixed pawl. The angular coordinates which define the positive direction of the pulley and the rear wheel are respectively θ_p and θ_{rw} are the angular coordinate which defines the pose of the pulley reference system pulley and θ_{rw}. The function of each component is described below.

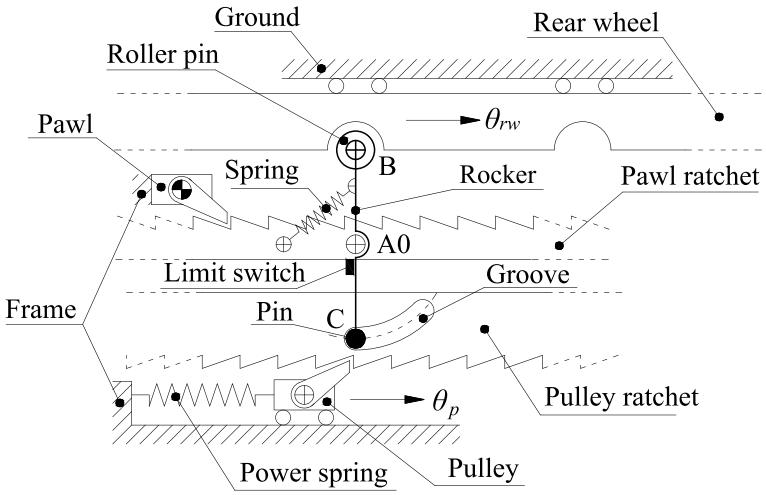

Figure 2.8: Linear functional design of the mechanism for the transmission of motion.

In the active phase, Figure 2.9, the user pulls the cable wrapped around the pulley. The pulley is connected to the frame with a power spring. During this phase, the power spring is loaded. The pulley transmits the motion to the pulley ratchet, as shown in circle 1.1. The groove limits the anti-clockwise rotation of the rocker around the joint A0, thanks to the pin labelled as 1.2, and the roller pin, 1.3, transmits the motion to the rear wheel. The pawl, 1.4, does not interfere in this phase. The light blue indicates line the components move together.

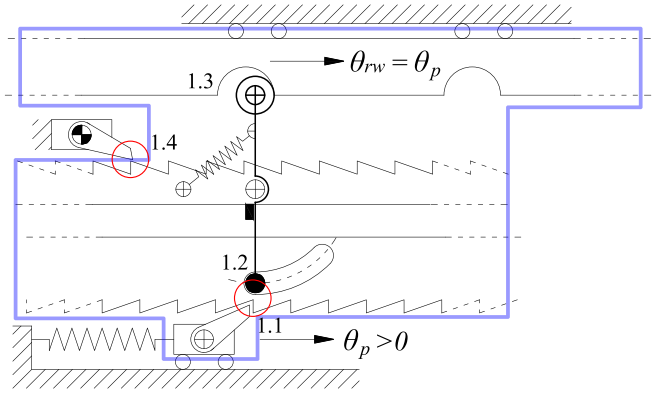

Figure 2.9: Mechanism in the active phase

In the recovery phase, Figure 2.10, the user does not pull the cable and so the power spring, previously loaded in the active phase, drags the pulley in the initial position. In this phase, the pulley and the pulley ratchet motions are decoupled,

circle 2.1. The limit switch limits the clockwise rotation of the rocker, 2.2. The rear wheel drags the barbell by means of the roller pin, 2.3, and the pulley ratchet due the pin, 2.4. The pawl, 2.5, does not interfere in this phase. The line light blue indicates the components that have the same kinematic.

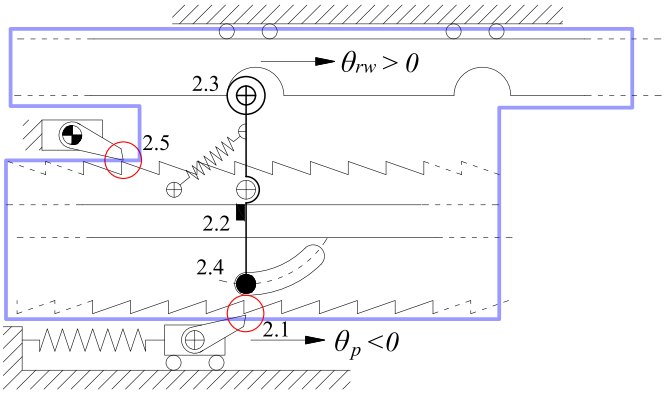

Figure 2.10: Mechanism in the recovery phase

The freewheel phase, Figure 2.11, is similar to the recovery phase, the only difference concerns the kinematic of the pulley. During this phase, the pulley angular speed is zero.

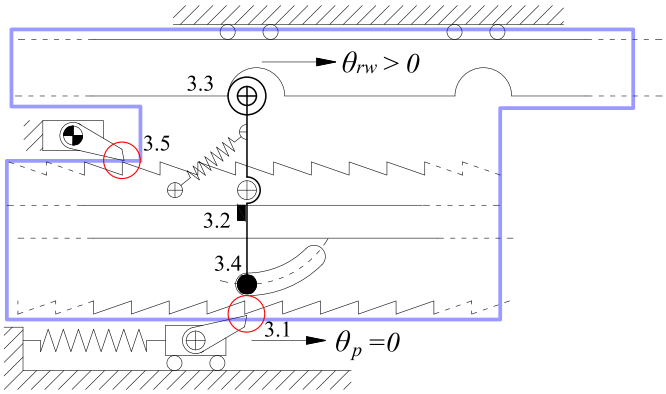

Figure 2.11: Mechanism in the freewheel phase

In the reverse phase, Figure 2.12, the angular speed of the rear wheel is negative. The pawl, 4.1, limits the motion of the pawl ratchet. The rocker rotates anti-clockwise around the fix joint A0, the pin is free to move in the groove, 4.2, and the spring is compressed, 4.3. The roller pin rotates around the joint B, 4.4.

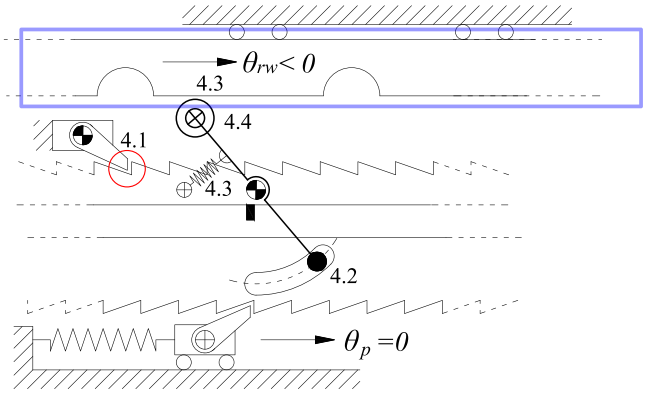

Figure 2.12: Mechanism in the reverse phase

The functional design of the mechanism described, respects the requirements described in the previous section.

2.2.3 Executive design and prototype

In Figure 2.13, the render of the executive design of Handwheelchair.q is reported. The executive design concerned the design of some components such as the return pulley, the pulley, the telescopic rod, and the integration of commercial components like the rear wheel, the hub with the mechanism, the brake, the brake lever, and the frame of the wheelchair.

a) b)

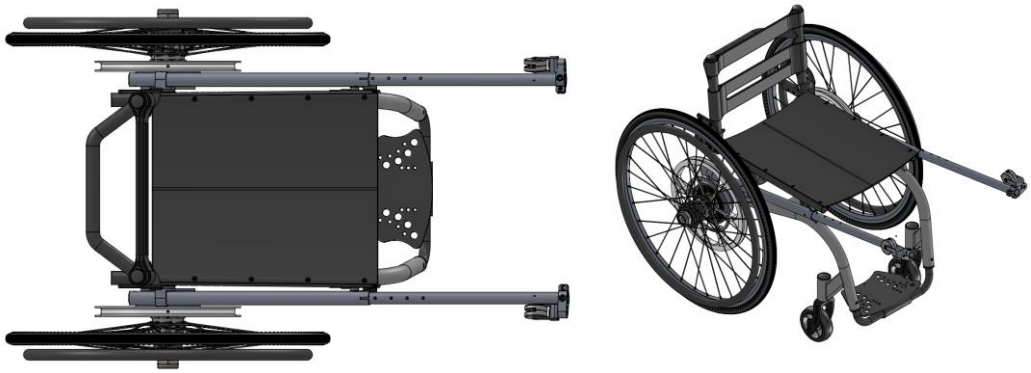

c) d)

Figure 2.13: Render of Handwheelchair.q a) lateral, b) front, c) top and d) axonometry

The executive design concerned in the design of an independent subsystem composed of the rear wheel, the hub, the telescopic rod, the pulley, the return pulley, the cable, the power spring, the handle, the brake and the lever brake as shown in Figure 2.14 and 2.15. In figure 2.14 the lateral distance of the brake and the axis of the cable from the axis of the telescopic rod respectively y_b and y_{rp} are shown.

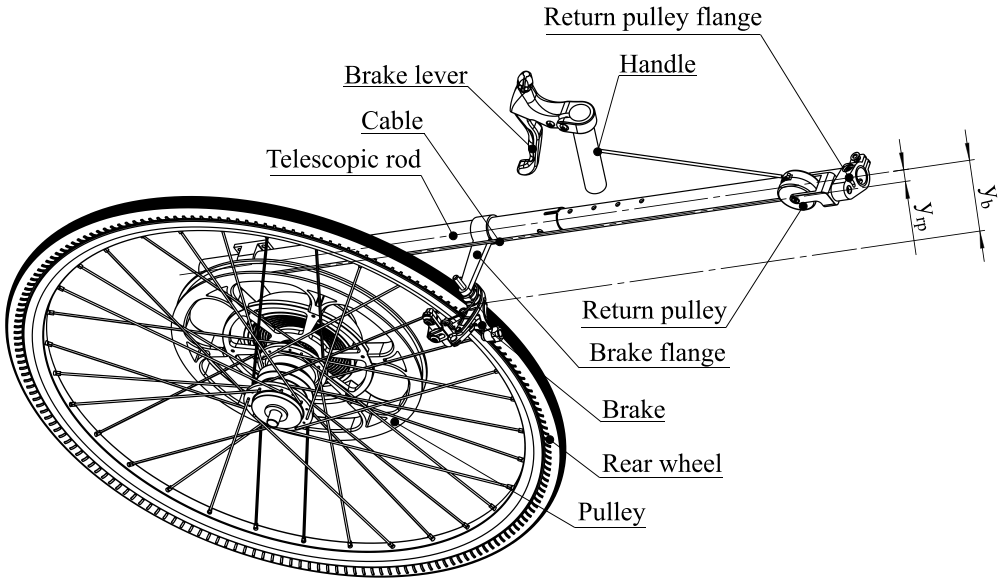

Figure 2.14: Axonometry of the complete subsystem that enables to implement the innovative system of propulsion.

In Figure 2.15 the lateral view of the complete subsystem is reported. Figure 2.15 highlights the light design obtained for the executive design.

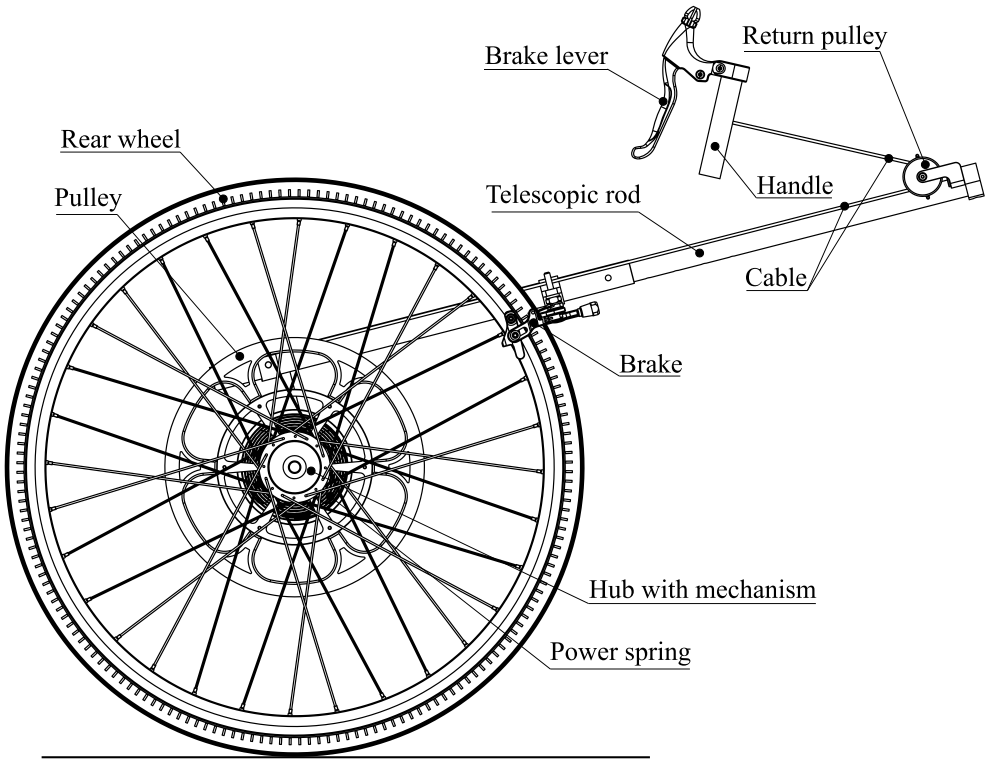

Figure 2.15: Lateral view of the complete subsystem.

This subsystem can be easily adapted on each manual wheelchair through two components: the shaft of the hub and a flange. All manual wheelchair has a component that supports the shaft. This component is the interface between the subsystem and the frame of the wheelchair as shown in Figure 2.16.

The mechanism of the transmission of motion, described in the previous paragraph, is based on a commercial components appropriately modified. The commercial component is a mechanism within the kinematic characteristics described in the section 2.2.2 employed in specific bike. At this component, a pulley and a power spring have been added obtaining the executive design shown in Figure 2.16. The internal extremity of the shaft is integral to the frame of the wheelchair. The pulley is supported on the shaft by two ball bearings. A power spring connects the pulley and an external shell integral with the shaft. The axial pawls enable to engage the pulley with the hub. In the external extremity of the shaft a nut lock axially the hub. The pulley is composed of two components: the external part with the groove and the internal part with the ball bearings. The external part can be

replaced in order to change the pulley radius. In the last prototype, the external part of the pulley has been designed with two grooves with different radii in order to simplify the experimental test.

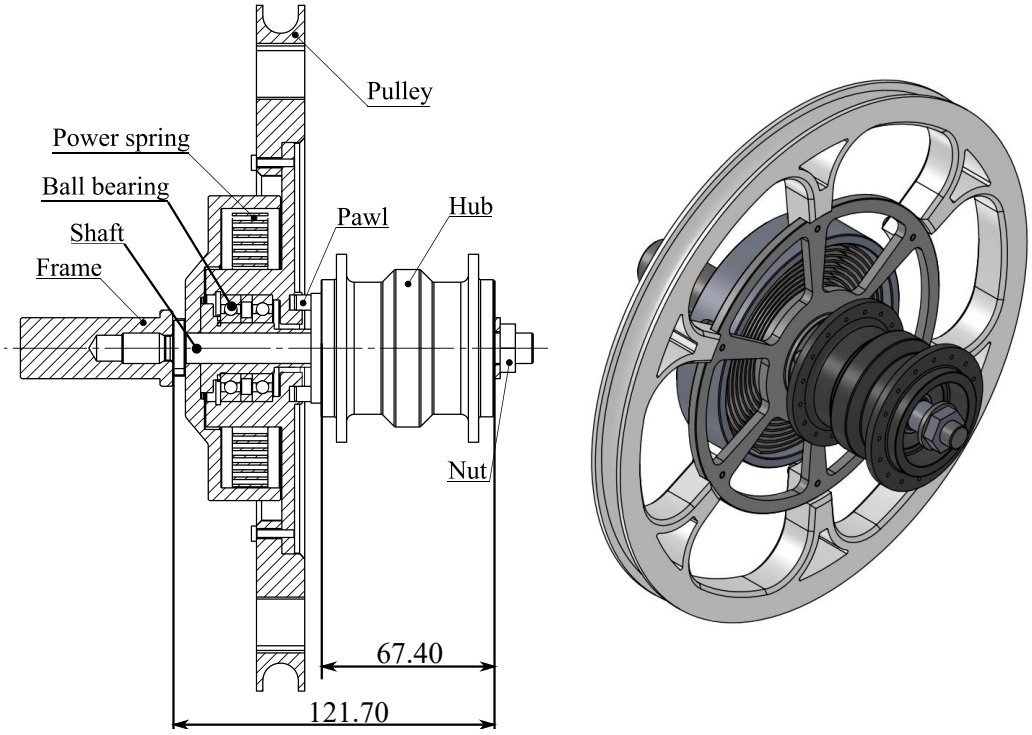

a) b)

Figure 2.16: a) Section and b) axonometry of the subsystem of the pulley.

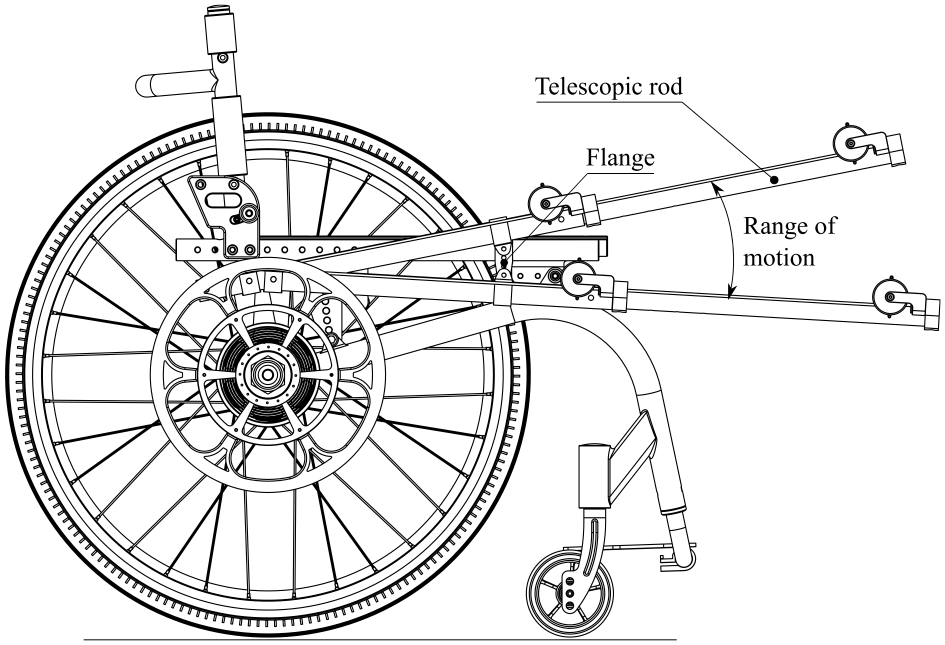

Figure 2.17: Lateral view of the wheelchair with the complete pulley-cable subsystem. The right rear wheel has been removed in order to highlight the flange.

The flange is a component that connects the telescopic rod and the frame of the wheelchair and it has two main functions, Figure 2.17. The first one is to avoid the rotation of the telescopic rod around the shaft and the second is to regulate the inclination of the telescopic rod. This component is the interface of the complete subsystem and the wheelchair. This component is specific for each wheelchair based on the wheelchair frame. The correct inclination of the telescopic rod has to be defined by doctors, physiatrists and physiotherapists according to the physical characteristics of each user and from the mechanic, biomechanics and electromyography data that are described in the next chapter.

In order to limit the friction of the cable on the groove of the return pulley, it has a passive degree of freedom that coincides with the axis of the cable that connects the pulley and the return pulley, namely, the axis of the groove of the pulley and the return pulley as shown in Figure 2.18.

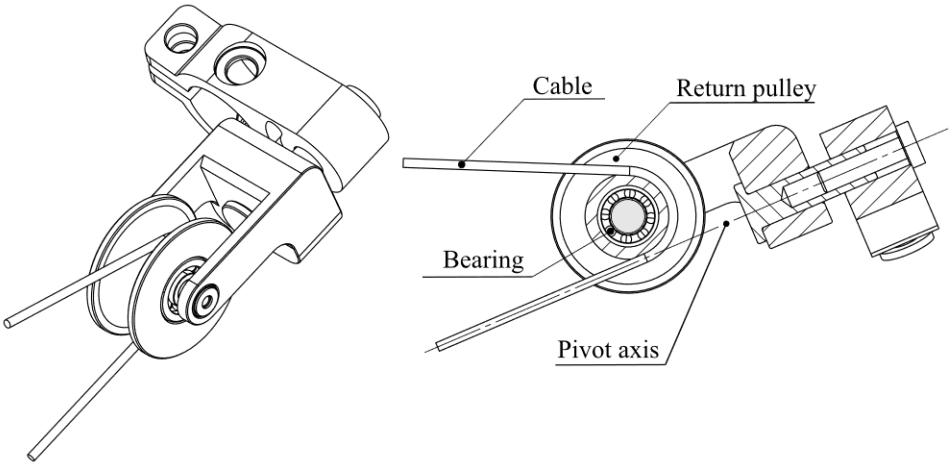

a)

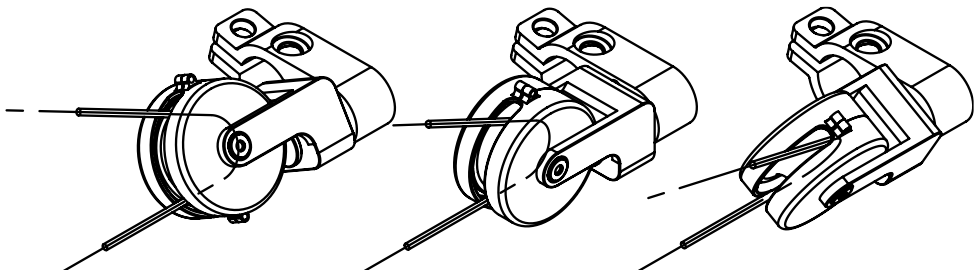

b)

Figure 2.18: a) section and axonometry of the return pulley and b) return pulley in different inclinations

In figure 2.19, the prototype of the return pulley is shown. In particular, it is possible to observe how the direction of the force does not modify the direction of the cable that connect the pulley and the return pulley.

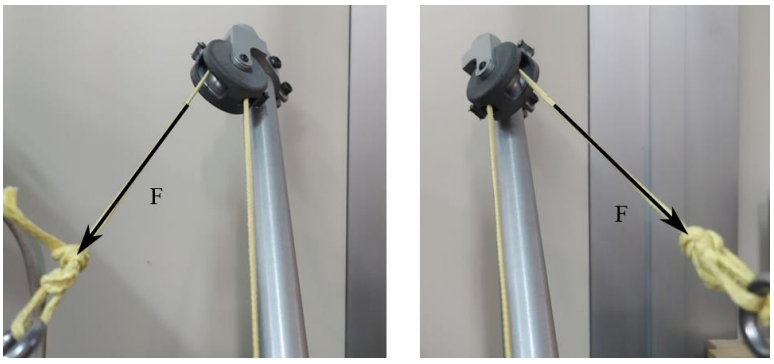

Figure 2.19: Photo of the return pulley in different inclination

In Figure 2.20 the prototype of the Handwheelchair.q is shown.

Figure 2.20: Prototype of Handwheelchair.q

Even in the prototyping phase, there was an attempt at limiting the visual impact of the prototype with a light prototype.

In the experimental phase, it has been necessary to test the wheelchair with different transmission ratio. For this reason, the aluminum pulley shown in figure 2.20 has been substituted with two pulley 3d printed, as shown in figure 2.21. The second pulley speeds up the procedure to change the transmission ratio.

Figure 2.21: 3d printed pulleys

The Figure 2.22 shows the first test in the prototyping phase in which the function of the prototype and the experimental apparatus have been tested. In particular, the figure 2.22a shows three frames of the active phase and in figure 2.22b shows three frames of the recovery phase. The active and the recovery phase will be described in detail in the next chapter.

a)

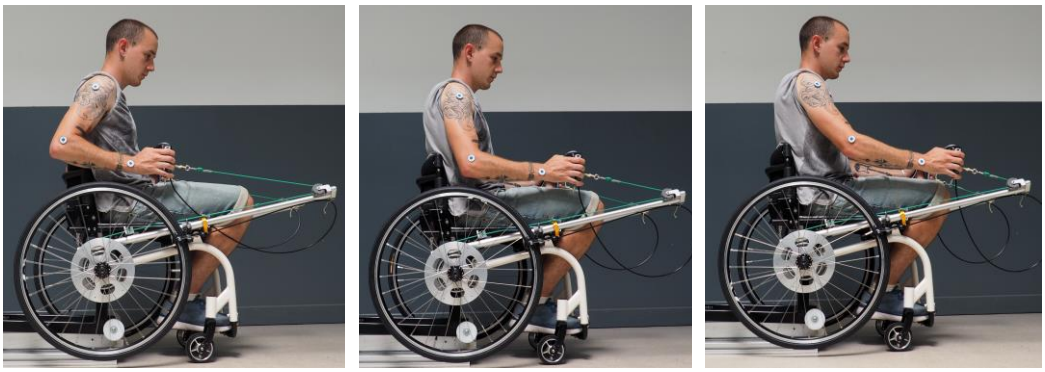

b)

Figure 2.22: a) Active and b) recovery phase

2.3 Handwheelchair.q racing

Handwheelchair.q racing is a prototype of a racing wheelchair with the same innovative system of propulsion inspired to the rowing motion proposed in Handwheelcahir.q for daily use, presented before. The prototype is based on a standard racing wheelchair with the addition of the pulley-cable system previously described, the concept of the idea is shown schematically in Figure 2.23.

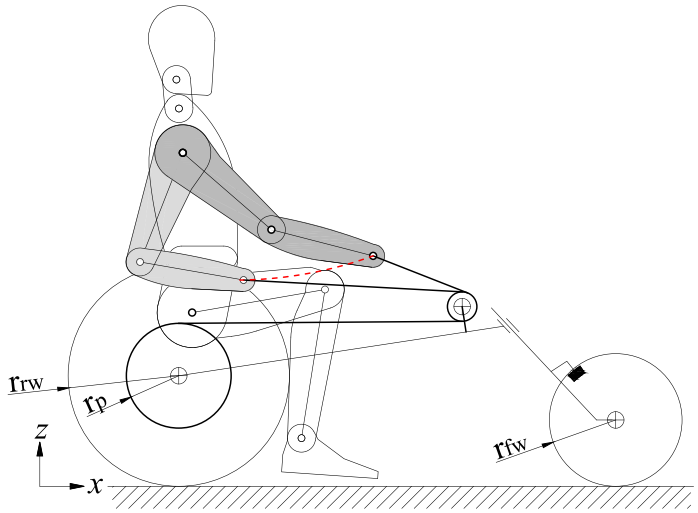

Figure 2.23: Concept of racing wheelchair with pulley-cable system

2.3.1 Requirements and dynamic model

The main goal of this work is to facilitate the mobility of a racing wheelchair, not only on the athletic track or on specially designed paths, but even on cycle paths, parks, city roads, and country roads. The trajectory of the racing wheelchair is controlled by a front steering wheel which is hand-operated by the user when the user does not push the handrims. The leading idea of this prototype is to design a steering system that the user can always control.

Before presenting the concept of this innovative steering system, some considerations about the dynamic of the vehicle are necessary. The standard racing wheelchair are composed of six subsystems, as shown in Figure 2.24: two rear wheels, the front fork, the front wheel, the steering compensator and the frame. The frame connects the two rear wheels and the fork with the front wheel. In addition, the steering compensator is a four-bar linkage mechanism that connects the fork and the frame. In general, as a result of the contact between the front wheel and the

ground, the front wheels are subjected to a force that can be decomposed in three components: longitudinal, lateral and normal force. These forces generate, among the others, a torque, T_S, around the steering axis, shown in Figure 2.24, that has to be compensated in order to keep the steering angle in the desired angular position. Because the user cannot constantly control the steering, a compensator steering is mandatory. In the standard racing wheelchair, the function of keeping the steering angle desired is entrusted to the steering compensator.

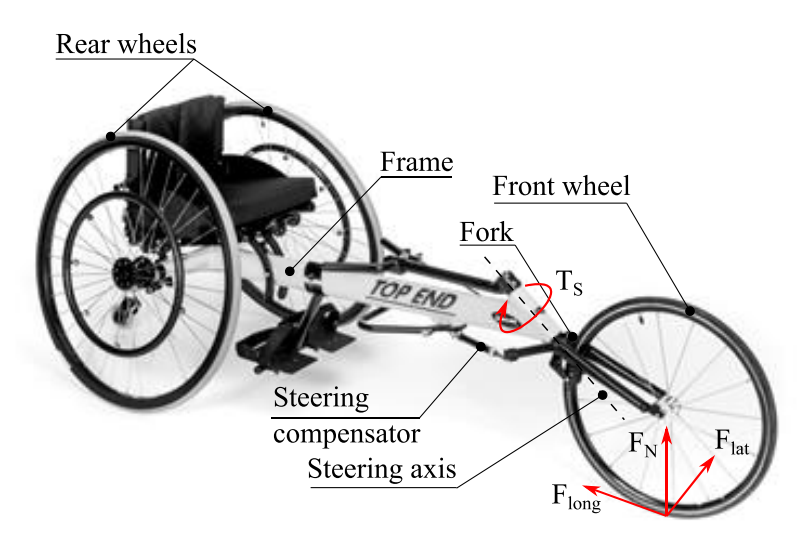

Figure 2.24: Racing wheelchair

The steering compensator is a four-bar linkage, A_0B-BC-CF_0 that connects the fork with the wheelchair frame, as reported in Figure 2.25. The axis of the joint A_0 and F_0 are not parallel, but the joint C and B are spherical joints. The fork rotates around the joint A_0 and it is fixed with the link A_0B. In the joint F_0 there is a friction torque, T_f, generated by the contact area of the link CF_0 and the wheelchair frame. The friction torque, T_f, can be regulated by modifying the contact force of the link CF_0 and the frame, through a nut. The friction torque, T_f, has to be regulated in order to avoid the free rotation of the fork due to the steering torque, Ts, generated by the wheel contact forces, F_{long}, F_N and F_{lat}, with the ground.

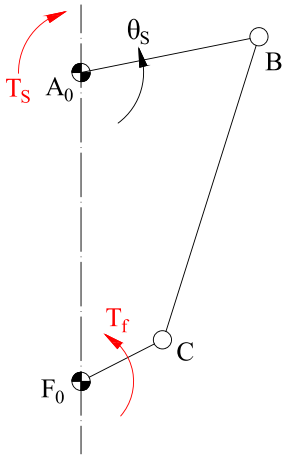

Figure 2.25: Four-bar linkage steering compensator

The torque on the steering axis depends on the magnitude and direction of the contact force on the ground and the position of the contact point of the wheel with the ground. The magnitude and the direction depend on the steering angle, the velocity and the friction parameters of the wheel/ground, while the position of the contact point depends only on the steering angle.

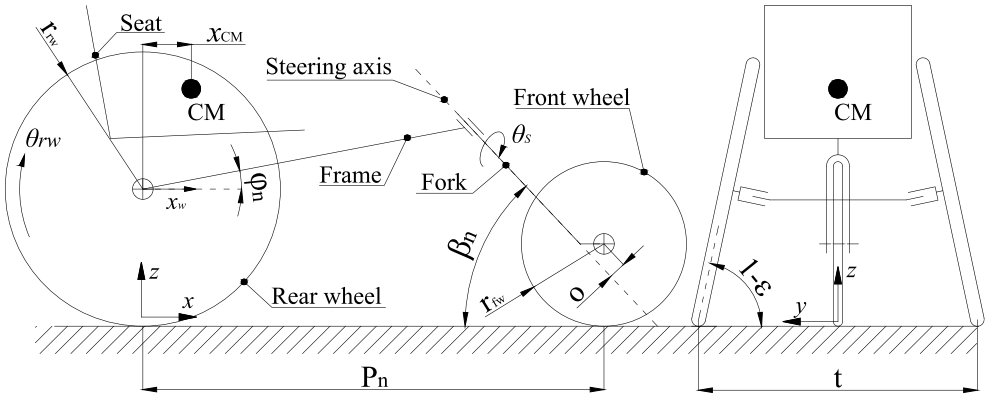

Figure 2.26: Geometrical parameters of the wheelchair racing

The relationship between the radius of curvature and the steering angle can be analysed through a dynamic model. In Figure 2.26, the scheme and the geometrical parameters of the racing wheelchair are presented and the values of the parameters employed in the dynamic model are summarized in table 2.1. The longitudinal position of the seat can be regulated and with it the position of the center of mass. The two extreme positions of the seat determine the minimum and maximum longitudinal coordinates of the user center of mass, values in table 2.1.

Table 2.1: Functional parameters of the racing wheelchair

Symbol	Description	Value
P_n	Nominal pass	1300 mm
t	Track	700 mm
φ_n	Inclination angle of the frame	6°
r_{rw}	Rear wheel radius	300 mm
r_{fw}	Front wheel radius	220 mm
x_{CM}	Longitudinal coordinate of the user center of mass	80 to 170 mm
ε	Camber rear wheel	12°
β_n	Nominal head angle	36°

The mass of the five components: frame, fork, front wheel and rear wheels have been determined by weighing each component. The inertia and the coordinates of the center of mass of the components have been estimated by a cad model knowing the real weight. The coordinates of the user center of mass have been calculated knowing the weight of the prototype, the weight of the user and the normal force of the ground measured by employing three scales.

The racing wheelchair has been modelled as a system composed of five elements: two rear wheels, a front wheel, the frame and the fork. Each component can be uniquely described through the adoption of reference frames, presented in Figure 2.27. In table 2.2 the kinematic and dynamic variables, that have been estimated in the model, are reported.

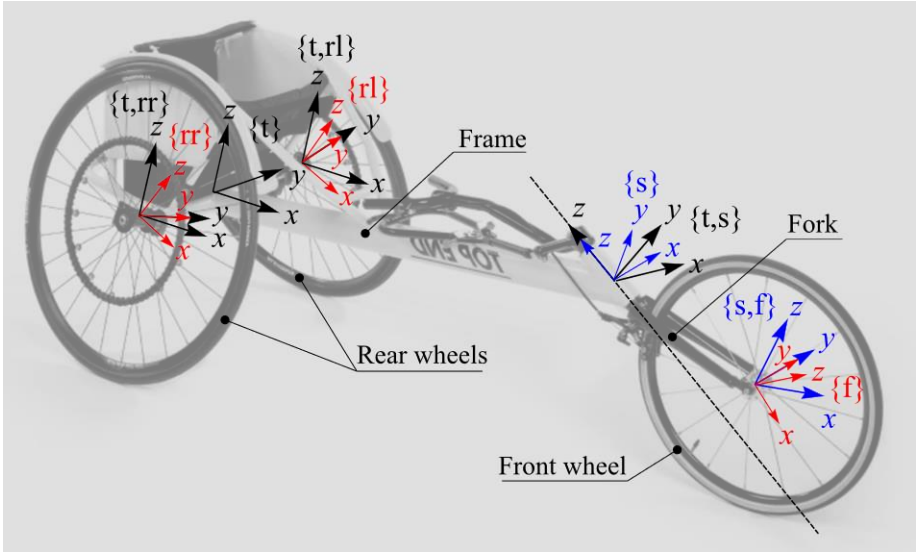

Figure 2.27: Dynamic model of racing wheelchair with the pose of the reference system

The reference frame {t} is fixed on the wheelchair and it identifies the pose of the vehicle.

Table 2.2: kinematic and dynamic variables

Symbol	Description	Note
$\theta_{rw}, \dot{\theta}_{rw}, \ddot{\theta}_{rw}$	Angular variables of the rear right wheel	Rotation of {rr}with respect to {t,rr} along the y axis of {t,rr} along the y ax
$\theta_{lw}, \dot{\theta}_{lw}, \ddot{\theta}_{lw}$	Angular variables of the rear left wheel	Rotation of {rl}with respect to {t,rl} along the y axis of {t,rl}
$\theta_{fw}, \dot{\theta}_{fw}, \ddot{\theta}_{fw}$	Angular variables of the front wheel	Rotation of {f}with respect to {s,f} along the y axis of {s,f}
$\theta_s, \dot{\theta}_s, \ddot{\theta}_s$	Angular variables of the steering	Rotation of {s}with respect to {t,s} along the z axis of {t,s}
T_S	Steering torque	Steering torque on the fork generated by the contact force on the ground

The model of the racing wheelchair has been implemented in the dynamic software simulation MSC Adams/View with the geometrical and dynamic

parameters shown previously. The ground-wheel contact model implemented is the "Pacejka's Magic Formula" [86], with the parameters determined in [87]. The input data of the model are the longitudinal wheelchair speed and the steering angle. The maximum range of motion of the steering angle, θ_S, in static condition is from -45° to 45°. The range of motion is wide and it has been reasonably limited depending on the wheelchair speed and checking the stability of the vehicle in the simulation. In table 2.3 the data of wheelchair speed and steering angle of each simulation are reported.

Table 2.3: Input data for the model

	$\dot{x}_w$: Wheelchair	θ_S: Steering angle
Run 1	0.05 m/s	[-45; +45°]
Run 2	0.5 m/s	[-35; +35°]
Run 3	2 m/s	[-25; +25°]
Run 4	8 m/s	[-20; +20°]

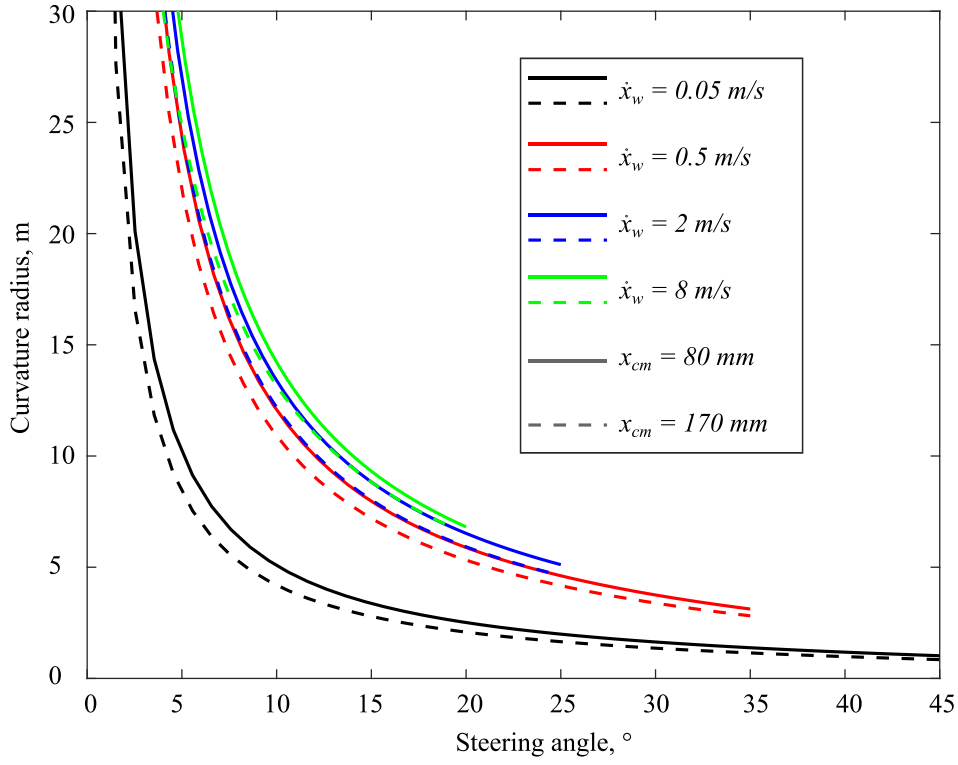

Figure 2.28: Curvature radius of the vehicle depends on the steering angle and the wheelchair speed

During the analysis, the system has been simulated multiple times: for each longitudinal speed of the vehicle the curvature radius has been evaluated with two different longitudinal coordinates of the center of mass. In Figure 2.28 the curvature radius of the wheelchair is shown, while in Figure 2.29 the steering torque is reported.

By increasing the wheelchair speed the curvature radius increases, and the range, in which the wheelchair is stable, is reduced. At the same speed, an increment of the longitudinal coordinate of the center of mass, which increments the normal force on the front wheel, results in a decrease of the curvature radius.

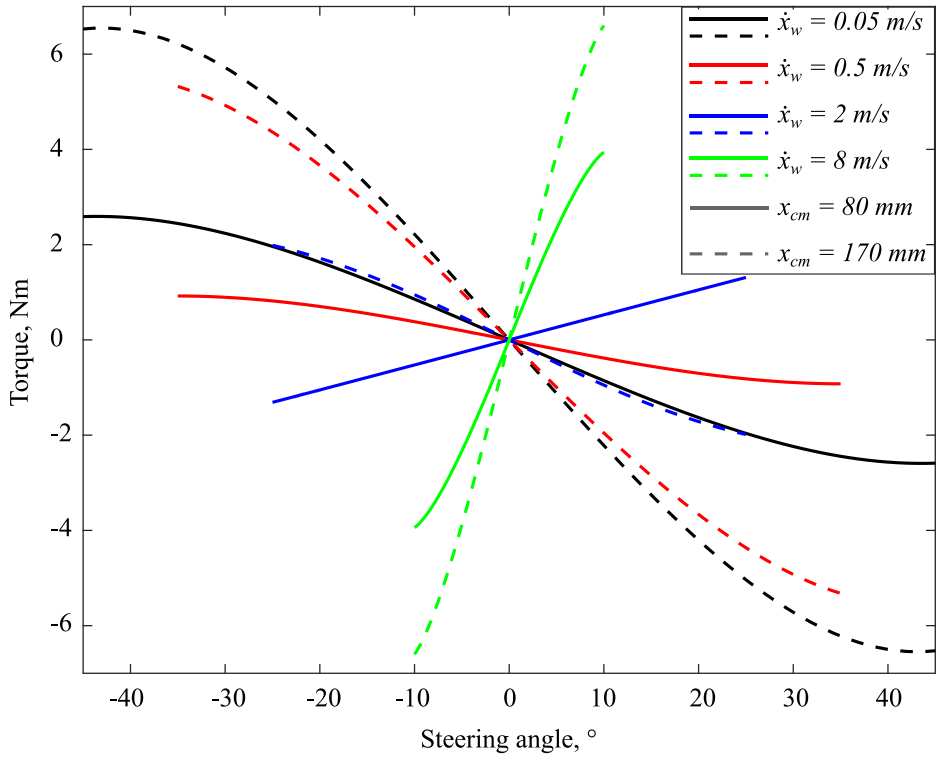

Figure 2.29: Steering torque depends on the steering angle and the wheelchair speed.

The steering torque depends on the magnitude and the direction of the three components of the contact force applied on the front wheel by the ground. Its magnitude and direction depend on the steering angle, the wheelchair speed and parameters of the model of the wheel. In general, the curves in the first and third quadrant are torques that stabilise the fork in the central position, thus the wheelchair steering angle is in a stable equilibrium, for example the green lines. On

the contrary, the curves in the second and fourth quadrant are torques that destabilize the fork from the central position, leading to an unstable equilibrium, for example the black lines. In general, at low speed the effect of the normal force is predominant, while at high speed the effect of the lateral and longitudinal forces is predominant. By increasing the normal force magnitude of the torque increases.

The results obtained depend strongly on the weight and the centre of mass of the user and on the wheelchair speed. The speed of 8 m/s is a velocity reached only by Paralympic athletes; thus it is a limited case. For non-athlete users the speed is limited to lower speeds. In addition, the speed is limited when the user takes a curve. Based on this consideration, in the next paragraph, the design of a new steering compensator mechanism is presented. Based on the previous results, the new steering compensator mechanism has been designed including multiple regulation systems which have been conceived for the experimental phase and which could be exploited to adapt the mechanism to the user preferences.

2.3.2 Functional design

Based on the commercial racing wheelchair previously presented, the prototype has been upgraded through the adoption of a pulley-cable subsystem composed of a rear wheel, a return pulley, a power spring, a mechanism for the transmission of motion and the handlebar with the system to control the steering angle, Figure 2.30.

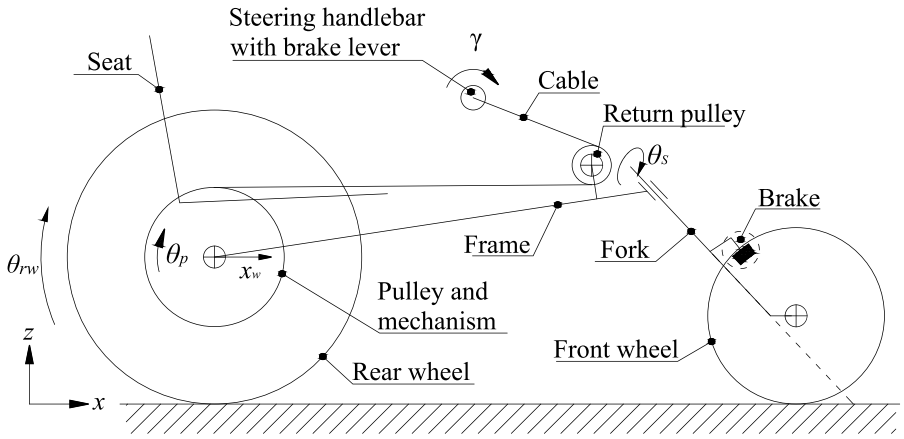

Figure 2.30: Functional sketch of the Handwheelchair.q racing, lateral view

Except for the steering handlebar and the compensator steering mechanism the other components were previously described from a functional point of view. Regarding the handlebar, the idea is to use a handlebar to propel the wheelchair and

to control the steering angle as shown in Figure 2.31. The handlebar is composed of two bars, right and left, that can rotate relatively. The relative rotation of the two bars determines the input, γ, of the steering mechanism, while the output is the steering angle θ_S. The right and left bar rotations are determined by the flexion-extension motion of the right and left wrist.

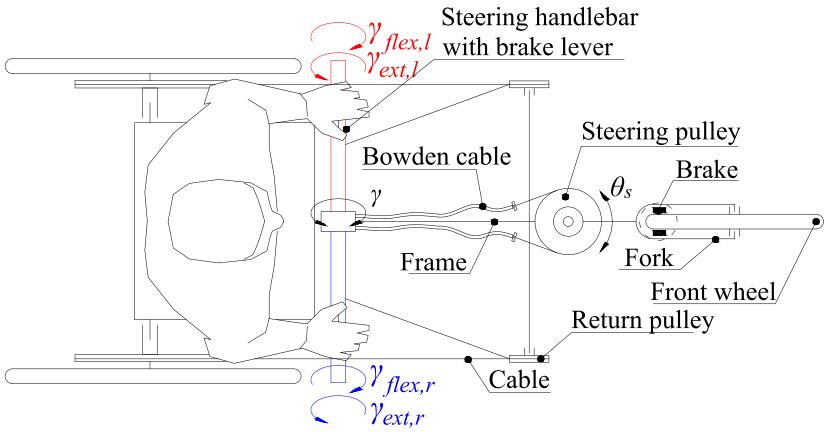

Figure 2.31: Functional sketch of the Handwheelchair.q racing, top view

The input angle γ is transmitted to the fork by a Bowden cable as shown in Figure 2.32. On the Handlebar side, the Bowden cable is wrapped around a pulley with radius r_{hp} and on the fork side, the Bowden cable is wrapped around a pulley with a radius r_{sp}. The link between the input and output is given by equation 2.1, where τ_S is the transmission ratio of the mechanism.

$$\theta_S r_{sp} = \gamma r_{hp} \rightarrow \theta_S = \tau_S \gamma \tag{2.1}$$

The input angle γ is the sum of the contribution of the right and left force, respectively γ_r and γ_l. The wrist flexion of the right hand, $\gamma_{flex,r}$, and the wrist extension of the left hand, $\gamma_{ext,l}$, give a positive contribution, while the wrist flexion of the left hand, $\gamma_{flex,l}$, and the wrist extension of the right hand, $\gamma_{ext,r}$, give a negative contribution, as shown in figure 2.33.

Considering the results of the curvature radius obtained by the dynamic model in Figure 2.28, the transmission ratio has been chosen lower than 1 for kinematic and dynamic reasons. From a kinematic point of view, a steering angle of 30° enables to cover a curve with a curvature radius of 2-3 m at low speed, which is acceptable and avoid the dynamic instability of steering angle higher than 30°. From a dynamic point of view, a transmission ratio lower than 1 enables to decrease the

torque perceived on the handlebar by the user. As described in the executive design, the limit is due to the maximum radius of the steering pulley that can be mounted on the prototype.

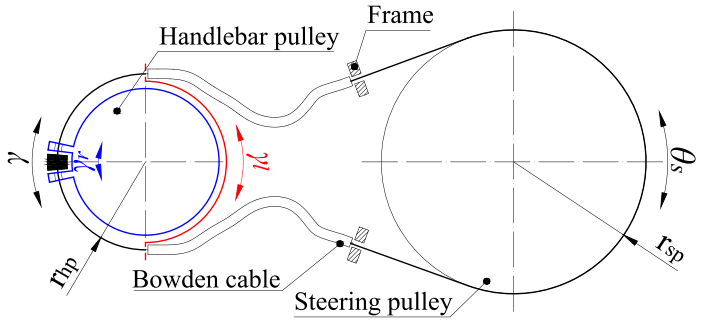

Figure 2.32: Functional design of the handlebar

In Figure 2.33 the input-output characteristic of the mechanism is reported with a transmission ratio equal to 1/2.

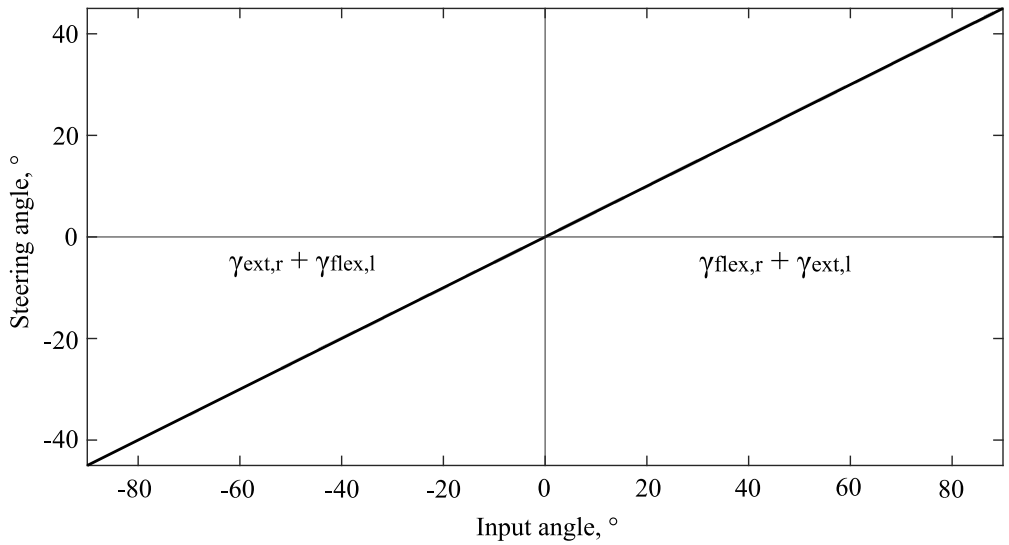

Figure 2.33: Input-output characteristic

The requirements are:

- minimum kinematic curvature radius of about 3 m;
- reduce the torque applied by the user to the handlebar to control the steering.

Considering to have a curvature radius of the wheelchair about 3 m the range of motion of the steering angle is limited about -30° to 30°. In order to reduce the torque applied by the user to the handlebar to control the angular position of the fork, the transmission ratio τ_S has to be the minimum possible. The maximum steering pulley radius that can be mounted on the racing wheelchair is 42.5 mm due to interference issues. The minimum radius of the handlebar pulley for technological reason is about 20 mm. These sizes define a transmission ratio τ_S equal to 1/2.

In Figure 2.34, the complete new steering compensator mechanism is reported. A steering pulley is fixed with the fork that rotates around the joint A_0. The rotation of the steering pulley and the fork are controlled by Bowden cables that come from the handlebar, as previously described, and they are fixed to the steering pulley by the limit stoppers right and left, $L4_R$ and $L4_L$. When the fork rotates anticlockwise, it engages with the link A_0E_R by means of the limit stopper $L1_R$ integral with the fork, while it engages with the link A_0E_L through the limit stopper $L1_L$, which moves with the fork, when it rotates clockwise. The links A_0E_R and A_0E_L are connected to the frame through two traction springs with stiffness equal to K, in the joint $D_{0,R}$ and $D_{0,L}$ respectively. The limit stoppers $L3_R$ and $L3_L$ limit respectively the anticlockwise and the clockwise rotations of the link A_0E_R and A_0E_L. In figure 2.34b the parameters of one side of the steering compensator mechanism are shown in order to simplify the functional design. The angle θ_S is the coordinate of the fork, $\theta_{S,i}$ is the shift angle and $\theta_{S,w}$ is the range of motion of the fork. The other parameters of interest are the distance d, namely the distance between the joint A_0 and D_0, and the length r of the link A_0E. The steering compensator mechanism generates a return torque, T_R, defined by equation 2.2. The force F_T is the useful component of F, defined by equation 2.3, while $F0$ is the pre-load.

$$T_R = F_T r \tag{2.2}$$

$$F = F0 + F_W = kl0 + k\Delta l \tag{2.3}$$

where k is the stiffness of the traction spring, r is the length of the link A_0E, Δl is the elongation and $F0$ is the preload. The elongation Δl is defined by equation 2.4.

$$\Delta l = \sqrt{(rcos(\theta_S) - d)^2 + (rsin(\theta_S))^2} - li \tag{2.4}$$

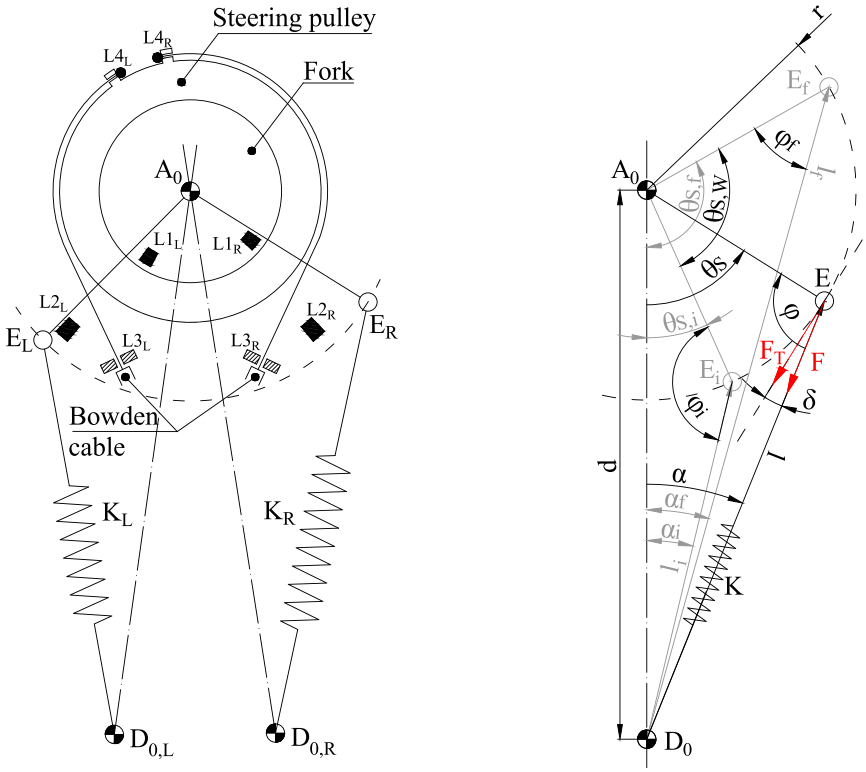

Figure 2.34: New steering compensator mechanism: a) functional sketch and b) functional design with the parameters and variables

Table 2.4: Complete nomenclature of the variables, parameters and components of the new steering compensator mechanism

Symbol	Description
α	Rotation of the link ED_0
θ_S	Steering angle, rotation of the link A_0E
φ	Angle between the link A_0E and ED_0
δ	Complementary angle of φ
l	Length of D_0E
r	Link A_0E
d	Link A_0D_0

$l0$	Initial elongation of the traction spring
$\theta_{S,i}$	Shift angle
li	Initial length of D0E
lf	Finale length of D0E
$L_{1,2,3,4}$	Mechanical stopper

In Figure 2.35, the parametric analysis of the mechanism is presented. The main parameters analyzed are a) the ratio *r/d*, b) the pre-load of the traction spring, c) the shift angle and d) the stiffness of the traction spring. The parameter *r/d* is a dimensionless parameter which defines the scale of the mechanism by defining the distance between the three joint *A0*, *E* and *D0*. When *r/d* increases, the return torque increases. The l0 is the pre-elongation of the traction spring. The pre-load generated by the traction spring increases with the pre-elongation proportionally. The shift angle influences the moment arm of the traction spring and modifies the trend of the return torque. An increment in the traction spring stiffness results in a proportional increment of the return torque.

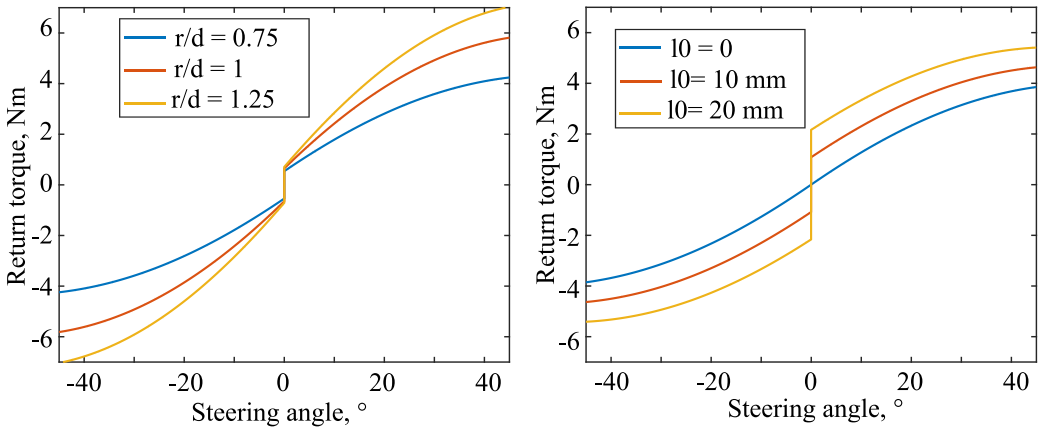

a) b)

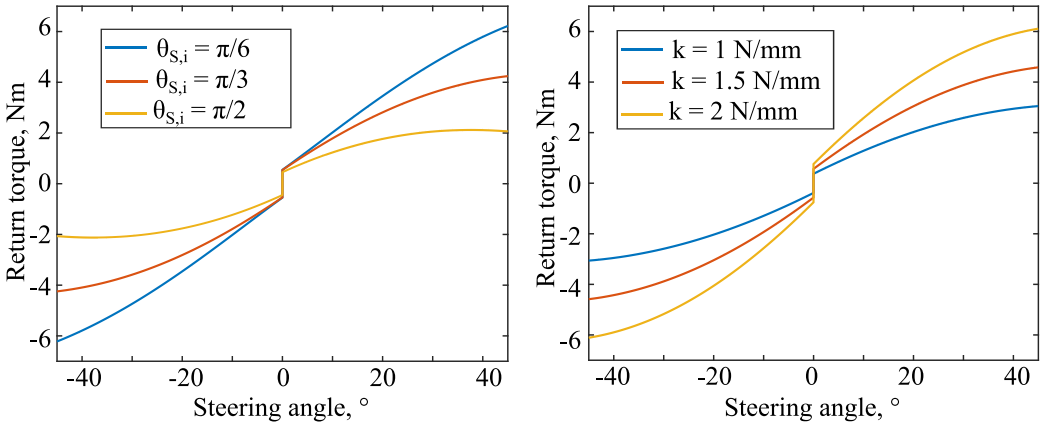

c) d)

Figure 2.35: Parametric analysis of the new steering compensator mechanism. Parameters: a) r/d, b) pre-load, c) shift angle and d) stiffness

The first parameter that has been defined is the length $d = 130\ mm$. This value is the maximum value that still allows for a compact and well-integrated steering compensator mechanism. As shown in Figure 2.29, the steering torque is influenced by the weight and the longitudinal position of the user and by the speed of the vehicle. For this reason, the steering compensator mechanism has been designed with variable parameters. The parameter d has five possible discrete values from 90 to 130 mm, while the length r has five regulations from 80 to 120 mm. These parameters define a transmission ratio τ_S variable from 0.61 to 1.33. The shift angle has five regulations from 30 to 80°, but the range of regulation can be easily increased as will be shown in the executive design in the next paragraph. The regulation of the pre-elongation l0 is continuous. Lastly, the stiffness regulation depends on the commercial component that satisfy the geometrical size and the required stroke. The mechanism has been defined considering that the stiffness of the commercial springs that satisfy the geometrical size are in the range of 1 to 2 N/mm.

2.3.3 Executive design and prototype

In Figure 2.36 the render of the executive design of the Handwheelchair.q racing is shown in the lateral, front, top view and the axonometry views.

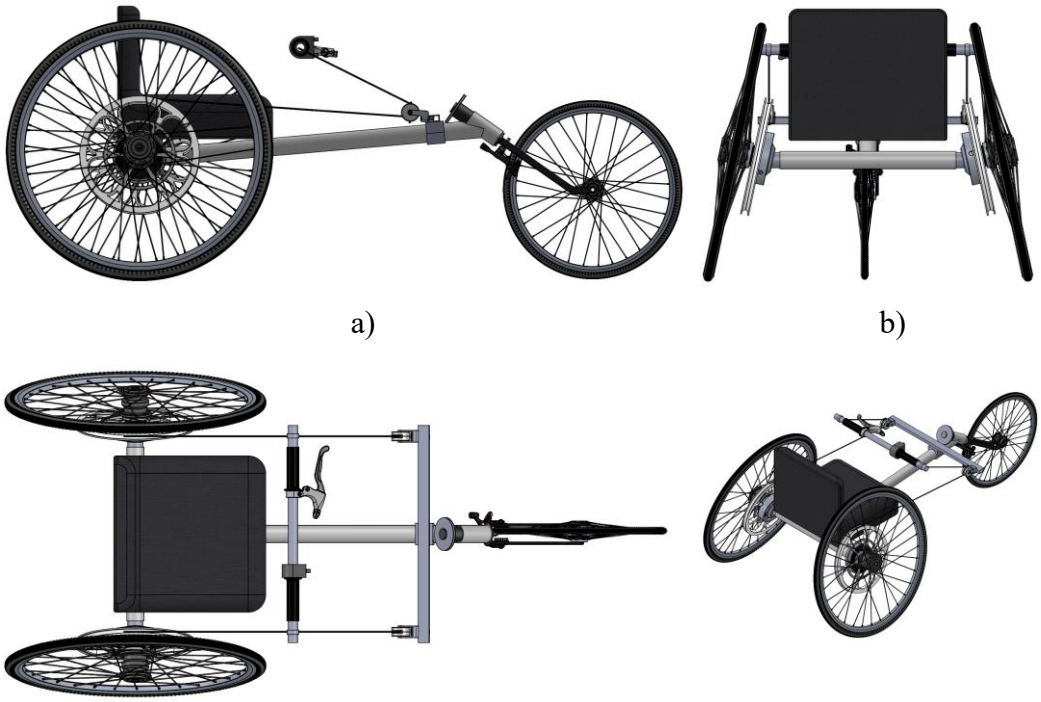

a) b)

c) d)

Figure 2.36: Render of the executive design of Handwheelchair.q racing

Starting from a commercial wheelchair, different subsystems has been substituted or added, as highlighted in Figure 2.37.

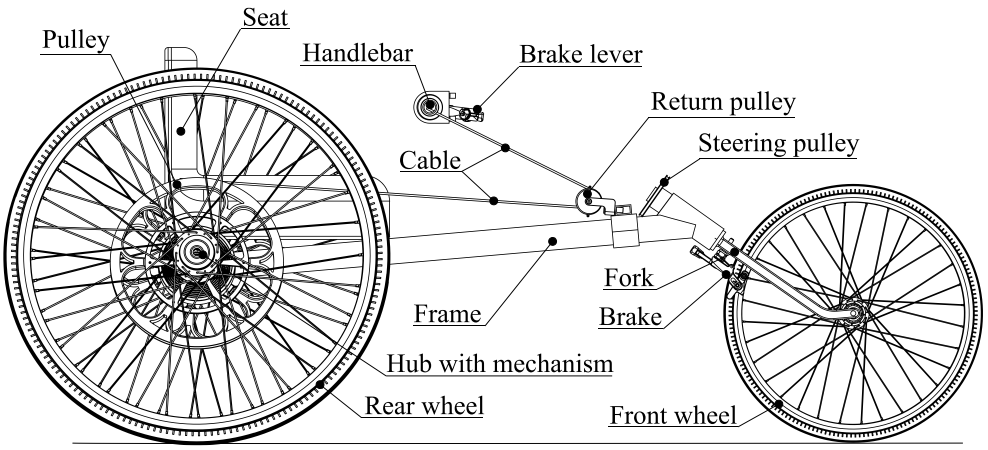

Figure 2.37: Executive design of Handhwheelchair.q racing, lateral view

First of all, the real wheels have been substituted with the subsystem of the rear wheel, hub and pulley presented in the section 2.2.3.

The only modification regards the camber angle, as shown in Figure 2.38.

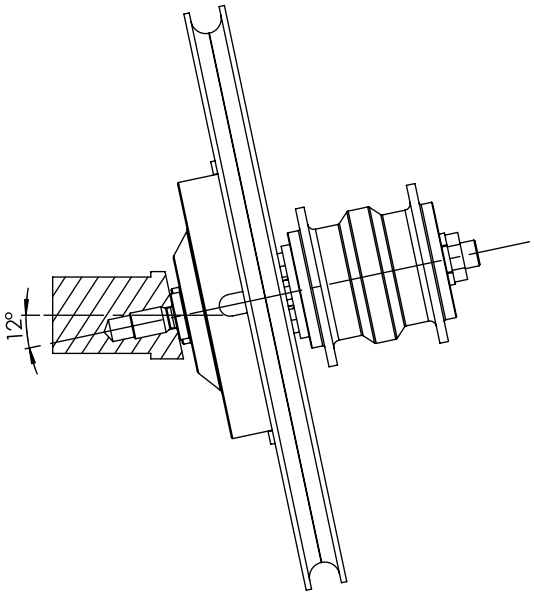

Figure 2.38: Rear wheel subsystem with a camber angle

The two return pulleys, Figure 2.39, have been mounted on a bar fixed to the frame. Also, these return pulleys have two degrees of freedom as described in the paragraph 2.2.2.

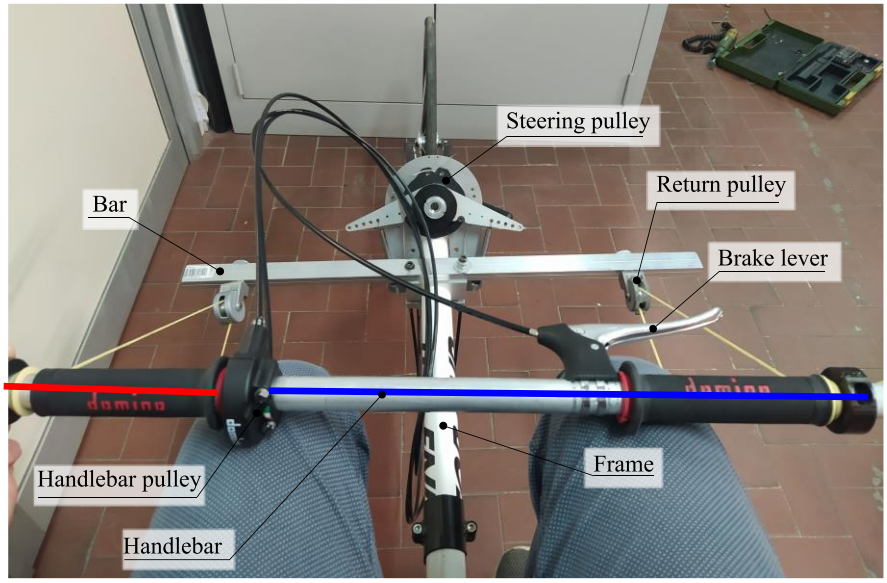

Figure 2.39: Prototype of Handhweelchair.q photographed by the point of view of the user

The right and left sides of the handlebar can rotate relatively, and the difference angle, γ, is transmitted to the fork by a Bowden cable. On the right side of the handlebar, a lever brake that controls the brake on the front wheel is mounted.

In Figure 2.40 the executive design of the compensator steering mechanism is reported with the nomenclature of the main parameters and its components. The flange represents the frame of the mechanism where the joints A_0, D_0 and the limit stopper L2 and L3 are positioned. The joint A_0 is centered on the fork axis and the steering pulley is fixed to the fork. The links A_0E_R and A_0E_L rotate with the steering pulley due to the limit stopper $L1_R$ and LI_L. The rotation in the opposite direction of each link is limited through the limit stopper $L2_R$ and $L2_L$ respectively. The limit stopper L1, L2 and the joints E, D_0 can be positioned in different positions to regulate the mechanism according to the specific user.

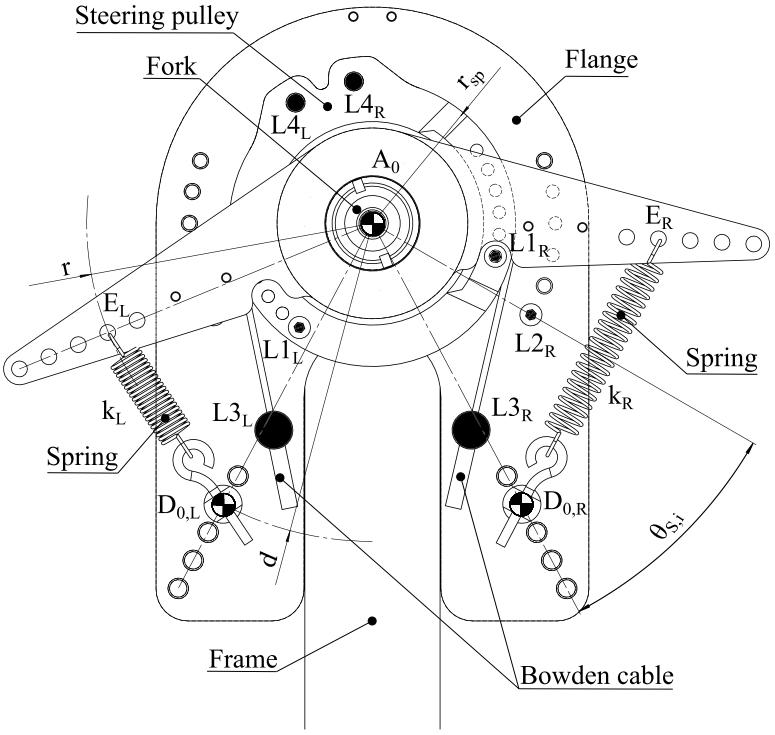

Figure 2.40: Top view of the new steering compensator mechanism, executive design

In Figure 2.41 the axonometry of the new steering compensator mechanism is reported. The two holes, on the top of the flange, need to support a potentiometer on the joint A_0 to measure the steering angle, as shown in Figure 2.42.

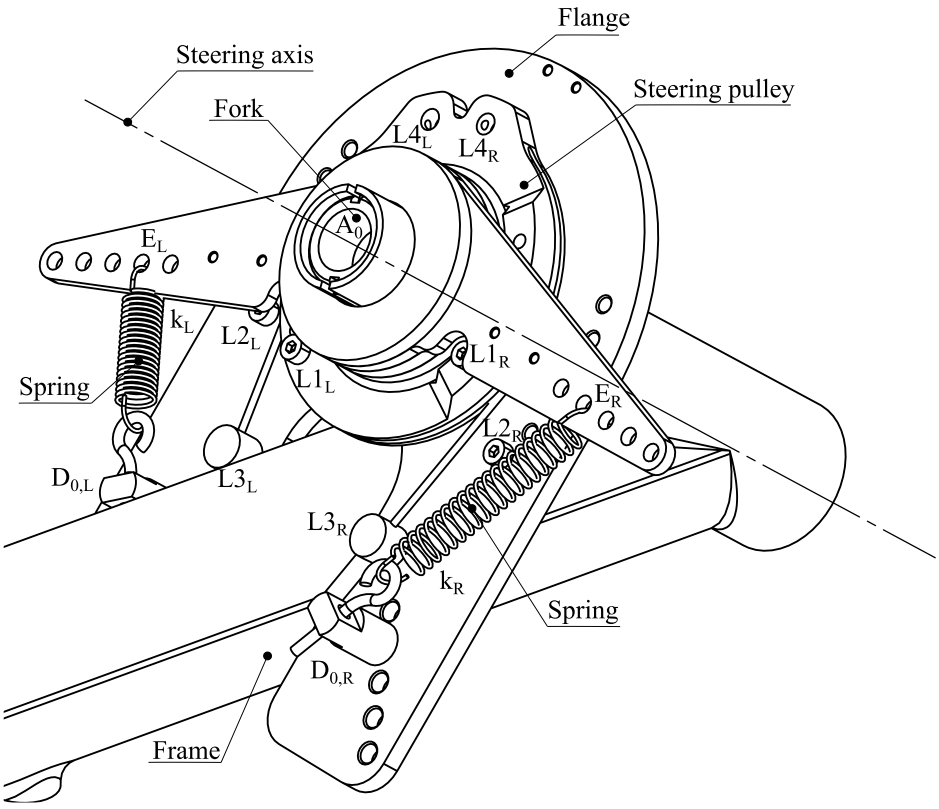

Figure 2.41: Axonometry of the new steering compensator, executive design

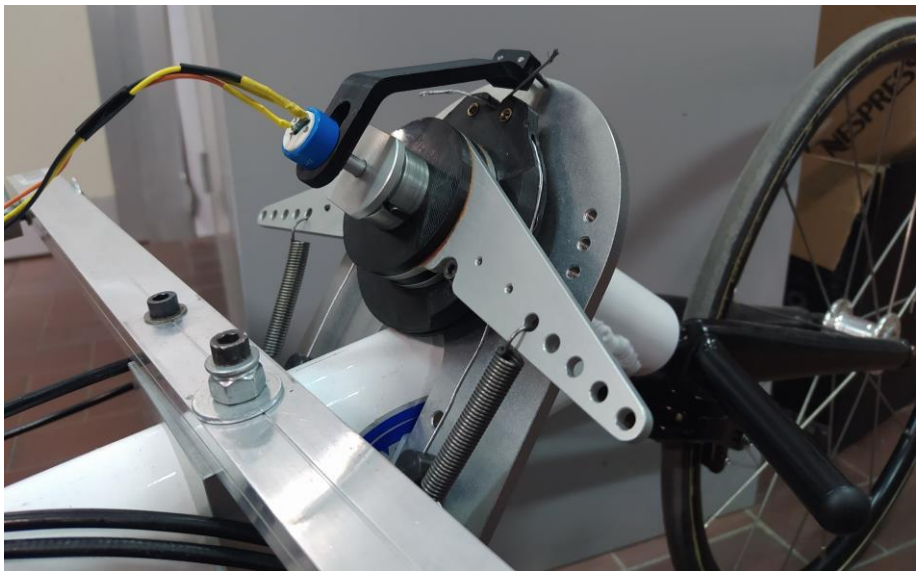

Figure 2.42: Prototype of the new steering compensator

In Figure 2.43 the prototype of Handwheelchair.q racing is reported. In the prototyping phase, the pulley has been upgraded with a new version characterized

by three grooves with three different radii. The alignment of the pulley and the return pulley is acceptable. The distance between the pulley and return pulley is about 0.7 m and each groove is wide 4 mm and the edge of each groove is 3 mm.

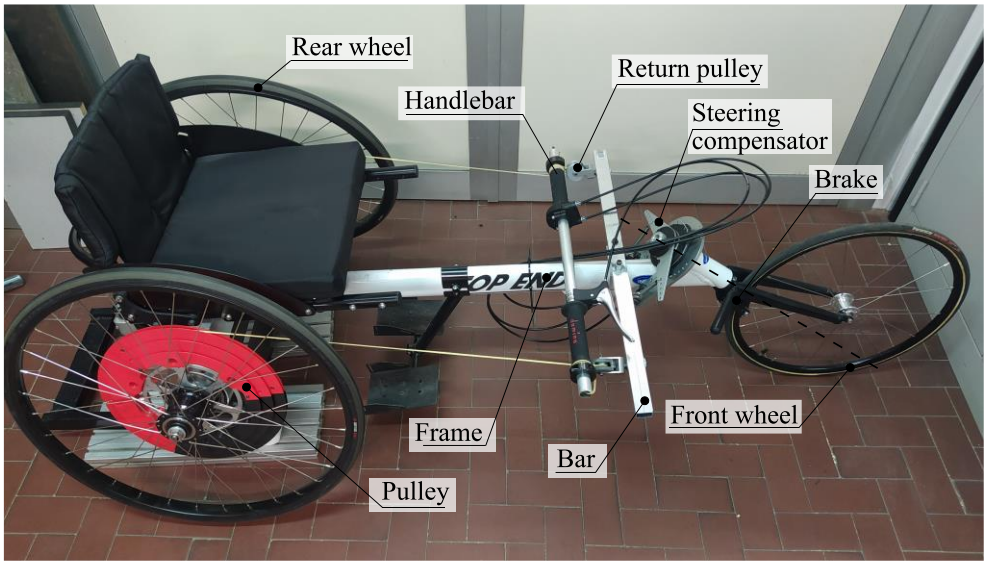

Figure 2.43: Prototype of the Handhwheelchair.q racing

Chapter 3

Experimental test

The pandemic situation has had a relevant impact on the experimental test. In 2019, the definition of experimental protocol with the doctors, physiatrists and physiotherapists of the U.S.U. (Unità Spinale Unipolare) in Turin was ongoing in order to conduct the experimental activity with spinal cord injury patients. The pandemic has interrupted the collaboration. In the follow paragraphs different tests have been conducted on able-bodied subjects. The following tests have a common goal, namely, to define a methodology, the experimental apparatus and the acquisition and elaboration data to test the innovative wheelchair. Each test has a specific goal discussed in its paragraph.

Experimental procedures conformed with the *Declaration of Helsinki* and were approved by the Local Ethics Committee.

3.1 Experimental apparatus

In general, the prototype has been equipped with different sensors. In Figure 3.1 the diagram of the experimental apparatus is reported.

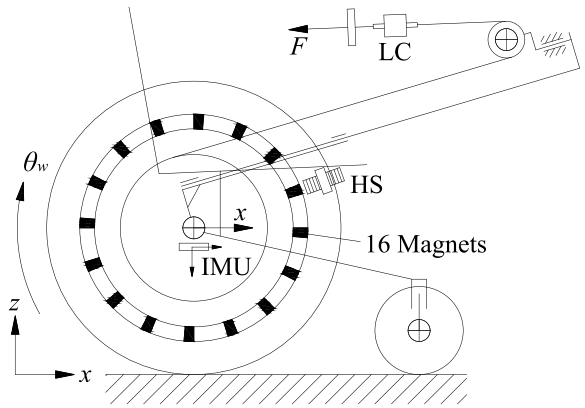

Figure 3.1: Diagram of the experimental apparatus

Two traction load cells (right and left), LC, connect the handle and the cable to measure the forces that the user applies to propel the wheelchair. Sixteen equidistant magnets are positioned on each rear wheel and two hall sensors detect the passage of the magnets. The signals of the Hall sensors are elaborated in order to obtain the wheelchair linear speed. An Inertial Measurement Unit, IMU, is located on the frame of the wheelchair. The data are recorded with an acquisition system on board.

3.1.1 Equipment

In Figure 3.2 the circuit diagram of the acquisition system is reported. A 24 V battery powers the load cells through the corresponding instrumental amplifier and the acquisition board. The acquisition board powers the hall sensors and the IMU. The signals of the sensors are acquired by the acquisition board and are logged by an on-board computer.

The load cell (DCE, LCM Systems Ltd, Newport, Isle of Wight, UK) outputs a differential signal, which is made by the paired signals Signal LC (+), mV and Signal LC (-), mV, that is proportional to the force applied on the load cell. Then, the instrumental amplifier (SGA, LCM Systems Ltd, Newport, Isle of Wight, UK) scales the differential signal up producing the Signal LC (+), V and Signal LC (-), V. The differential of the amplified signals of each load cell LC (+) and LC (-) define the signal of the right and left cell, V_r and V_l.

Signals $V_{H,rw}$ and $V_{H,lw}$ are the signal generated by the right and left hall sensors (SS41, Honeywell, Charlotte, North Caroline, USA), respectively. The signal is an analog voltage included between 0 and 5 V. When the hall sensor does not detect a magnetic field the output signal is 2.5 V, otherwise, when the hall sensor detects a magnetic field, the output is proportional to the intensity of the magnetic field.

The IMU (MPU-6050, TDK InvenSense, San Jose, California, USA) is a 6-axis accelerometer. (Aggiungere info sull'output digitale, Chiedere a Luigi)

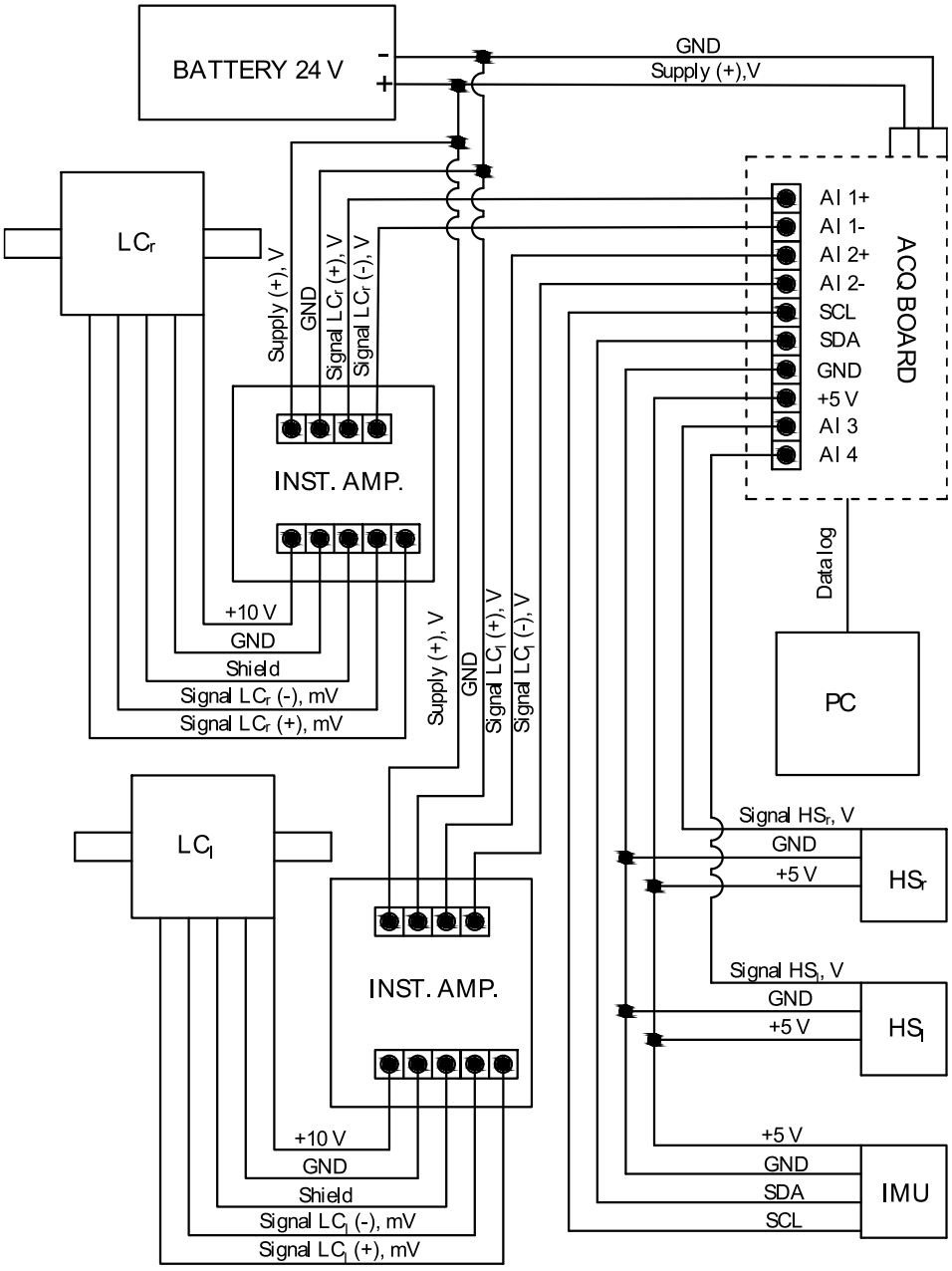

Figure 3.2: Circuit diagram of the acquisition system

3.1.2 Experimental data conditioning methodology

In this section the methodology of the elaboration data is reported. In the next tests, if not specified, this represents the methodology employed for the elaboration data. The two hall sensors detect the passage of 16 magnets mounted on each rear wheel, left and right. The angular distance of each magnet is defined by the following eq. (3.1):

$$\Delta\theta = \frac{2\pi}{16} = \frac{\pi}{8} \tag{3.1}$$

From the signals, $V_{H,rw}$ and $V_{H,lw}$, of the Hall sensors, Figure 3.3, the frequency of the passage of the magnets, f_{rw} and f_{lw}, is identified by a trigger V_s, defined by eq. (3.2) for each wheel. Knowing the angular distance and the frequency, the angular position of each rear wheel, θ_{rw} and θ_{lw}, is defined by eq. (3.3) and it shows in Figure 3.3.

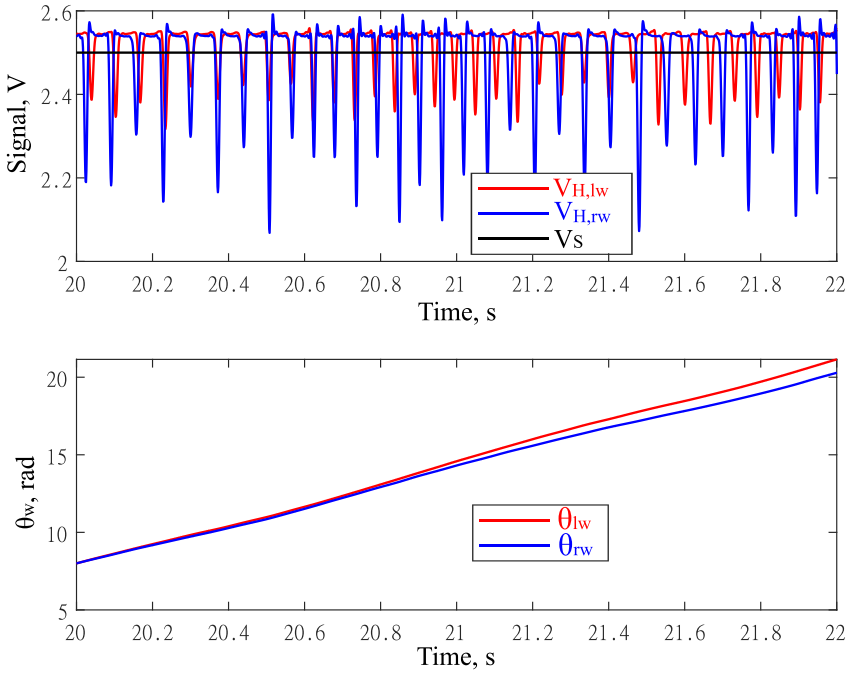

Figure 3.3: Output signal of the Hall sensor, top, and angular position of the rear wheel, below.

$$\begin{cases} f_{rw} = f_{rw} + 1; & V_{H,rw} \geqslant V_S \wedge \dot{V}_{H,rw} > 0 \\ f_{rw} = f_{rw}; & Otherwise \end{cases}$$
$$\begin{cases} f_{lw} = f_{lw} + 1; & V_{H,lw} \geqslant V_S \wedge \dot{V}_{H,lw} > 0 \\ f_{lw} = f_{lw}; & Otherwise \end{cases} \quad (3.2)$$

$$\theta_{rw} = f_{rw}\Delta\theta \; ; \; \theta_{lw} = f_{lw}\Delta\theta \quad (3.3)$$

From the angular position of each rear wheel, the longitudinal position of the wheelchair, its longitudinal speed and its longitudinal acceleration are defined respectively by eq. (3.4a), (3.4b) and (3.4c), with the hypothesis of pure rolling motion.

$$x_w = \frac{\theta_{rw} + \theta_{lw}}{2} r_w \quad (3.4a)$$

$$\dot{x}_w = \frac{dx_w}{dt} \quad (3.4b)$$

$$\ddot{x}_w = \frac{d\dot{x}_w}{dt} \quad (3.4c)$$

In Figure 3.4, the wheelchair longitudinal displacement, the wheelchair longitudinal speed and the wheelchair longitudinal acceleration are reported.

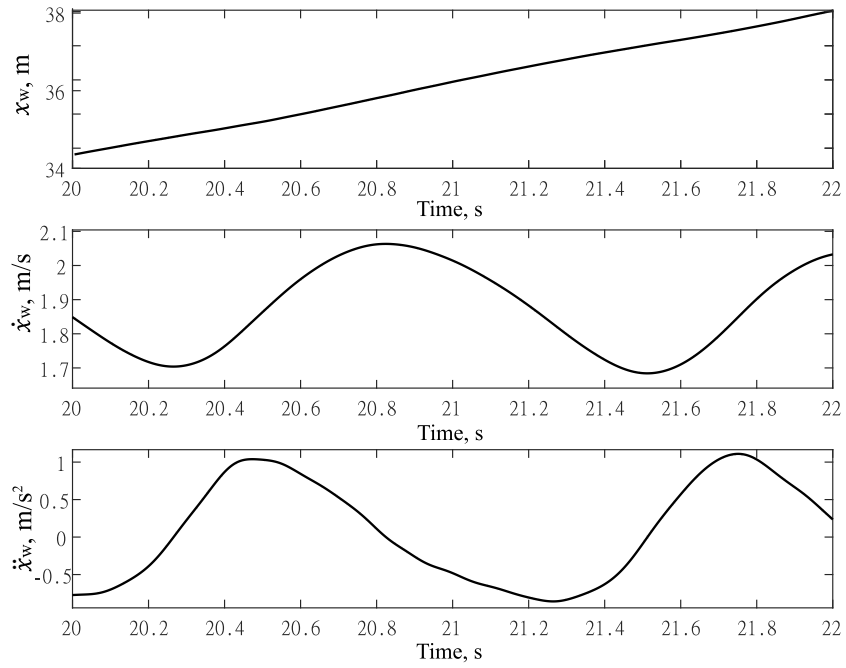

Figure 3.4: Longitudinal displacement, speed and acceleration of the wheelchair computed by the Hall sensor

With the hypothesis that the cable is inextensible, it is possible to evaluate the stroke of the user during the active phase with eq. 3.5.

$$x_u = x_w \frac{r_p}{r_w} \tag{3.5}$$

The cable employed in the prototype is a cable of "Kevlar", an Aramid fiber, with a breaking load of 3 kN and a breaking elongation of 2% [CITARE]. Considering that, in this application, the peaks of force on the single cable is less than 100 N, the hypothesis is acceptable.

From the differential signals of the two load cells, V_r and V_l, and the respectively gain, K_r and K_l, the right and left forces, F_r and F_l, that the user applies on the wheelchair are defined by eq. (3.6). Figure 3.5 shows right and left measured forces and their sum, F, after being filtered by a zero-phase digital filter.

$$F_l = V_l K_l;\ F_r = V_r K_r \tag{3.6}$$

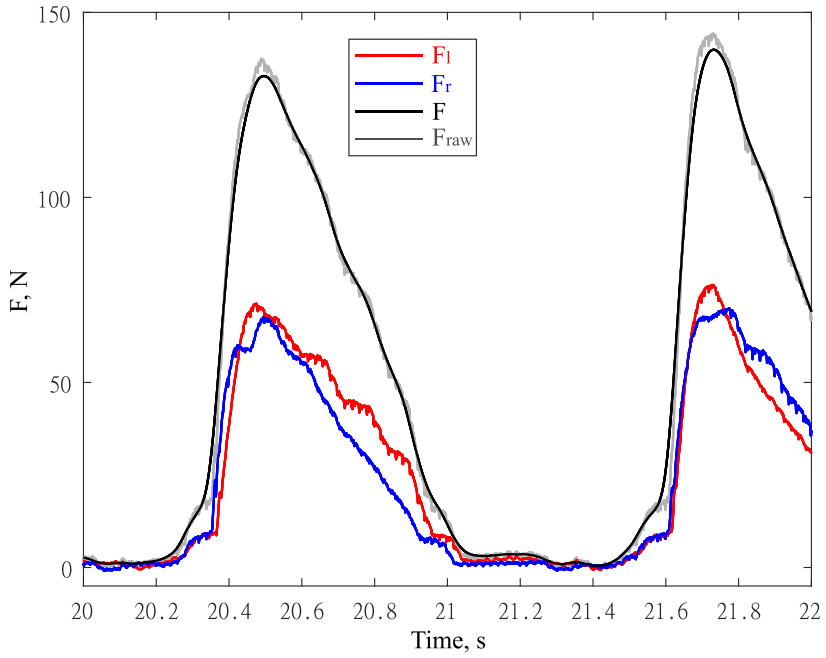

Figure 3.5: Right, left and total force computed by the right and left load cells.

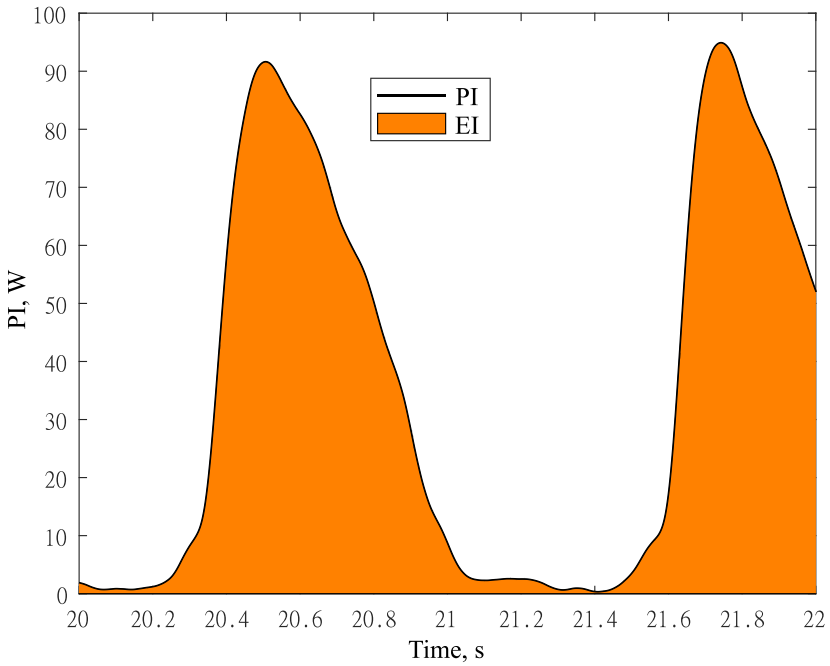

Figure 3.6: Input power and energy computed by the load cells and the Hall sensors

From the kinematic and dynamic data, the input power, *PI*, and the energy input, *EI*, Figure 3.6, are defined respectively by the eq. (3.7) and (3.8), where r_w is the rear wheel radius.

$$PI = F_l \dot{\theta}_{lw} r_w + F_r \dot{\theta}_{rw} r_w \tag{3.7}$$

$$EI = \int PI \, dt \tag{3.8}$$

3.1.3 Data analysis methodology

Each propulsion gesture cycle is composed of two phases: the active phase and the recovery one. The active phase occurs when the user transmits force to the wheelchair, whereas the recovery phase arises when the user does not transmit force. Based on this consideration, the active phase is identifiable when the force exceeds a threshold value. Accordingly, the recovery phase is defined as the phase between two active phases. T_A and T_R represent the time of the active and recovery phase, respectively. For each cycle is possible to identify the kinematic and dynamic parameters collected in Table 3.1. In general, the subscript "*A*" refers to the average value of the variable in the active phase, the subscript "*i*" refers to the average value of the variable in the cycle *i-th* and the subscript "*avg*" refers to average value of the variables *i-th*. An example of the nomenclature is reported in Figure 3.7.

In addition, it is possible to define a new parameter that represents the general trend of the cycles of some variables, and it is indicated with the subscript *-mean*. In the follow, an example of the procedure that defines the F_{mean} is reported. In Figure 3.8a, the curves in grey are the force of each cycle F_i. The eq. (3.9) defines the normalized force *i-th*, $F_{i,norm}$, that are reported in Figure 3.8b in grey. The eq. (3.10) defines the mean of the normalized force *i-th*, $F_{mean,norm}$ that is reported in Figure 3.8b in black, where N is the number of the cycle. Lastly, the mean force, F_{mean}, is defined by the eq. (3.11) and it is reported in Figure 3.8b in black.

Table 3.1: Kinematic and dynamic parameters

Symbol	Description
$T_i, T_{A,i}, T_{R,i}$	Cycle, active and recovery time of the cycle *i-th*
$T_{avg}, T_{A,avg}, T_{R,avg}$	Average value of $T_i, T_{A,i}, T_{R,i}$
F	Sum of right and left forces
$F_{A,i}$	Mean force of the cycle *i-th* in the active phase
$F_{A,avg}$	Average value of $F_{A,i}$
$F_{max,i}$	Peak of force of the cycle *i-th*
$F_{max,avg}$	Average value of $F_{max,i}$
PI	Input power
PI_i	Mean input power of the cycle *i-th* in the complete cycle
PI_{avg}	Average value of PI_i
$PI_{A,i}$	Mean input power of the cycle *i-th* in the active phase
$PI_{A,avg}$	Average value of $PI_{A,i}$
EI_i	Energy input of the cycle *i* in the active phase
EI_{avg}	Average value of EI_i
$x_W, \dot{x}_W$	Displacement and speed of the wheelchair
x_u	Stroke of the user hand
$x_{W,i}, \dot{x}_{W,i}$	Mean wheelchair displacement and speed of the cycle
$x_{u,i}$	Mean user hand stroke of the cycle *i-th*
$x_{W,avg}, \dot{x}_{W,avg}$	Average value of $x_{W,i}$ and $\dot{x}_{W,i}$
$x_{u,avg}$	Average value of $x_{u,i}$

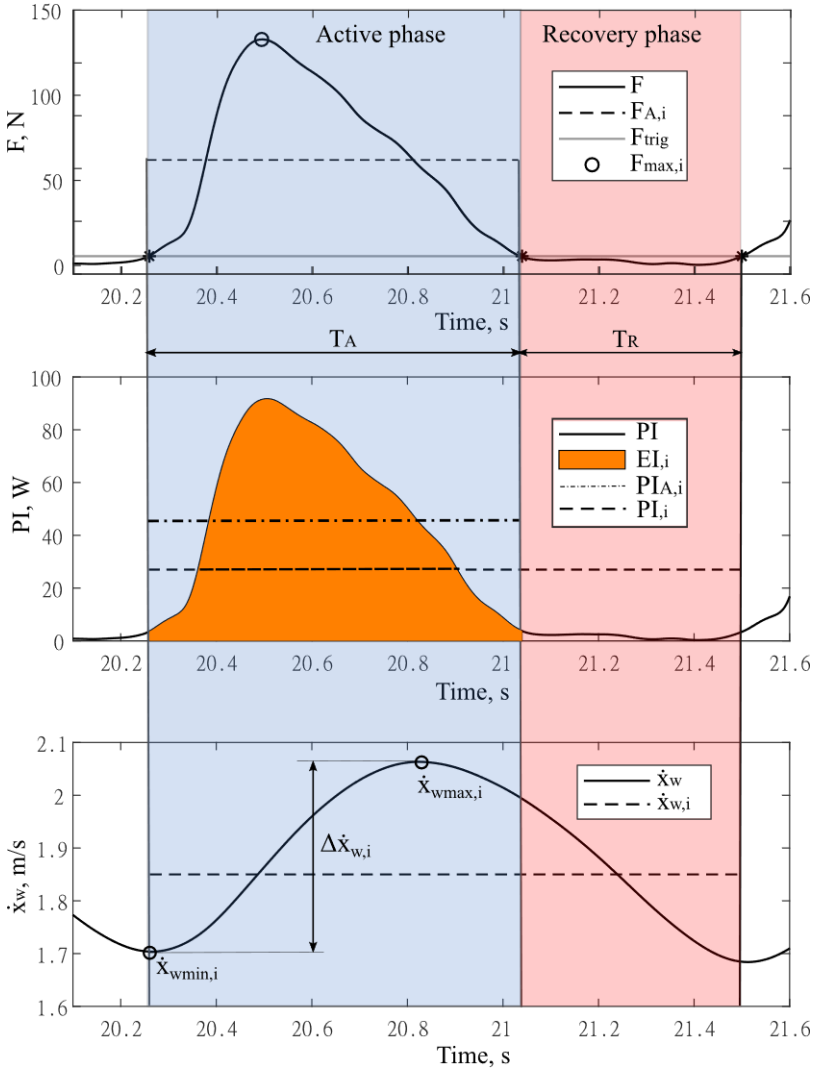

Figure 3.7: Example of main nomenclature

$$F_{i,norm} = F_i(\tau = \frac{Time}{T_{A,i}}) \tag{3.9}$$

$$F_{mean,norm} = \frac{\sum F_{i,norm}}{N} \tag{3.10}$$

$$F_{mean} = F_{mean,norm}(\tau\, T_{A,avg}) \tag{3.11}$$

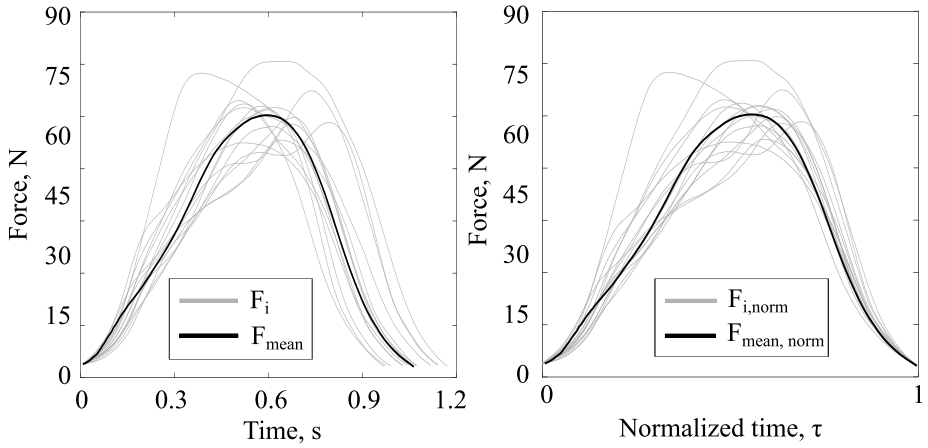

Figure 3.8: Procedure for the definition of the F_{mean}

As shown in the literature [88], the magnitude of the force on the shoulder joint influences the shoulder pain. Obviously, the magnitude of the force depends on the use of the wheelchair (e.g., indoor, sport, climbing a ramp, etc). This work proposes a new index, named *POF*, Peak of Force defined by equation 3.13.

$$POF = \frac{F}{F_A} \tag{3.13}$$

Thus, the index is an evaluation about how F_A and F compares, in particular, the specific condition about how F_A and F_{max} compares. The average force in the active phase, F_A, is a characteristic parameter that can be calculated for each system of propulsion: handrim, handbike and lever system. The average force depends on the use and the intensity of the activity. In addition, the average force depends on the system of propulsion because each system of propulsion has its own transmission ratio as seen in paragraph 1.5. The index *POF* is an index that can be an interesting parameter to compare the peaks of force and the average force for different systems of propulsion.

During the prototyping phase, the characteristic of the power spring has been defined. The power spring is loaded in the active phase, while in the recovery phase it has to rotate the pulley in the opposite direction in order to rewind the cable. The return torque generates by the power spring has to be as low as possible in order to keep higher efficiency of the wheelchair, but, at the same time, it must be sufficient to guarantee the correct rewind of the cable. The power spring has been realized by

using a harmonic steel tape. The return torque depends on the width, thickness of the tape and the external radius of winding. Tapes with different characteristics have been tested in order to find the best solution for the application. In Figure 3.8 the return torque of the right and left power spring, $T_{PS,l}$ and $T_{PS,r}$ respectively, are reported.

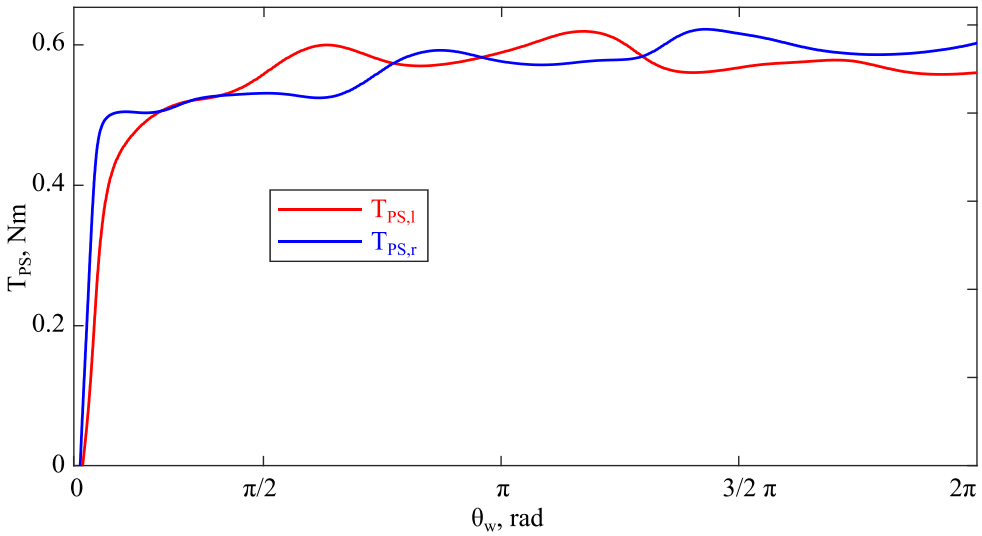

Figure 3.8: Characteristic of the right and left return torque of the return pulley

3.2 Test 2: Kinematic and dynamic analysis

This test represents the first test of the innovative manual wheelchair named Handwheelchair.q. This test investigates the dynamic and kinematic characteristics of the prototype. In this test different subjects were involved, and the wheelchair was tested in different setups and different levels of external load. The second goal of this test is to evaluate the correct functioning of all complete experimental apparatus, from the equipment to the data elaboration.

3.2.1 Methods

Three able-bodied subjects not familiar with wheelchair use participated in the experiment. The experimental tests consisted of propelling Handwheelchair.q from a standing start on a flat hallway. The users were asked to drive the wheelchair for about 60 m, as shown in Figure 3.9, at different intensities (low or high) and different transmission ratios. The low intensity has been defined as the intensity at which the user does not perceive fatigue, comparable to a walk on a flat surface for an able-bodied. The high intensity has been defined as increasing the wheelchair

speed by about 50%. In the tests, the users were able to check the wheelchair speed in real-time with a speedometer. Four sets of tests were performed

- Set 1 “Low Speed, LS” with the radius pulley r_{p1};
- Set 2: “High Speed, HS” with the radius pulley r_{p1};
- Set 3: “Low Speed, LS” with the radius pulley r_{p2};
- Set 4: “High Speed, HS” with the radius pulley r_{p2}.

Subjects were first asked to practice on Handwheelchair.q. During this familiarisation session, each user has chosen the height of the return pulley in order to get a comfortable rowing motion and then the position of the return pulley was kept constant during the test. Two different pulley radii were available: r_{p1} = 130 mm and r_{p2} = 108 mm and the radius of the rear wheels was r_w = 292 mm. In the test, the Handhweelchair.q is equipped with two load cells, two Hall sensors and an Inertial Measurement Unit, I.M.U.

3.2.2 Results

Each run is composed of two phases: the acceleration phase and the steady-state phase. During the acceleration phase, the wheelchair accelerates from zero to the steady-state speed. During the steady-state phase, the wheelchair speed oscillates around an average speed, as shown in Figure 3.9. In Figure 3.9 is also reported the displacement during the test. At the beginning of the acceleration phase, the wheelchair starts with a speed equal to zero. After some cycles, the steady-state speed is reached. The steady-state phase starts when the wheelchair speed reaches the steady-state speed that is defined as the average speed in the central part of the test. At the beginning of the acceleration phase, the time of the active phase, T_A, is large and then decreases.

In Figure 3.10 are reported the right, left forces and their sum, in blue, red and black respectively. In general, it is possible to observe as the major peaks of the force are in the acceleration phase. In the steady-state phase, the peaks of force are lower.

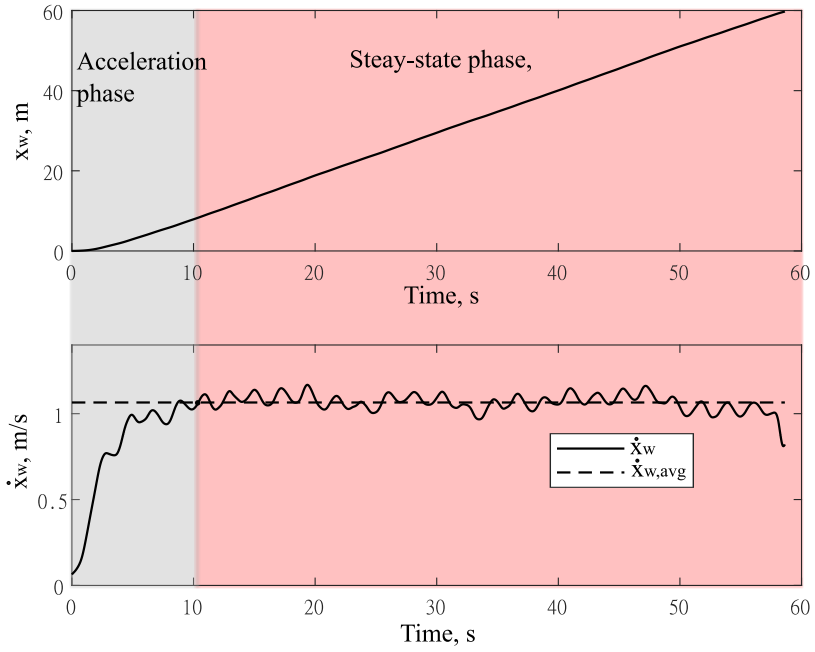

Figure 3.9: Displacement and speed of the wheelchair during the test.

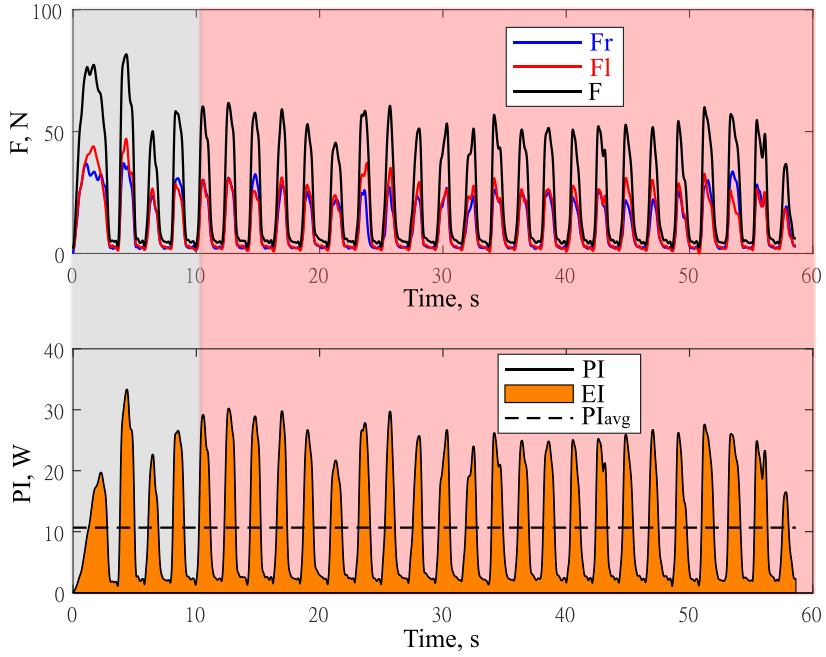

Figure 3.10: Right, left and total force of the user and the input power during the test.

In Figure 3.11, the wheelchair speed and the forces of the acceleration phase are reported. This figure represents a general trend of the results of the different subjects and the overall results are reported in Table 3.1. In the first cycles, the time of the cycles are longer: the time of the first cycle is about 3.8 s and the cycle time of the 4th and 5th are about 2 s. In the first cycles, the peaks of force are higher than the next cycles. The steady-state speed is reached in the third, fourth or fifth cycle. In general, for Sets 1 and 3, namely the low speed runs, the steady-state speed is reached before than in Sets 2 and 4.

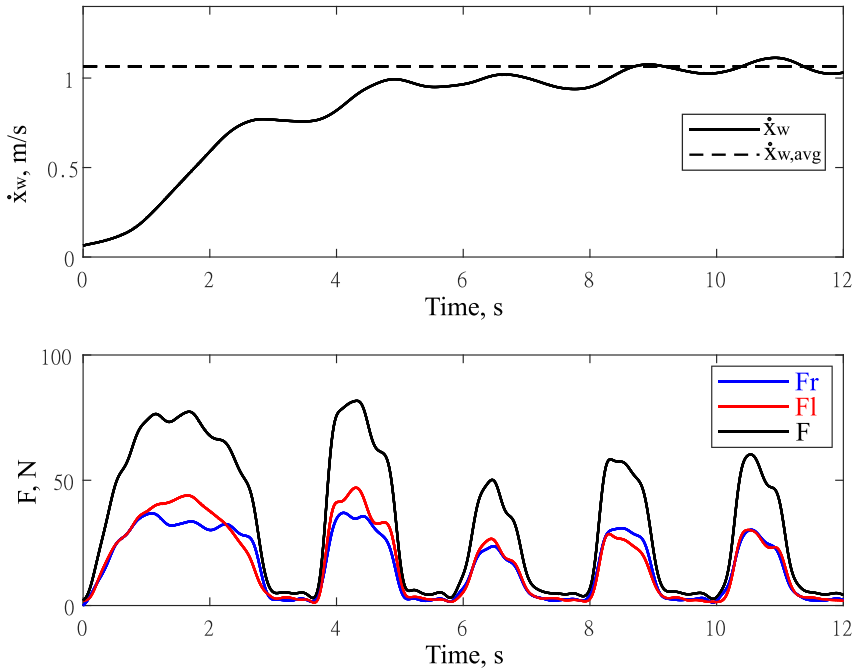

Figure 3.11: User's Force and wheelchair speed in the acceleration phase

In Figure 3.12, the data force in the acceleration phase of the subjects 1, 2 and 3. The data refer to the Set 4, namely with the smaller pulley radius at high intensity. For all subjects, as also reported in Table 3.2, the general trend shows that the peaks of force decrease in the first three or four cycles (Except for the subject 2 between the second and third cycle) and also the active time decrease.

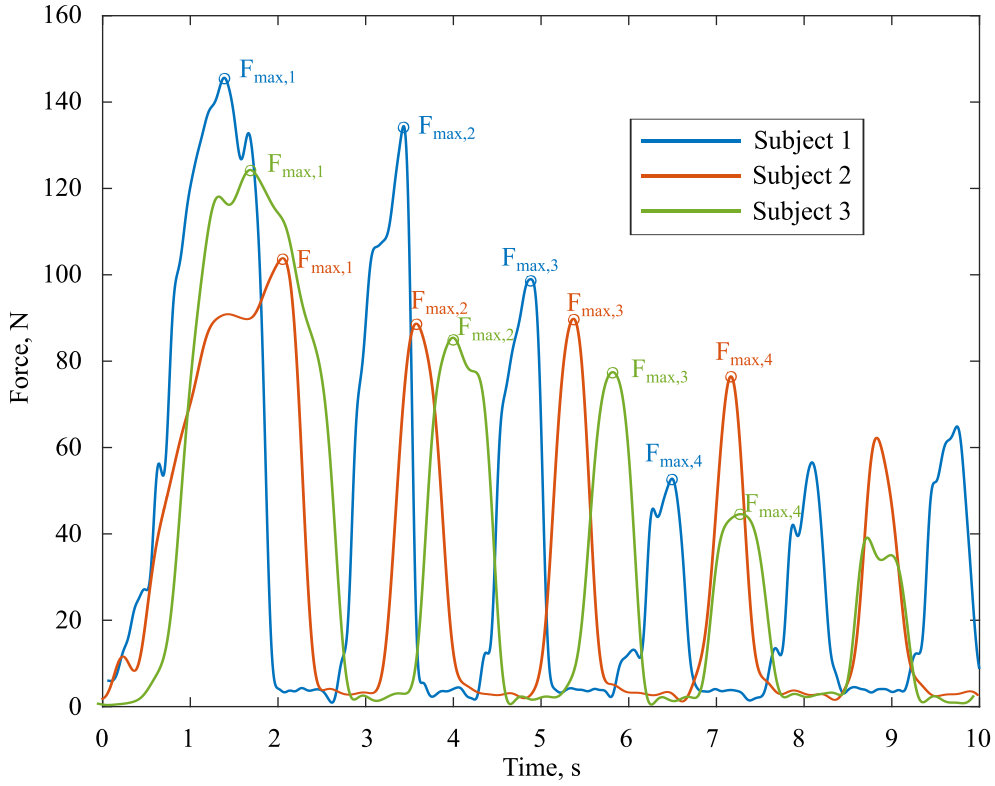

Figure 3.12: Data force in the acceleration phase for all three subjects during the set four.

In Table 3.2 some variables of the first four cycles are reported. In particular, the variables reported are the active time T_A, the peak of force F_{max}, the average force in the active phase F_A, the average power in the active phase PI_A and the wheelchair displacement in the active phase x_{WA}. The general trend shows as the maximum peaks of force and the maximum active time are in the first cycle while the maximum value of the average power during the active phase, PI_A, are in the second cycle. It is interesting to note that the wheelchair displacement in the active phase x_{WA} is almost constant for each cycle of each set, but it increases as the wheelchair speed rises, and as expected, it increases when the pulley radius decreases.

Table 3.2: Variables in the acceleration phase, Test 2

Variables	Set 1: r_{p1}	Set 2: r_{p1}	Set 3: r_{p2}	Set 4: r_{p2}
$T_{A,1}, s$	2.56	2.08	2.7	2.75
$F_{max,1}, N$	88.4	124.0	96.6	123.7
$F_{A,1}, N$	52.4	80.3	59.1	81.2
$PI_{A,1}, W$	12.1	19.6	11.2	23.8
$x_{WA,1}, m$	0.99	1.03	1.28	1.54
$T_{A,2}, s$	1.36	0.93	1.38	1.17
$F_{max,2}, N$	68.2	107.1	78.5	107.7
$F_{A,2}, N$	44.6	67.1	51.1	69.0
$PI_{A,2}, W$	16.6	36.9	18.2	33.3
$x_{WA,2}, m$	0.96	1.11	1.34	1.56
$T_{A,3}, s$	0.96	0.78	1.25	1.00
$F_{max,3}, N$	64.6	83.0	64.0	91.7
$F_{A,3}, N$	41.2	52.5	38.0	60.2
$PI_{A,3}, W$	16.9	33.6	15.3	35.5
$x_{WA,3}, m$	0.99	1.11	1.33	1.61
$T_{A,4}, s$	1.01	0.76	1.28	0.90
$F_{max,4}, N$	51.4	64.3	66.8	93.0
$F_{A,4}, N$	33.6	38.3	36.0	53.5
$PI_{A,4}, W$	13.6	26.0	15.1	41.3
$x_{WA,4}, m$	1.01	1.18	1.38	1.63

During the steady-state phase, the wheelchair speed, $\dot{x}_W$ oscillates around the average value $\dot{x}_{W,avg}$, as shown in Figure 3.12, and the peaks of force are almost constant for each set. In Table 3.3 are reported the average value of all three subject of the variables in the steady-state phase. It is interesting to note the amplitude of

the average power, PI_{avg}. In Sets 1 and 3, the average speed was about 1 and 1.16 m/s, respectively, which correspond to 3.6 km/h and 4 km/h, and the average power was about 10 W. In Sets 2 and 4 the wheelchair speed was respectively 5.5 km/h and 6.5 km/h and the average power was about 14 W and 20 W, respectively. Comparing the forces, F_A and F_{max}, of the steady-state phase with the forces of the first cycle, the forces in the first cycle are from 60% to 95% higher than the forces in the steady state phase. In particular, the percentage is higher in Sets 2 and 4, namely when the intensity is higher. Another interesting aspect concerns the cycle times T_A, T_R and T. The recovery time T_R is almost constant in the range between 0.88 s and 0.95 s. It means that in the recovery phase and in these conditions of external load, the kinematic of the motion of the user is always almost similar. On the contrary, the active time T_A is very different since it ranges between 0.82 s and 1.27 s and it depends on the external load and from the radius of the return pulley.

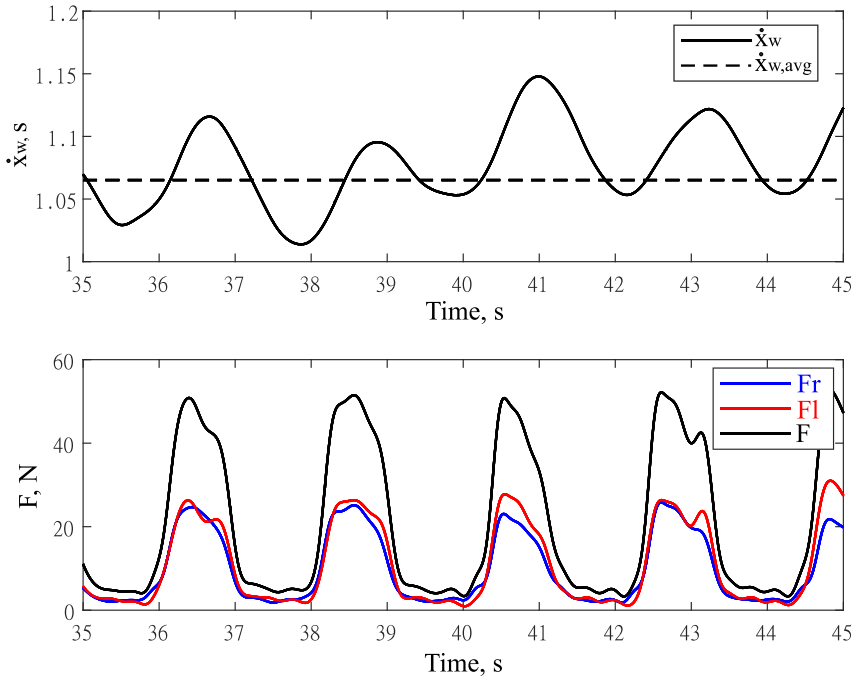

Figure 3.13: User's Force and wheelchair speed in the steady-state phase

The Figure 3.14 shows the overlap of forces, in grey, of the cycles in the steady-state phase for a single subject. In particular, the data reported in Figure 3.14 refer to the Set 2. The Figure shows as the maximum peak of force in the acceleration phase is about 92 N and the minimum peak of force is about 65 N. The time of the active phase is about between 0.95 and 1.2 s. The black curve is determined as the

instantaneous mean of all normalized cycles, named instantaneous normalized mean, as described in detail as follow. All cycles have been normalized respect the time, then for each instant has been determined the mean value. In Figure 3.14 are not reported the normalized cycles but the real cycles and the mean normalized has been scaled respect the time by multiplying the average value $T_{A,avg}$, named instantaneous mean, in order to highlight the difference of the cycle time for each cycle. The peak and the active time of the black curve are not the average value of $F_{max,avg}$ reported in Table 3.3

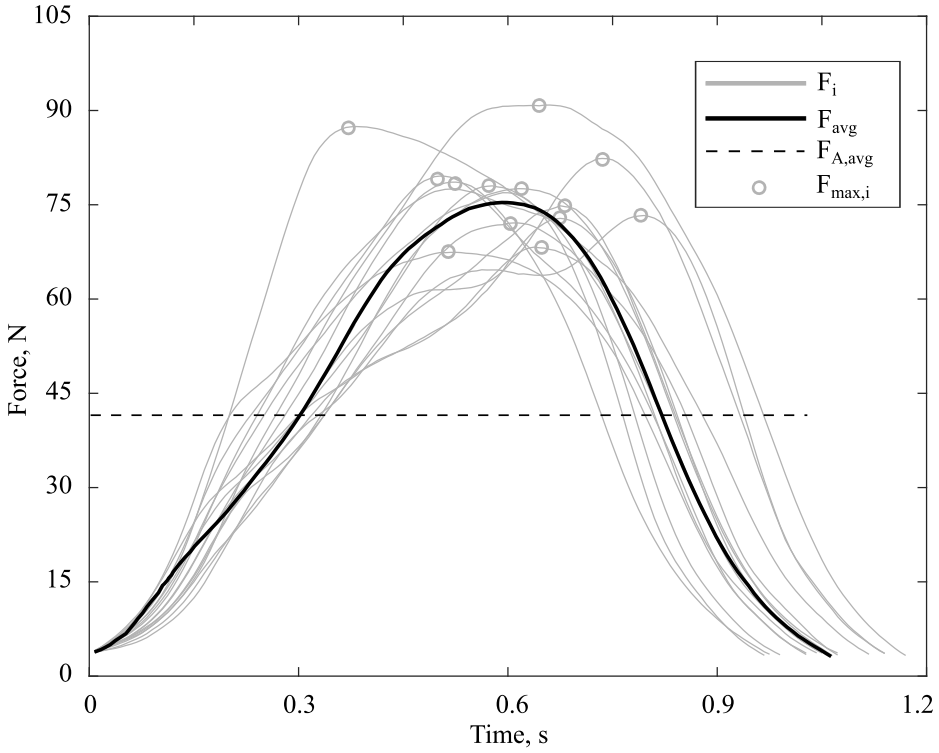

Figure 3.14: Overlap of the curves of force in grey and the instantaneous mean in black

For each Set, the instantaneous mean of the normalized cycles has been reported for all three subjects. In addition, the average value $F_{A,avg}$ is reported.

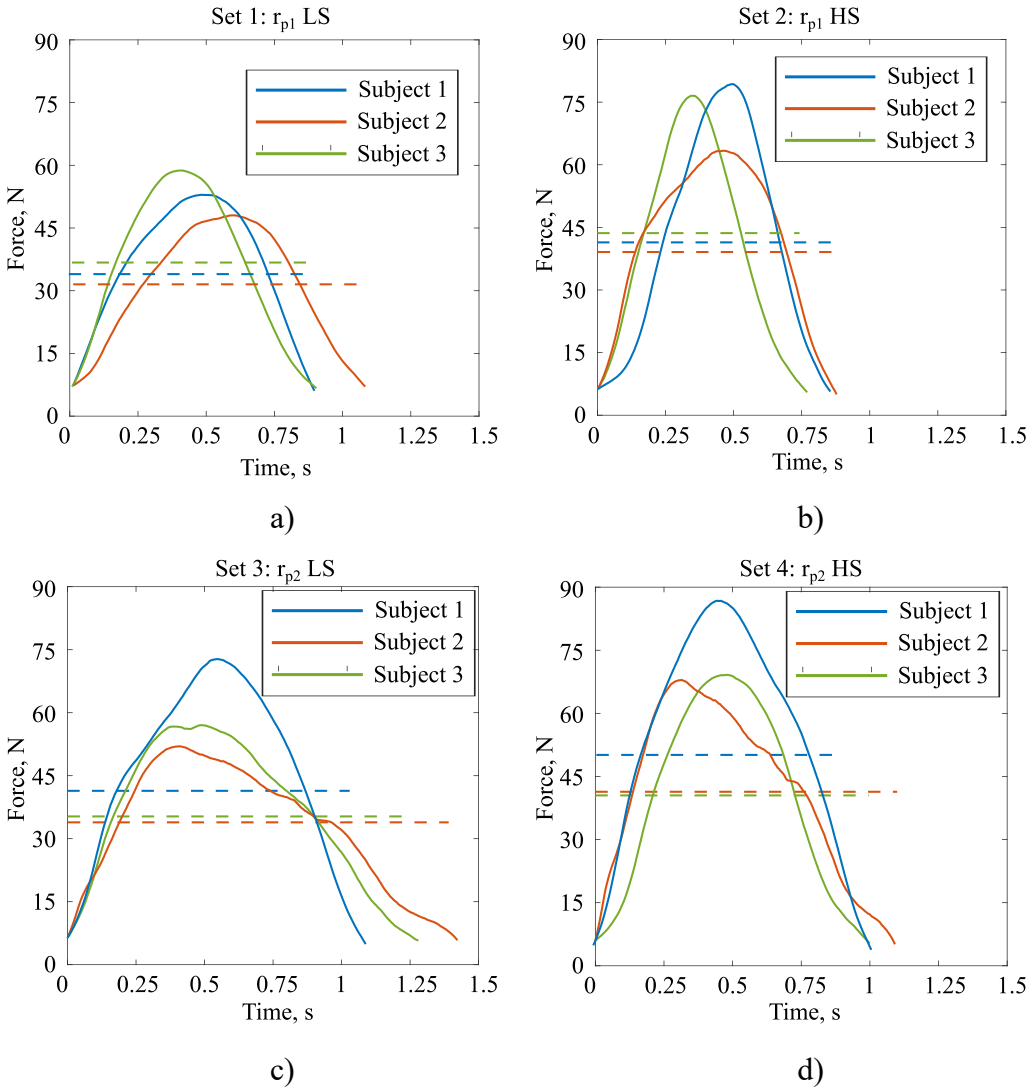

Figure 3.15: Instantaneous mean of force for all subject for different set

Table 3.3: Variables in the steady-state phase, Test 1

Variables	**Set 1: r_{p1}**	**Set 2:**	**Set 3:**	**Set 4:**
$T_{A,avg}, s$	0.97	0.82	1.27	1.01
$T_{R,avg}, s$	0.91	0.92	0.95	0.88
T_{avg}, s	1.88	1.74	2.22	1.89
$x_{WA,avg}, m$	0.97	1.18	1.41	1.64

$x_{UA,avg}, m$	0.43	0.52	0.52	0.60
$\dot{x}_{W,avg}, m/s$	1.04	1.54	1.16	1.75
$F_{A,avg}, N$	33.2	42.7	37.3	44.4
$F_{max,avg}, N$	51.7r	72.6	59.3	73.3
PI_{avg}, W	8.5	14.3	11.5	19.9
$PI_{A,avg}, W$	15.2	27.8	18.8	32.8
EI_{avg}, J	14.8	22.8	24.0	32.9

The index *POF*, previously defined by eq. 3.9, is an index that evaluates the instantaneous force *F* with the average force of the cycle *i-th* in the active phase $F_{A,i}$. It is also interesting to monitor the maximum value of the index *POF* in order to evaluate different systems of propulsion. Based on this consideration, it is possible to evaluate simply the index *POF* as the ratio of the average maximum force $F_{max,avg}$ and the average force in the active phase $F_{A,avg}$ as in the eq. 3.10

$$POF_{avg} = \frac{F_{max,avg}}{F_{A,avg}} \tag{3.10}$$

In the steady-state phase, the index for Sets 1, 2, 3 and 4 is respectively equal to: 1.69, 1.70, 1.58 and 1.65. It means that for this system of propulsion, in these conditions of external load, the peak values are about 60-70% larger than the average force in the active phases. This data can be compared with different systems of propulsion, namely handrims and handbikes.

In Figure 3.16, the longitudinal acceleration data of the wheelchair, calculated in different ways are shown. The blue line represents the longitudinal acceleration calculated from the hall sensors data of by numerical deriving two times the position. The red line represents the longitudinal acceleration measured by the Inertial Measurement Units, IMU, fixed on the wheelchair frame. The comparison of these data has an important goal, namely, to check the same variable measured with different technologies. In addition, the IMU can be used to evaluate the lateral and vertical accelerations. The vertical acceleration can be an interesting parameter to analyze the comfort of the user.

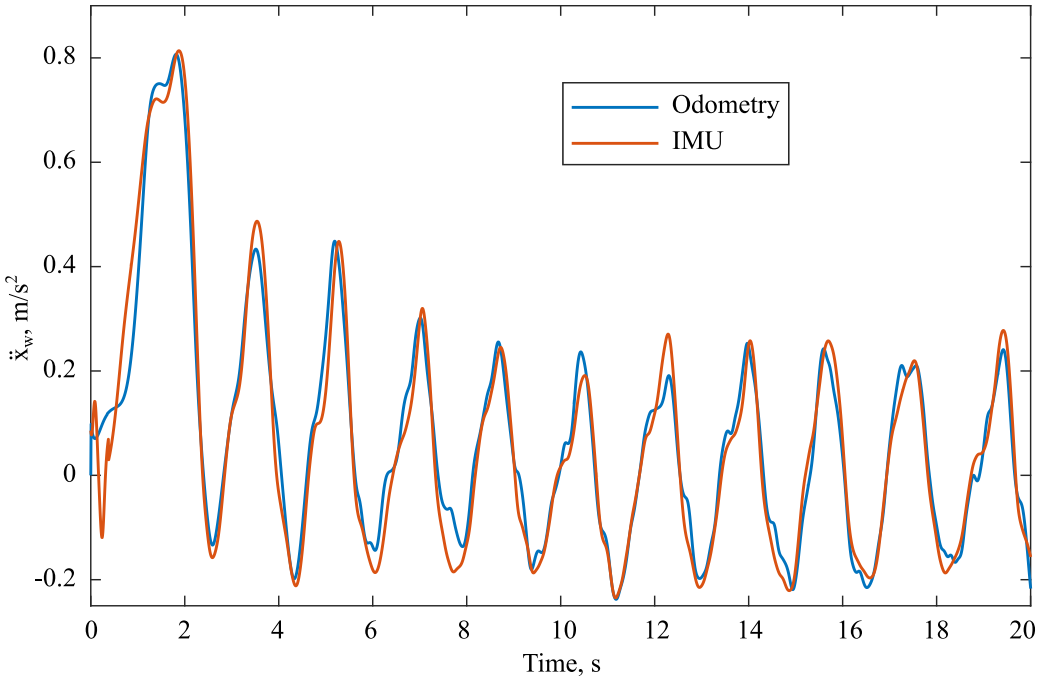

Figure 3.16: Longitudinal acceleration of the wheelchair computed from odometry, in blue, and measured by IMU

3.2.3 Discussions

The aim of this test was to analyse the propulsion force of a manual wheelchair with an innovative system of propulsion, Handwheelchair.q. The force and the wheelchair speed were monitored during the acceleration and steady-state phases of an experimental campaign. The test showed that the force magnitude depends on the wheelchair speed, external load condition, and pulley radius. The input power was obtained by the wheels angular speed and the user applied forces. Future studies should focus on comparing the efficiency in the same test conditions of different manual wheelchair drive systems, such as lever systems, handbikes, and handrims.

For equal or similar wheelchair speeds, the larger pulley radius reduced the average and the maximum force, which is a significative outcome to reduce the stress on the upper limb. A variable transmission ratio could be implemented on the proposed wheelchair in order to reduce the peak of force during the acceleration phase. F_{max} remains a fundamental parameter in order to evaluate a manual wheelchair, in addition, the direction of the force is relevant because it defines whether the shoulder and elbow joints are compressed or in traction.

3.3 Test 2: Roller bench

In this test, the Handwheelchair.q was tested on a test roller bench in order to evaluate the effect of the cadence of the motion. The Figure 3.17 shows the wheelchair on the test roller bench. The rear wheels are positioned on a couple of rollers and the front wheels is supported by the frame that enables to do not modify the longitudinal inclination of the wheelchair. The goal of this test is to evaluate the effect of the cadence, based on the external load, in order to optimize the efficiency and to reduce the dangerous peaks of force. The friction and inertia data of the roller bench are unknown.

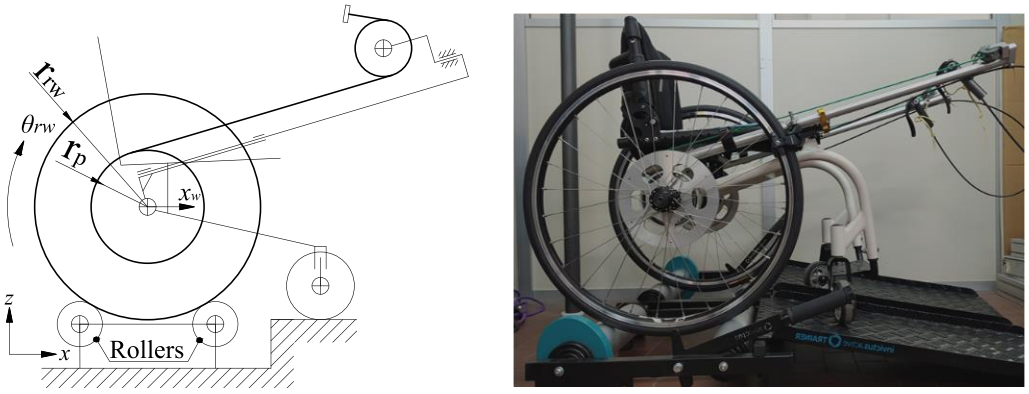

a) b)

Figure 3.17: Functional sketch of the Handhweelchair.q on the test roller bench a) and prototype b)

3.3.1 Methods

One able-bodied non-wheelchairs user (29 years old, 170 cm, 65 kg) participated in the experiment. This experimental test was a preliminary analysis hence nobody else was involved. The experimental tests consisted of propelling from standing start Handwheelchair.q on a test roller bench for 60 seconds at different cadence of the gesture. In addition, the user was asked to keep a constant amplitude of the propulsion gesture, namely the stroke. In order to facilitate this task, the cable has been marked with two markers distant 0.55 m. This distance was evaluated previously as an average value. There is not a mechanical stop in order to avoid possible peaks of force. The test was performed with two different pulley radii, r_{p1} = 130 mm and r_{p2} = 108 mm. For each radius six runs were performed, each run

with for a minute, the first run was performed with a cadence of the gesture of 30 rpm, the second at 35 rpm and then the cadence was increased by 5 rpm every run, concluding with the *six-th* run with a cadence of the gesture of 55 rpm. The amplitude of the stroke was kept constants for all tests. The data acquired have been elaborated as described in the paragraph 3.1.

3.3.2 Results

In Figure 3.18, the mean displacement of the wheelchair in the active phase is shown, each line represents the mean displacement at different cadence of gesture. As expected, the mean displacement with the pulley with the smallest radius is higher than the mean displacement obtained with the other pulley. The average value of the mean displacement with the pulley with radius equal to 108 mm is $x_{W,avg}=1.48$ m, while the mean displacement with the pulley radius of 130 mm is $x_{W,avg}=1.28$ m. The mean displacements correspond respectively to a stroke of the user equal to $x_{u,avg}=0.54$ and $x_{u,avg}=0.56$, respectively. In the six runs with the r_{p1} pulley radius, the mean displacement increases increasing the cadence of the gesture, from 1.18 m to 1.40 m while with the pulley rp2 the mean displacement is from 1.42 m to 1.55 m. In the curves of the Figure 3.18, it is noted that the curves at minor cadence, in the initial phase they have a smaller inclination and then the inclination increases. The reason of this characteristics is a consequence of the speed that the run at low cadence at the beginning of each phase the speed is very low, as shown in Figure 3.19.

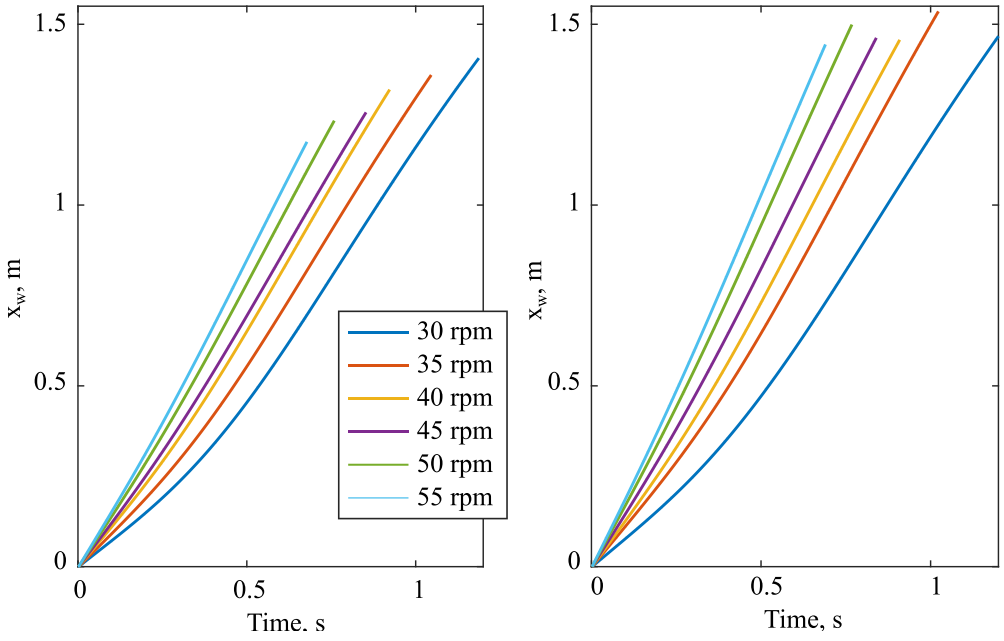

Figure 3.18: Mean of wheelchair displacement with a) r_{p1} = 130 mm and b) r_{p2} = 108 mm

The Figure 3.19 shows the mean of the wheelchair speed. As expected, the mean wheelchair speed increases with increasing the frequency and it increases when the pulley radius decrease. The second important aspect is that increasing the cadence, the difference of maximum and minimum speed, $\Delta\dot{x}_w$ decreases, in other word, the mean wheelchair acceleration decrease increasing the cadence, as will be shown examining the acceleration. The last particular characteristics is that at the end of the active phase the wheelchair speed decreases. These characteristics depend on the external load.

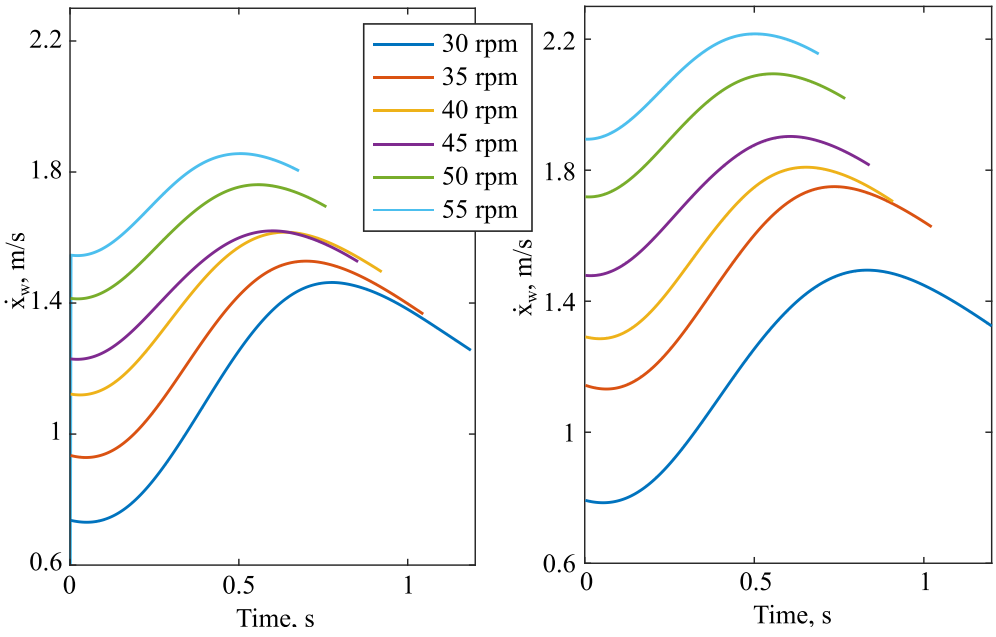

Figure 3.19: Mean of wheelchair speed with a) rp1 = 130 mm and b) rp2 = 108 mm

In Figure 3.20 the mean of the longitudinal acceleration of the wheelchair is reported. The general trend shows as increasing the frequency the mean longitudinal acceleration decreases. In general, the maximum efficiency of a mechanical system is when speed is constant, therefore, based on this consideration, it is important to reduce the mean longitudinal acceleration. The mean accelerations do not depend strongly on the pulley radius, with this condition of external load, with the exception of the frequency of 30 rpm.

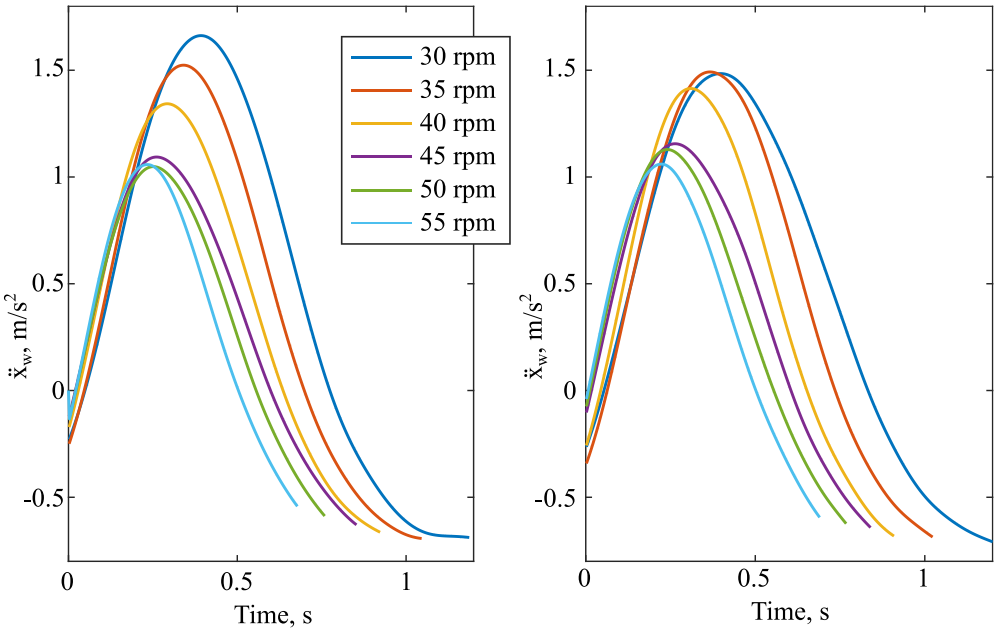

Figure 3.20: Mean of the longitudinal acceleration with a) r_{p1} = 130 mm and b) r_{p2} = 108 mm

In Figure 3.21, the mean of the total force, the sum of right and left force, applied to the cable by the user is shown. As expected, the mean forces with the smaller radius, b), are higher. The influence of the cadence is minimal, since the user exerts almost the same force for every run. Yet, the cadence seems to have a more significant effect on the duration of the period when the mean force is applied, in particular when the larger pulley was used.

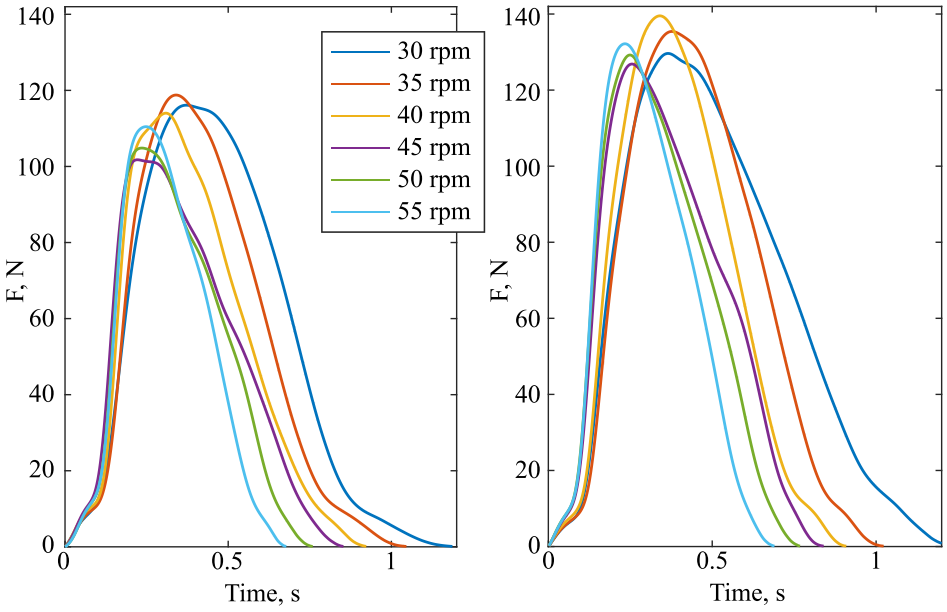

Figure 3.21: Mean of total force with a) r_{p1} = 130 mm and b) r_{p2} = 108 mm

In Figure 3.22, the mean input power is shown.

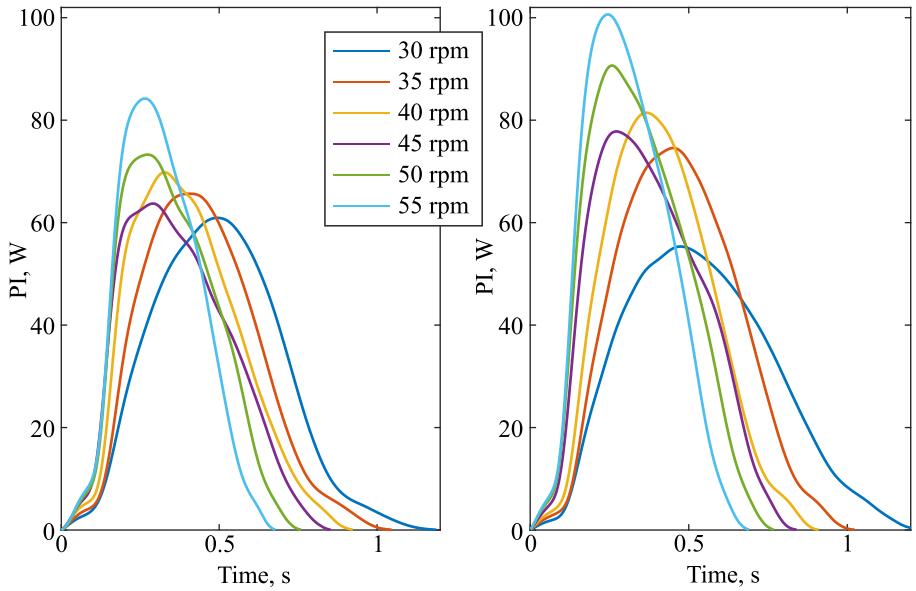

Figure 3.22: Mean of input power with a) r_{p1} = 130 mm and b) r_{p2} = 108 mm

As expected, the user power in the runs with the larger radius, a), are lower. The influence of the cadence shows that the intuitive result that, overall, the user has to generate an increasing amount of power to achieve a faster cadence.

In Table 3.3, the average value in the active phase of the speed, $\dot{x}_{W,avg}$, force, $F_{A,avg}$, input power, $PI_{A,avg}$, and energy, EI_{avg}, are reported. The average speed and the average power increase with increasing the frequency for both the pulley radii, as expected. The trend of the average force, F_A, is independent from the cadence. The results about the energy are variable with respect to the cadence. The results with the r_{p1} = 130 mm the energy decrease increasing the cadence, but the results obtained with the radius r_{p2}, = 108 is independent from the cadence.

Table 3.4: Variables, Test 2

r_p,	Cadence,	$\dot{x}_{W,avg}, m/s$	$F_{A,avg}, N$	$PI_{A,avg}, W$	EI_{avg}, J
130	**30**	1.18	54.4	27.9	31.2
	35	1.29	53.2	30.4	30.2
	40	1.42	52.8	33.2	29.7
	45	1.46	50.9	33.4	27.4
	50	1.61	52.0	37.7	27.6
	55	1.71	52.4	40.7	26.8
108	**30**	1.22	62.6	27.8	33.1
	35	1.49	65.9	36.5	36
	40	1.59	65.6	38.8	34.2
	45	1.73	65.0	41.8	33.9
	50	1.94	64.9	46.9	35.0
	55	2.08	64.6	50.2	33.5

3.3.3 Indices analysis

The index *POF*, defined by eq. (3.9), evaluates the magnitude of the force compared with the average value of force in the active phase. In Figure 3.23, the mean index *POF* of this test is reported. The Figure shows that the index *POF* was not influenced by the pulley radius and the cadence in this condition of external load.

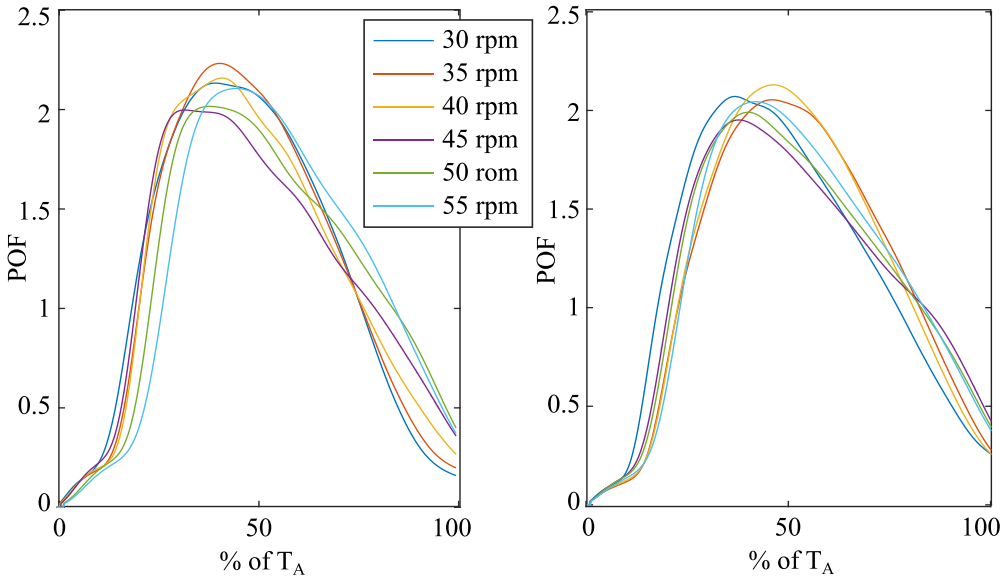

a) b)

Figure 3.23: Mean index POF, Peak of Force.

The *FEF* index was defined for the handrim system as the ratio between the tangential force that represents the useful force and the total force that the user applied on the handrim, sum of lateral, normal and tangential force. The *FEF* index can be adapted for the pulley cable system considering the ratio of the useful force and the total force. The total force is the tension of the cable measured by the load cell. The useful force is calculated as the total force minus the return force generated by the power spring, reported in Figure 3.24. The mean index *FEF* increases at the beginning, and it reaches the maximum value of 80%-90% at the 10%-20% of T_A. Then it decreases to about 70% when around 80% of T_A and then it keep decreasing. Compared to conventional handrim wheelchairs and handbike, the *FEF* index of the proposed architecture is different, as shown in the literature [56], [89]–[94], both in magnitude and for the trend.

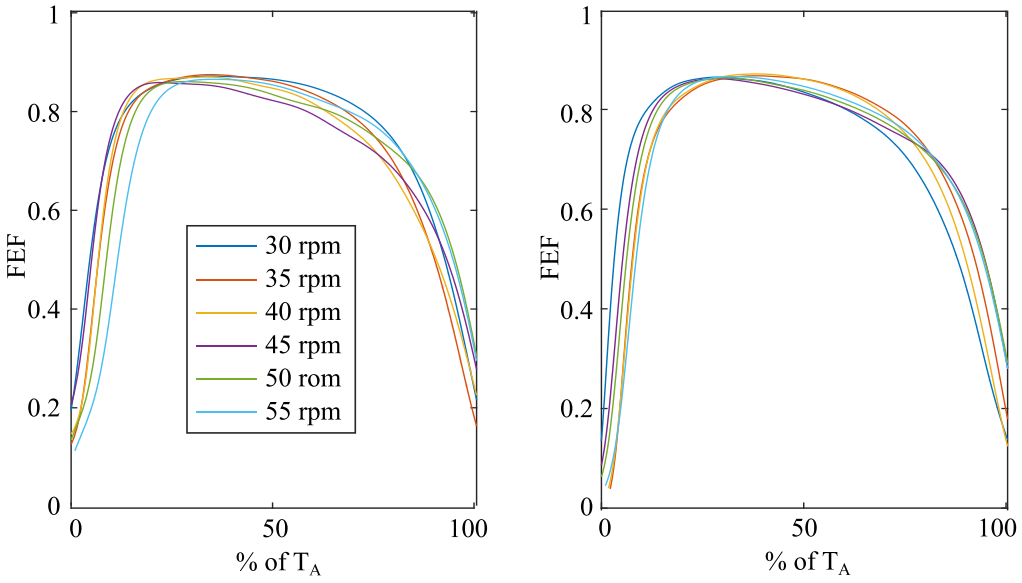

Figure 3.24: Mean index *FEF*

3.3.4 Discussion

The prototype was tested on a roller test bench. In the test, the influence of the cadence of the gesture and the pulley radii on the kinematic and dynamic of the wheelchair has been presented. In addition, the new index POF and the index FEF have been calculated and the index FEF was compared for a different system of propulsion, namely a conventional handrim wheelchair. The influence of the cadence in this condition of external load is variable across the results. This test can be adopted for sport use. In addition, monitoring the output power, for example by sensorising the roller bench, it is possible to evaluate the efficiency of the wheelchair related to the cadence and pulley radii. It will be interesting to have an active test bench in order to modify the condition of the external load.

3.4 Test 3: Different front wheel devices

In this test, Handwheelchair.Q was tested in three different front wheel configurations. The goal of this test was to evaluate the efficiency of the prototype with different front wheel designs. If the efficiency of these configurations are similar, the second fundamental step is to have the prototype tested by wheelchair users in order to evaluate manoeuvrability, stability, ergonomy and in general the subjective perception of different configurations knowing their efficiency.

In the first configuration, Figure 3.25a-b, named “Standard”, the wheelchair was provided with two pivoting wheels with a small radius. In the second and the third configuration, Figure 3.25c-d and 3.25e-f respectively, the wheelchair was provided with two different commercial pivoting wheels, named respectively “Freewheel” and “Easywheel”. Both commercial pivoting wheels have a radius larger than the pivoting wheels of the Standard configuration as reported in Table 3.4.

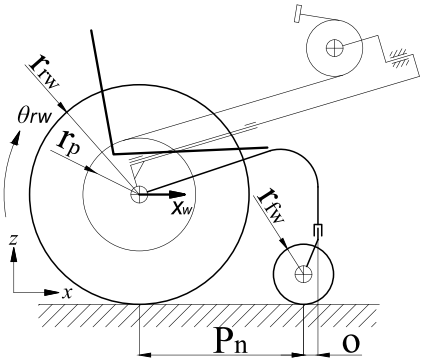

a)

b)

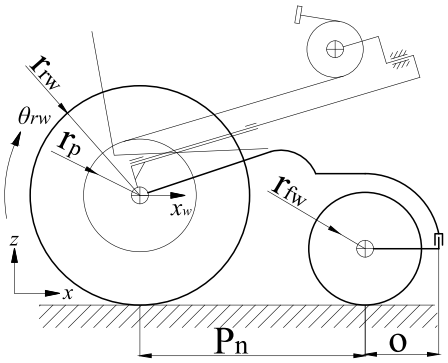

c)

d)

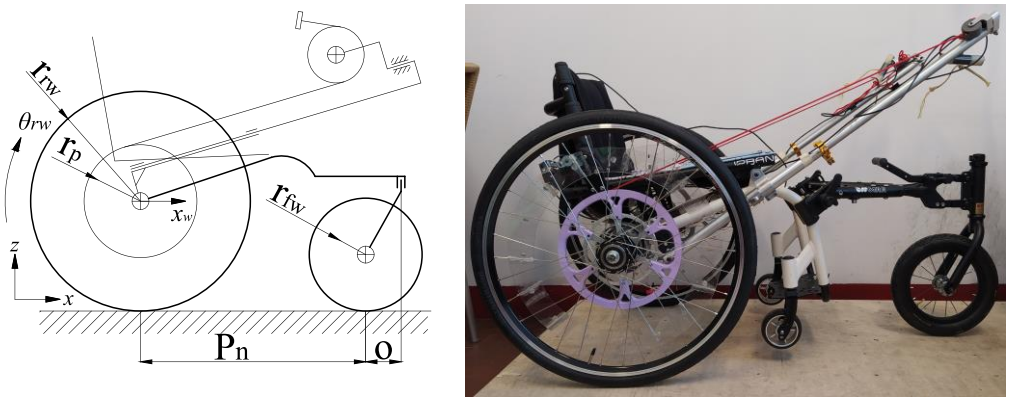

e) f)

Figure 3.25: Standard configuration a) functional sketch and b) prototype, Freewheel configuration c) functional sketch and d) prototype and Easywheel configuration e) functional sketch and f) prototype

Table 3.5: Parameters of the wheelchair with different front wheel devices

Configuration	Mass, kg	r_{Fw}, m	*Pn*, m	*o*, m
Standard	15.5	0.045	0.4	0.035
Easywheel	19.0	0.145	0.84	0.08
Freewheel	17.5	0.155	0.72	0.18

The main technological differences concern the nominal wheelbase, *Pn*, the offset, *o*, the front wheel radius and the weight. The nominal wheelbase has an influence on the distribution of the normal forces on the ground. The offset mainly influences the manoeuvrability during turns. The front wheel radius affects the comfort of the user.

3.4.1 Methods

One able-bodied non-wheelchairs user (29 years old, 170 cm, 65 kg) participated in the experiment. This experimental test was a preliminary analysis about the efficiency of a manual wheelchair, hence nobody else was involved. The limitation of having just one able-bodied male user is clear, however, each test was repeated ten times in order to obtain more fair results. The experimental tests consisted of propelling from standing start Handwheelchair.q on a flat hallway covered with

smooth flooring. The user was asked to drive the wheelchair at approximately 1 m/s, and to do so the user was able to check the wheelchair speed in real-time with a speedometer. To test each configuration, three sets, one per front wheel, of 10 runs each were done. The radius of the return pulley employed in this test is $r_p = 108\ mm$. The acquired data have been elaborated as described in paragraph 3.1.

3.4.2 Results

In table 3.6 the complete results of the test have been reported. In absolute terms, it is not possible to compare the three solutions because there is not a constant term for example: speed, force or power. However, the 4th run of the standard configuration, the 7th run of the Easywheel configuration, and the 4th run of the Freewheel configuration were done at exact the same speed of 1.03 m/s, it can be interesting to compare these 3 runs, reported in table 3.7.

Table 3.6: Variables, Test 3

Symbols	Standard	Easywheel	Freewheel
$T_{A,avg}, s$	1.51	1.39	1.47
$T_{R,avg}, s$	0.77	0.83	0.83
T_{avg}, s	2,28	2,22	2,30
$\dot{x}_{W,avg}, m/s$	1.02	1.09	0.98
$F_{A,avg}, N$	43.7	41.2	42.4
PI_{avg}, W	11.1	10.2	9.8
$PI_{A,avg}, W$	16.4	16.6	15.3
EI_{avg}, W	25.3	22.7	22.5
$\Delta\dot{x}_{w,avg}, m/s$	0.033	0.027	0.030

Table 3.7: Variables at the same speed, Test 3

Symbols	Standard	Easywheel	Freewheel
$T_{A,avg}, s$	1.48	1.46	1.41
$T_{R,avg}, s$	0.76	0.87	0.83
T_{avg}, s	2.24	2.33	2.24
$\dot{x}_{W,avg}, m/s$	1.03	1.03	1.03
$F_{A,avg}, N$	44.75	40.62	42.82
PI_{avg}, W	11.22	9.72	10.28
$PI_{A,avg}, W$	16.97	15.52	16.31
EI_{avg}, W	25.14	22.60	23.02
$\Delta\dot{x}_{w,avg}, m$	0.037	0.025	0.027

In terms of speed and input power, the Easywheel configuration seems to be the best in the specific conditions of the test even if it is the heaviest configuration. The percentage difference of the best and the worst configuration in terms of the average input power, $PI_{A,avg}$, and the average force in the active phase, $F_{A,avg}$, are both about 10%. Considering instead the difference of maximum and minimum wheelchair speed for each cycle, $\Delta\dot{x}_w$, and then the average value $\Delta\dot{x}_{w,avg}$, it is interesting to note that this parameter is higher in the standard configuration. Probably this result is due to two reasons: a) the standard configuration is the lightest which means the inertia effect is reduced and b) the two front wheels have low efficiency.

3.4.2 Discussion

This preliminary test has compared the efficiency of the prototype Handwheelchair.Q in three different configurations. The inertia effect and the rolling friction of the front wheel affect the global efficiency of the wheelchair. In addition, is important to point out that the technological characteristics of the front wheels have an important role in terms of efficiency of the wheelchair. Another important effect concerns the distribution of the normal force on the ground as shown in the literature [The effect of caster types on global rolling resistance in manual wheelchairs on indoor and outdoor surfaces, The effect of caster wheel diameter and mass distribution on drag forces in manual wheelchairs].

This work represents the preliminary test of a wide experimental campaign that will be executed in the future, where many aspects will be considered. First of all, the front wheels represent just one specific configuration, but other parameters can be varied to evaluate their effects, such as the position of the return pulley, the radius of the pulley that defines the transmission ratio, and the position of the centre of mass of the user will be examined in detail among others. Secondly, specific tests will be carried out in order to optimise the efficiency of the transmission of motion and the biomechanical motion depending on the anthropometry characteristic of the user. A specific methodology will be defined in order to optimise the different parameters for each user. The above-mentioned aspects will be examined in different conditions as different speeds and terrains (asphalt, dirt road, cycle path, smooth surface, …) and depending on the use: sport, light physical or recreational activities, speed up moving in around the city etc. In conclusion, the tests will involve different subjects, especially people with disabilities.

3.5 Test 4: EMG

In this study, the neuromuscular demands and the degree of mobility provided by our innovative wheelchair is evaluated to specifically ask whether the pulley-cable propulsion system would lead to a more efficient movement when compared with the standard, handrim approach. Recent studies have reported a diminished excitation of the shoulder muscles when subjects were asked to reproduce the movement necessary to move a wheelchair using reverse propulsion [Electromyographic Activities of Shoulder Muscles during Forward and Reverse Manual Wheelchair Propulsion] and lever system [Shoulder Muscular Demand During Lever-Activated Vs Pushrim Wheelchair Propulsion In Persons With Spinal Cord Injury] approaches than when relying on the standard pushrim propulsion system. While these results are encouraging, the efficiency of the movement with these innovative systems remains an issue, at least in paraplegia. Movement efficiency was assessed in terms of speed and travelled distance and excitation of the shoulder muscles for both wheelchair propulsion systems. Given the pulley-cable propulsion demands the shoulder extension rather than flexion during the propulsion phase, a smaller or comparable degree of muscle excitation it is expected to be observed. Moreover, as the pulling propulsion is ensured by a pulley system, which radius is remarkably smaller than that of the wheel, individual movement cycles are expected to result in greater speeds and distances for the pulley-cable rather than the handrim propulsion system.

This test examined the hypothesis that subjects are able to move with less muscle effort on Handwheelchair.Q, than the traditional handrim wheelchair, handrim, through the surface electromyography. Eight muscles of the arm and shoulder were analysed propelling two different types of wheelchairs at two different speeds.

3.5.1 Methods

Seven able-bodied adults (six male) were recruited to participate in the study (range values; age: 24-40 yrs; height: 168-183 cm; body mass: 55-75 kg). None of the subjects reported any musculoskeletal disorders that could affect their upper limb movements at the occasion of experiments, which commenced after subjects provided written informed consent. Able-bodied subjects, inexpert on the use of wheelchairs, were chosen because otherwise it would be difficult to discriminate the effect of experience and wheelchair propulsion system on the degree of muscle excitation and performance. Subjects were first asked to practice on a wheelchair specifically designed to accommodate both pulley-cable and handrim propulsion systems, namely Handwheelchair.q. The familiarisation session lasted about 5 minutes and comprised practicing with both propulsion systems at variable speeds. After that, participants were asked to propel the wheelchair using the pulley-cable and the handrim systems, at low and high speeds, for a total of four trials. Each of these four trials lasted roughly 2 min, ensuring at least 30 movement cycles per trial. Low and high speeds were self-selected, according to the instruction given to subjects: to perform at a comfortable speed, as if they had to move around normally (low speed), and to perform twice as fast (high speed) as for the comfortable speed condition. Each trial was applied twice, providing a total of eight recordings. Trials were applied in random order, with rest periods of 2 min in-between. For all trials, Handwheelchair.q was positioned over the commercial roller test bench described in the paragraph 3.3. Figure 3.26 shows the experimental setup, and the position of bipolar electrodes, reflective markers, the Hall sensor and the 16 magnets, on the right side. The ten muscles assessed were Biceps Brachii (BB), Triceps Brachii (TB), Upper (UT) and Middle (MT, not shown) Trapezius, Pectoralis Major (PM), Infraspinatus (IS, not shown), Supraspinatus (SS, not shown) and Anterior (AP), Middle (MD) and Posterior (PD) Deltoid.

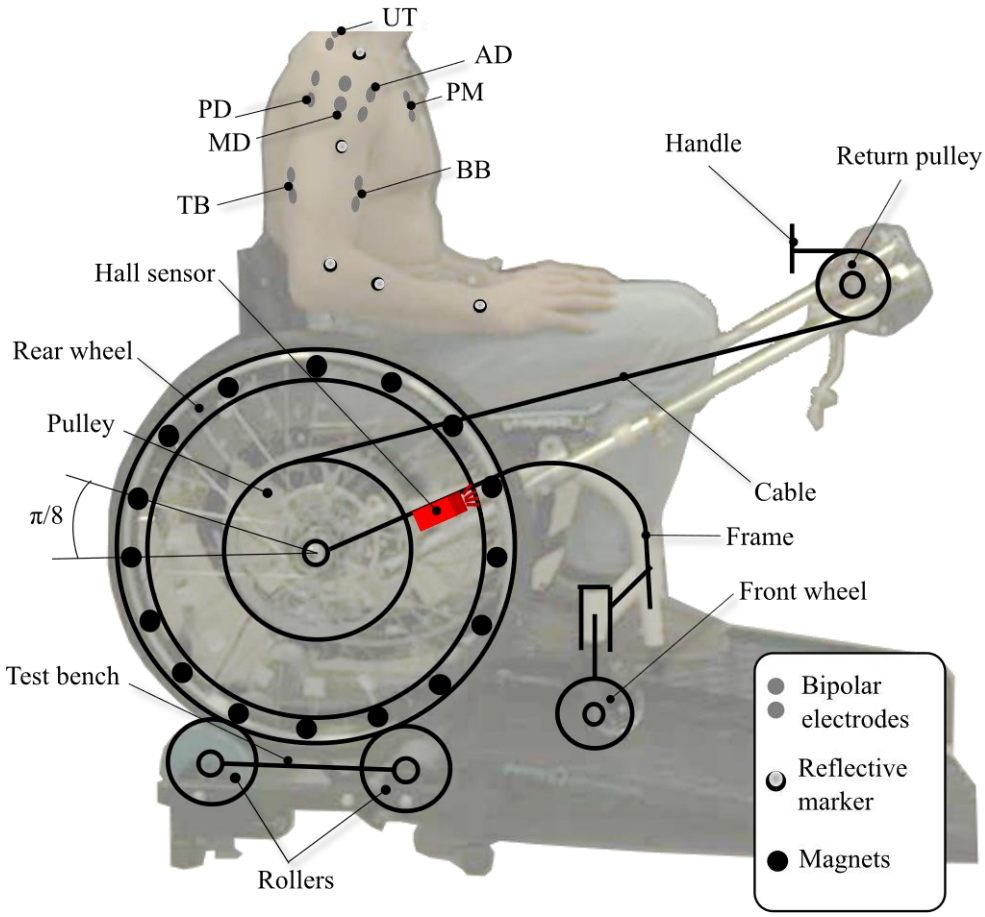

Figure 3.26: Illustrative example of the experimental setup, showing the position of bipolar electrodes, reflective markers, the Hall sensor and the 16 magnets, on the right side

Kinematics data were obtained after labelling a set of 17, reflective markers, which coordinates were captured by a 12 cameras VICON system (100 Hz, Vero v2.2, Vicon Motion System, Oxford, UK). Markers were positioned bilaterally in the upper limbs according to a modified version of the full-body, plug-in gait marker protocol (Nexus Plug-in Gait marker set, Oxford Metrics, Oxford, UK), so as to model only the trunk, arm and forearm segments. After sampling (100 Hz) and labelling the coordinates of each marker, Cardan angles were computed for the shoulder and elbow joints using the Nexus software (Nexus 2.11 software, Vicon Motion System, Oxford, UK).

Pairs of circular surface electrodes (24 mm diameter with roughly 30 mm center-to-center distance, Spes Medica, Battipaglia, Italy) were used to collect

surface electromyograms (EMGs) from ten muscles in the dominant side: anterior deltoid (AD), middle deltoid (MD), posterior deltoid (PD), middle trapezius (MT), upper trapezius (UT), infraspinatus (IS), supraspinatus (SS), pectoralis major, biceps brachii (BB) long head and triceps brachii (TB) lateral head. The selected muscles are either prime movers or stabilisers of the shoulder [16,17] and represent an extended set in relation to that considered in previous studies comparing different wheelchair propulsions [32], [33]. After carefully shaving and cleaning the skin with abrasive paste, surface electrodes were positioned on the skin surface over the muscles of interest, as shown in Figure 3.26. Pairs were centred at locations recommended by SENIAM [95], except for infraspinatus and supraspinatus, for which the positioning procedure was as described by [96]. Bipolar EMGs were recorded with a wireless system (200 V/V gain; 10–500 Hz bandwidth amplifier; DuePro system, OTBioelettronica and LISiN, Politecnico di Torino, Turin, Italy). EMGs were digitized at 1,000 Hz with a 16 bits A/D converter, synchronously with the sampling of markers' coordinates (Nexus 2.11 software, Vicon Motion System, Oxford, UK).In addition to biomechanical and physiological data, the kinematic of the wheelchair was assessed as described previously.

There is an important difference about the previously test. In this test the active and recovery phases were then identified based on instants when acceleration values crossed the 0-reference value, Figure 3.27. Crossings from negative to positive values denote a transition from recovery to active whereas crossings from positive to negative values indicate a transition from active to recovery. A single cycle was defined by consecutive instants corresponding to the transition from active to recovery. Once cycles were identified, the first five cycles were discarded to remove any transient effects associated with the commencement of the trial. The projected travelled distance and the average linear speed of the wheelchair have been further computed from the wheel velocity data.

The range of motion of the shoulder joint and the timing and degree of muscle excitation were computed separately for each cycle and subject. Range of motion values were defined as the maximal, flexion-extension excursion of the shoulder and elbow joints within cycles. The timing of muscle excitation was estimated as detailed in [Detection of onset and termination of muscle activity in surface electromyograms]. Briefly, after full-wave rectification, EMGs were low pass-filtered (2nd order Butterworth filter; 30 Hz cut-off) into their envelopes [97]. Then the baseline level has been computed as the mean plus three times the standard deviations of the EMG envelope during the first second of acquisition (rest). Within

each movement cycle, for each time sample, it has been computed how many out of the 200 (200 ms) preceding and the 200 succeeding samples did not and did respectively exceed the baseline level. The time sample providing the greatest count was deemed as the onset of muscle excitation [98]. The onset of silencing was defined using the same procedure, considering though the sum of preceding samples exceeding and succeeding samples not exceeding the baseline level. Onsets were identified separately for each muscle and cycle. Occasionally, multiple maxima and minima were observed in the counts, indicating multiple bursts of excitation were present. Whenever it occurred, the burst providing the greatest time-integrated envelope value was retained. In addition to the timing of muscle excitation, the duty cycle of muscle excitation has been computed, considering all bursts identified within cycles, together with the average amplitude of EMG envelopes, computed over samples for which the muscle was indeed excited. Subjects for which no onset values could be identified, because the muscle was either not excited or did not rest within cycles, a duty cycle of 100% or 0% was respectively assigned. Figure 3.23 shows the linear acceleration and velocity data for the wheelchair computed for both propulsion systems, on top. Periods of negative and positive acceleration respectively define the recovery and active phases. The middle panel shows elbow and shoulder joint angles in the parasagittal plane. Raw bipolar EMGs are shown in the bottom panel for the Posterior (PD) and Anterior (AD) Deltoid muscles. Periods within which the muscle was excited are indicated with horizontal, grey lines; only EMG bursts with the highest Root Mean Square (RMS) values within each cycle were considered for analysis.

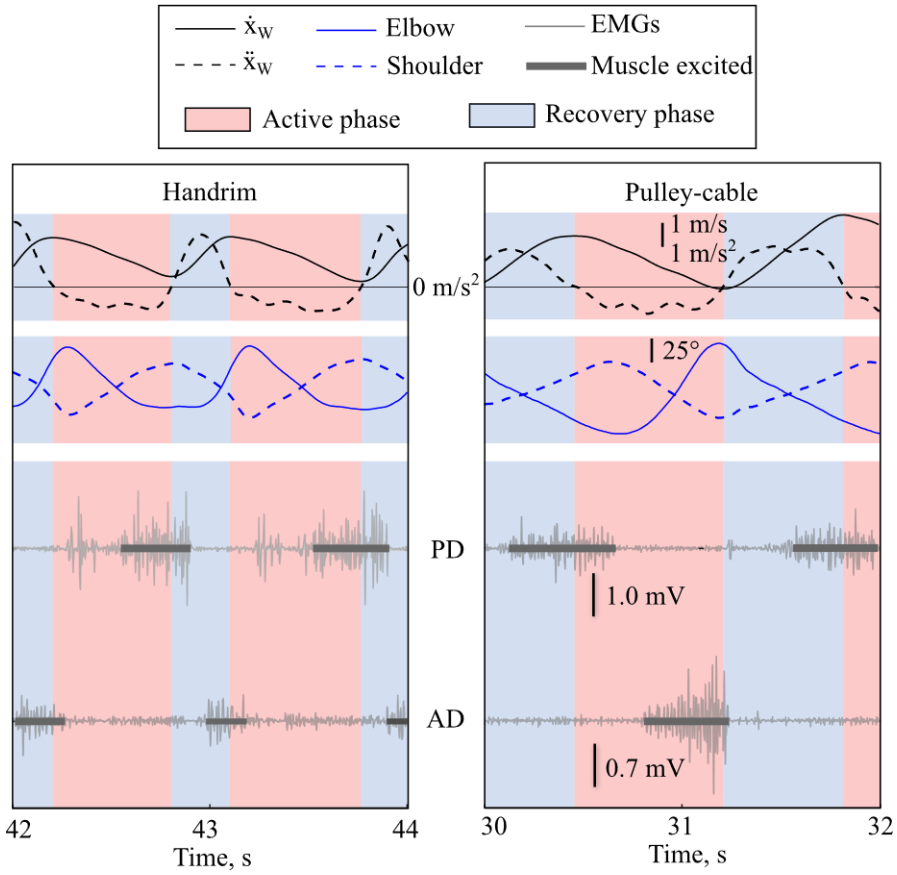

Figure 3.27: Wheelchair and joint kinematic data and surface electromyograms (EMGs) of PD and AD

Parametric, inferential statistics was used to assess the effect of test conditions on kinematic data, after ensuring their distribution was Gaussian (Shapiro-Wilk test, $p>0.15$) and the homogeneity of variances (Levene's test, $p>0.2$). Two-way ANOVA was applied to assess whether the propulsion system, taken as repeated measures and the movement speed affected the duration of cycles and their phases, the joint range of motion, and the chair speed and displacement. The assumption of equal variances for the different groups (propulsions and speeds) was not verified for muscle excitation data. Therefore, the Wilcoxon test was applied to assess the separate effect of propulsion and movement speed on the onset of muscle excitation and silencing, the duty cycle and the RMS amplitude, after applying Bonferroni correction to compensate for the inflation of type I error.

3.5.2 Results

Qualitative differences in wheelchair mobility, joint kinematics and muscle excitation can be appreciated for the representative data shown in Figure 3.27. The same time scale (2 s) was used to represent data for both propulsion systems, highlighting the shorter time taken to complete a cycle with the handrim than pulley-cable propulsion. During the active phase, elbow and shoulder moved in opposite directions, both for the handrim and pulley-cable propulsion systems, with the latter being associated with a roughly 20° greater elbow range of motion (cf. traces in Figure 3.23 middle panel). Excitation of posterior and anterior deltoid took place at different, relative instants of the movement cycle, with the former and latter being respectively elicited at recovery and drive for the handrim propulsion and vice-versa for the pulley-cable propulsion, Figure 3.27. As reported below, group results confirm the observations just made for a single subject.

Even though it was not possible to control the movement cadence in real time, subjects performed the tasks at a consistent cadence. For the two propulsion systems and the two movement speeds, the coefficient of variation of the duration of active and recovery phases did not exceed 8%. Similarly, the relative duration of active and recovery phases did not change with both the propulsion system (ANOVA $F<0.4$, $p>0.59$) and the movement speed ($F<4.2$, $p>0.07$; Figure 3.28, left side). The duration of cycles was however significantly greater for the pulley-cable system and the low, movement speed (ANOVA main effect, $F>7.4$, $p<0.02$).

Regardless of the propulsion system, the fast movement speed resulted in greater and faster, linear displacements of the wheelchair ($F>31.1$, $p<0.01$; Figure 3.28 right side, top). The pulley-cable propulsion led to wheelchair displacements roughly three times greater in relation to the handrim propulsion ($F=46.0$, $p<0.01$), even though no effect on the wheelchair speed was observed ($F=2.8$, $p=0.12$).

When considering joint kinematics, the pulley-cable propulsion demanded a greater range of elbow ($F=12.0$, $p<0.01$) though not shoulder (ANOVA $F=0.3$, $p=0.62$) flexion-extension (Figure 3.24 right side, down). No effect was observed for movement speed (ANOVA $F<0.5$, $p>0.47$).

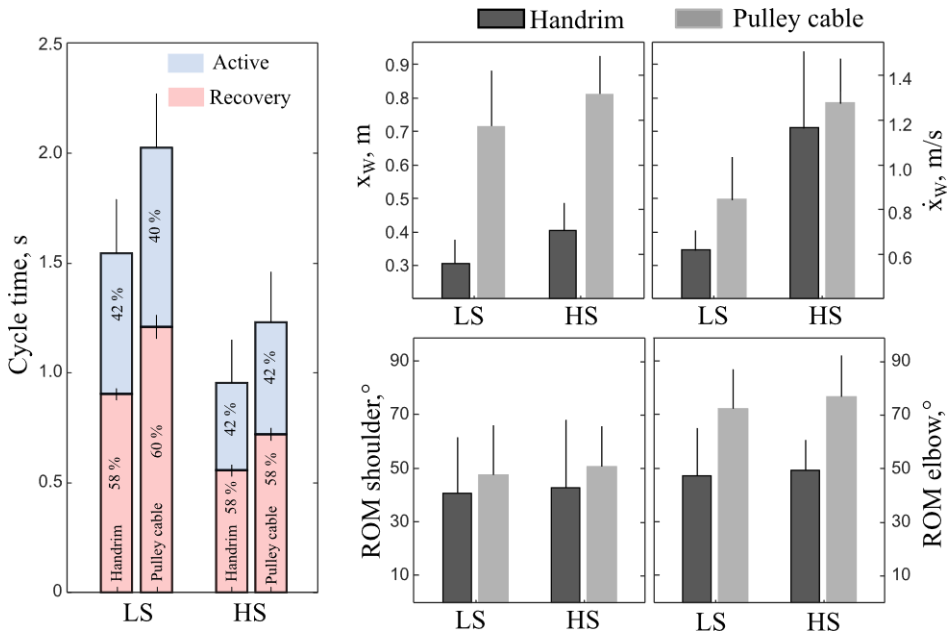

Figure 3.28: Mean (bars) and standard deviation (whiskers) values are shown for the duration of movement cycles, left side. The displacement and the velocity of the wheelchair, top, right side. Range of shoulder and elbow motion in the parasagittal plane, down, right side.

For both movement speeds, the onset of muscle excitation and silencing depended on the propulsion system. Except for the anterior deltoid, which was excited and silenced at roughly mid drive and early recovery respectively, muscles were excited early in recovery and silenced at mid drive for the handrim propulsion (Figure 3.29). The opposite was observed for the pulley-cable propulsion, resulting in significantly different onset values for all muscles represented (Figure 3.29; Wilcoxon paired test; Onset excitation: $p<0.035$; Onset silencing: $p<0.045$; henceforth all p values are reported after Bonferroni correction for multiple comparisons). Results for pectoralis major and upper trapezius were not presented because onsets could not be computed for all subjects, as EMG amplitude did not exceed the baseline for the former (0% duty cycle) and was always greater than the baseline for the latter (100% duty cycle).

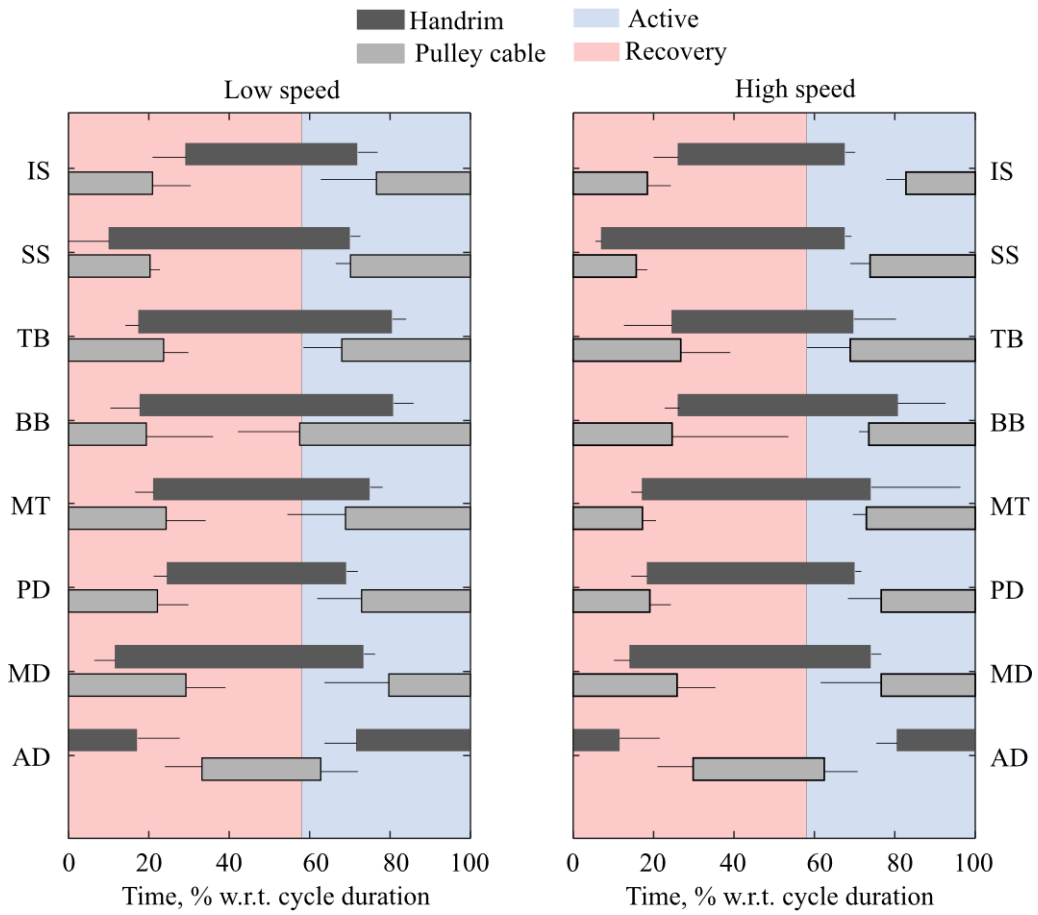

Figure 3.29: Mean (bars) and standard deviation (whiskers) values are shown for the onset of muscle excitation and silencing.

Movement speed did not affect the duty cycle for all muscles tested (Wilcoxon paired test; p>0.22). With respect to the propulsion system, pulley-cable propulsion resulted in greater duty cycles for posterior deltoid and supraspinatus and smaller duty cycles for pectoralis major (Figure 3.30; $p<0.04$). Regarding the RMS amplitude of EMGs, movement speed affected eight out of the ten muscles tested, with faster movements leading to greater amplitude values (Wilcoxon paired test; $p<0.04$). The effect of the propulsion system was variable across muscles, with the pulley-cable propulsion leading to smaller RMS values for middle trapezius, supraspinatus and middle and posterior deltoid (Wilcoxon paired test; $p<0.05$) and greater amplitude values for anterior deltoid, upper trapezius, biceps brachii and infraspinatus (Wilcoxon paired test; $p<0.04$).

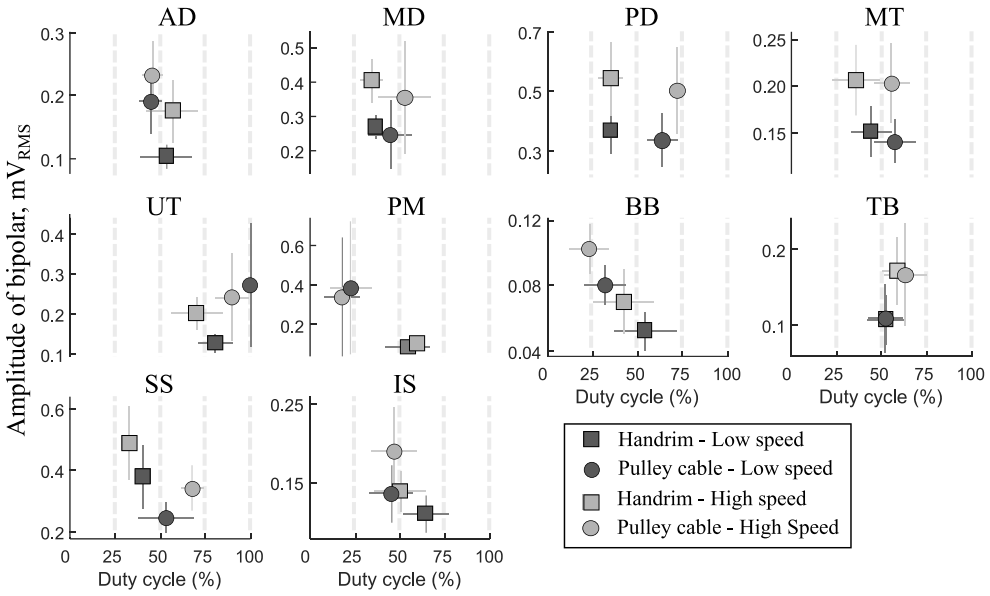

Figure 3.30: Mean and standard deviation (whiskers) values are shown for the RMS amplitude of surface EMGs (y axis) and the duty cycle (x axis), separately for each of the ten muscles assessed

The propulsion gesture is composed mainly by the flexion-extension of the shoulder and elbow joints, both for Handrim and Pulley cable system. In Figure 3.31, the flexion-extension of the shoulder joint for alle tests (low and high speed, Handrim and Pulley cable) and the flexion-extension of the elbow joint for all tests are reported. The figures 3.31 refer to the subject number one. The grey curves represent the angle normalized of each cycle and the black curve is the normalized mean of the angle. The vertical dashed grey line is the average ROM and the horizontal dashed black line is the average active time normalized.

In general, the ROM at high speed is greater than the ROM at low speed both for the Handrim and Pulley-cable system. In addition, the ROM of the Pulley-cable system is greater than the Handrim system. These results are in line with the results of the ROM in the parasagittal plane show in figure 3.28.

In the active phase, it is possible to note the difference between the Handrim and the Pulley-cable system of propulsion. In the Handrim motion, in the active phase, the gesture is composed of the shoulder flexion and elbow extension. In the Pulley-cable system the gesture is composed of the opposite motion namely the shoulder extension and the elbow flexion.

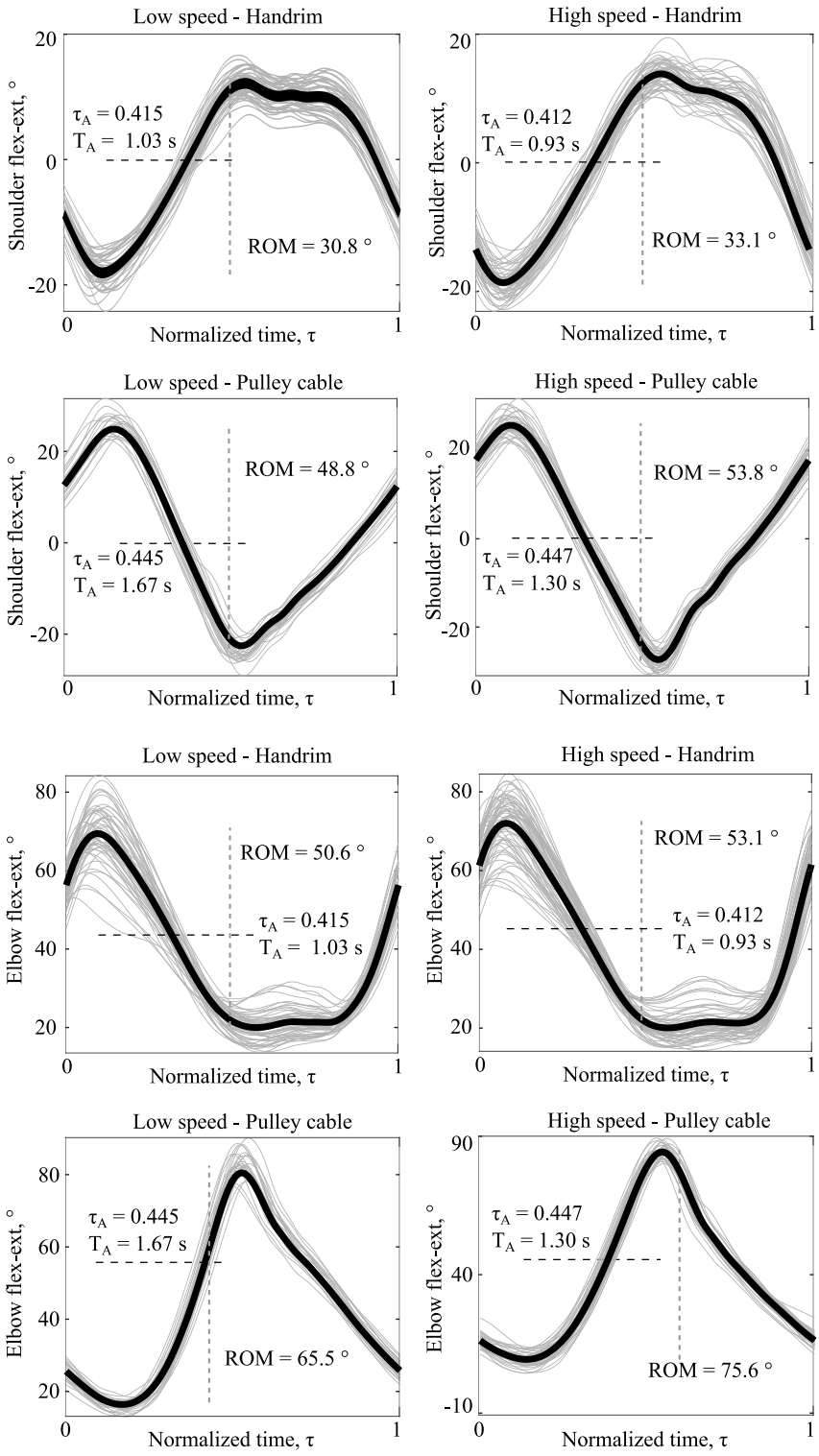

Figure 3.31: Flexion-extension of shoulder and elbow joint of the Handrim and Pulley-cable system at different speeds

In Figure 3.32, the conventions about the flexion-extension of shoulder and elbow joint are reported, according with the literature.

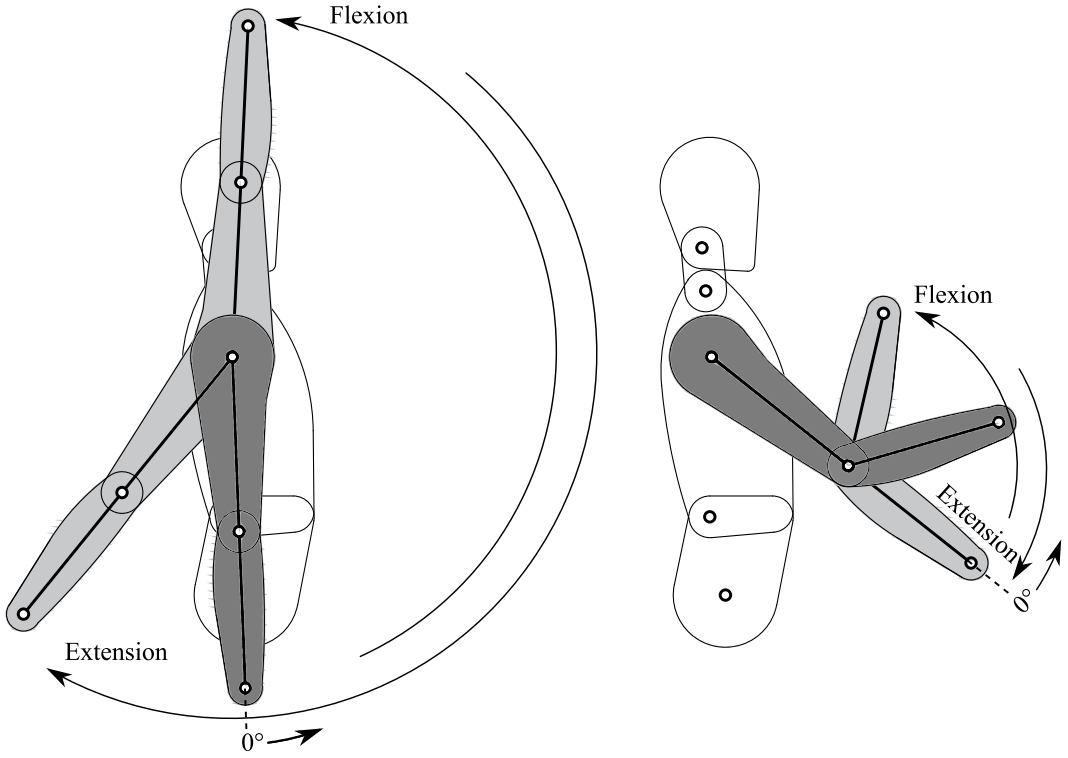

Figure 3.32: Conventions of flexion-extension of the shoulder and elbow joint

3.5.2 Discussions and conclusions

Seven able-bodied subjects, inexpert on the use of wheelchairs, were chosen to examine the excitation of ten shoulder muscles with two systems of propulsion: the handrim and the pulley-cable systems. The able-bodied subjects were chosen because it would be difficult to discriminate the effect of experience from that of the wheelchair propulsion system (handrim and pulley-cable) on the degree of muscle excitation and performance.

The excitation and silencing phases (Figure 3.30) of all ten muscles analysed were in opposition when comparing the handrim and the pulley-cable propulsion systems. Except for AD, the muscles analysed were excited when the angle between arm and forearm was smallest. In fact, this phase coincides with the transition from the recovery to the drive phase for the handrim propulsion and the transition from recovery to drive for the pulley-cable propulsion. This result is presumably due to

the opposite demands for muscle loading between propulsion systems: while handrim propulsion demands shoulder flexion and elbow extension during the drive phase the pulley cable propulsion demands shoulder extension and elbow flexion. The results of muscle excitation reported here corroborate those documented in a previous study [Electromyographic Activities of Shoulder Muscles during Forward and Reverse Manual Wheelchair Propulsion], focused on the assessment of excitation of six muscles during forward and reverse-wheeling propulsion. As for the pulley-cable propulsion, the active phase in reverse-wheeling propulsion is characterized by shoulder extension and elbow flexion and thus by out-of-phase excitation of trapezius and deltoid muscles when compared to the forward-wheeling propulsion [32].

The effect of the propulsion system on the degree and timing of muscle excitation was observed to be variable (Figure 3.29). More specifically, the handrim and the pulley-cable propulsion demanded longer and more active loading of different muscles: some muscles (AD, UT, PM, BB, and IS) were more strongly excited during handrim whereas others (MD, PD, MT and SS) were more strongly excited during pulley-cable propulsion. This difference, expectedly due to the different kinematics imposed by both propulsion systems, suggests the amount of active loading of the upper limb muscles per movement cycle may be comparable. The balanced excitation of different muscles between does not however indicate the two propulsion systems are associated with a similar efficiency. Indeed, the linear displacement of the wheelchair with the pulley-cable system of propulsion is approximately three times greater with respect to the handrim propulsion per cycle (Figure 3.28). This fact is likely due to the longer propulsion time required by the pulley-cable propulsion system (Figure 3.28). The difference in propulsion time between systems is attributable to the different transmission ratios between the two systems. In fact, the transmission ratio for the handrim system is defined by the ratio between the radius of the rear wheel, r_{rw}, and the radius of the handrim, r_h, being thus approximately equal to one. Conversely, the transmission ratio of the pulley-cable system is defined by the ratio between the radius of the rear wheel and the radius of the pulley, r_p: this ratio is nearly 2.2 times greater than that for the handrim system. In addition, the range of motion of the shoulder is similar for the two systems of propulsion (Figure 3.28) while the range of motion of the elbow is roughly 50% higher for the pulley-cable system. Collectively, these results suggest greater distance may be travelled when moving with the proposed pulley-cable propulsion system, for a presumably similar demand for active muscle loading.

The effect of the speed was observed to influence the degree of excitation of the ten muscles tested. In fact, the amplitude of bipolar EMG collected from the ten muscles assessed increased with the increase in movement speed, while the duty cycle was generally variable across muscles and propulsion systems (Figure 3.30). Similar results have been reported in [33] regarding the handrim and the lever, propulsion systems. More specifically, these authors reported an increase in the EMG amplitude with increases in movement speed in all muscles analysed, while only 3 out of the 4 muscles assessed showed a longer period of activity [33].

An additional important difference between the two systems is that the trajectory of the hand in the handrim system is fixed; namely the trajectory of the handrim or of the lever while with the pulley-cable system the hand trajectory is not constrained. It seems therefore plausible to state that with the pulley-cable propulsion system users can rely on different kinematic strategies to propel the wheelchair, likely adopting that associated with an optimal ergonomic propulsion. In addition, when following a fixed trajectory the user force on the handrim, or lever, has three components, but only one is useful for the transmission of motion, namely the tangential force, while with the pulley-cable system the end-point force wholly contributes to the generation of the angular momentum driving the wheelchair.

3.6 Test 5: Trajectory of the Handwheelchair.q racing

This test represents the experimental validation of the new steering compensator mechanism described previously. The prototype has been equipped with a potentiometer that evaluates the steering angle, namely the angle of the fork respect to the frame. The potentiometer has been shown in Figure 2.42 in the previous chapter. In addition, each rear wheel has been equipped with 16 magnets and two hall sensors detect the passage of the magnets as described in the section 3.1.

3.6.1 Methods

The test consists of two different tests. The first one, concerns the analysis of the minimum curvature radius of the Handhweelchair.q racing. In this test the user drives the Handhweelchair.q racing on a circular trajectory by imposing the maximum steering angle to obtain the minimum curvature radius. The second test concerns the preliminary test about the maneuverability of the prototype. In the second test, the user drives the Handwheelchair.q racing on a zigzag path.

The coordinates of the center of mass of the wheelchair, are defined as follow eq. (3.11).

$$\begin{bmatrix} x_{cm} \\ y_{cm} \end{bmatrix} = \begin{bmatrix} \int_0^t \frac{\dot{x}_{rw}\cos\psi + \dot{y}_{lw}\cos\psi}{2} dt \\ \int_0^t \frac{\dot{x}_{rw}\sin\psi + \dot{y}_{lw}\sin\psi}{2} dt \end{bmatrix} \tag{3.11}$$

Where ψ is the yaw of the wheelchair determined as reported in eq. (3.12).

$$\psi = \int_0^t \dot{\psi} dt = \int_0^t \frac{\dot{x}_{rw} + \dot{x}_{lw}}{t} dt \tag{3.12}$$

Lastly, the curvature radii of the right and left wheel are defined by the eq. 3.13

$$\rho_r = \dot{x}_{rw} tan\alpha;\ \rho_l = \dot{x}_{lw} tan\alpha \tag{3.13}$$

Where α is defined by the eq. (3.14)

$$\alpha = \text{atan}\ \frac{t}{\dot{x}_{rw} - \dot{y}_{rw}} \tag{3.14}$$

3.6.2 Results

The goal of the first test was to evaluate the minimum curvature radius related to the maximum steering angle. In Figure 3.33, the trajectory of the right, left wheel and the center of mass of the wheelchair are reported. The curvature radius of the right and left wheel are respectively: ρ_r = 3.10 m and ρ_l = 2.35 m. The curvature radius of the center of mass of the wheelchair has been calculated as follow, eq. 3.15:

$$\rho_{cm} = \frac{\rho_r + \rho_l}{2} \tag{3.15}$$

The curvature radius of the center of mass of the wheelchair is equal to 2.725 m. The difference of the curvature radius of the right and left wheel il 705 mm, very close with the track, “t”, of the wheelchair of 700 mm.

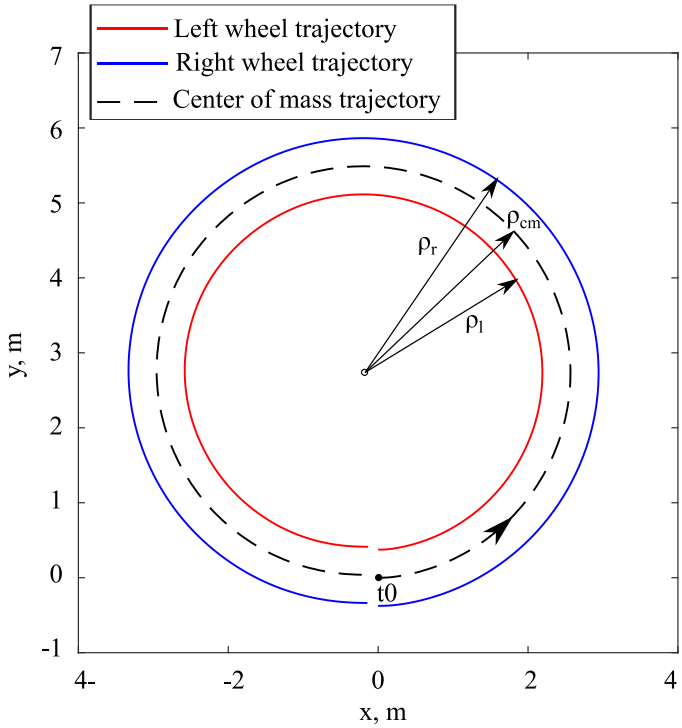

Figure 3.33: Trajectory of the left, right wheel and the center of mass of the wheelchair.

At the same time, the steering angle was detected by a potentiometer, Figure 3.34. The average value is about 32-33°. It is possible to affirm that a low speed (< 0.5 m/s), the minimum curvature radius of the center of mass of the wheelchair is 2.725 m with a steering angle of 32.5°. This result is comparable with the result obtained with the dynamic model, in the previous chapter, shown in Figure 2.28.

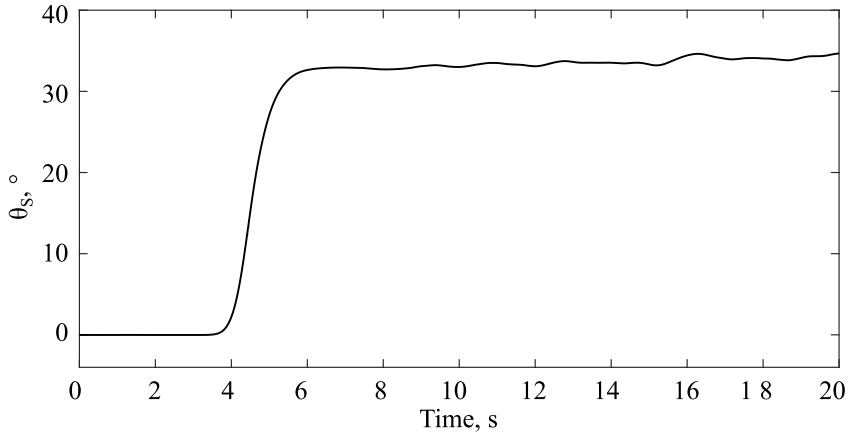

Figure: 3.34: Steering angle measured with the potentiometer

Lastly, a zig zag course has been travelled in order to verify the maneuverability. In Figure 3.35, the trajectory of the wheelchair is reported. It is possible to note the zig zag trajectory.

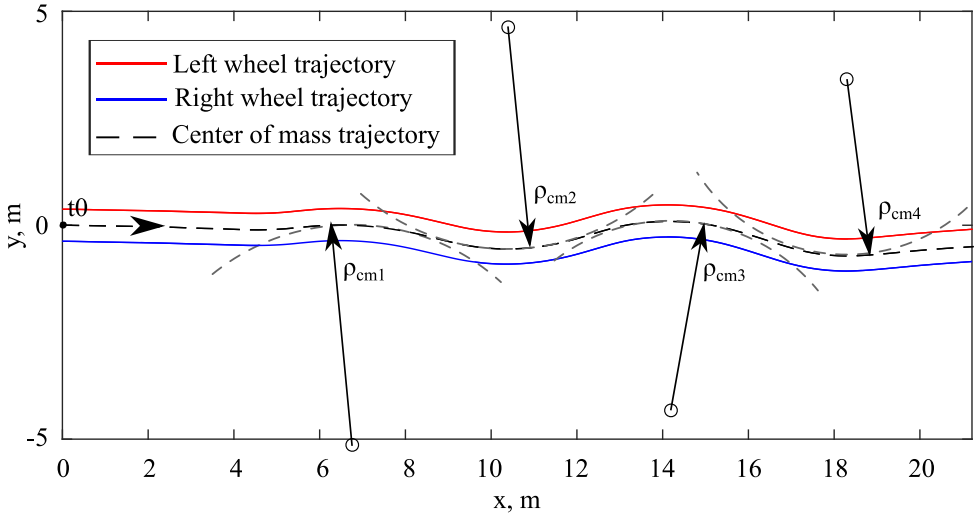

Figure 3.35: Trajectory of the left, right wheel and the center of mass of the wheelchair.

In Figure 3.36, the steering angle measured with the potentiometer and the curvature radius are reported.

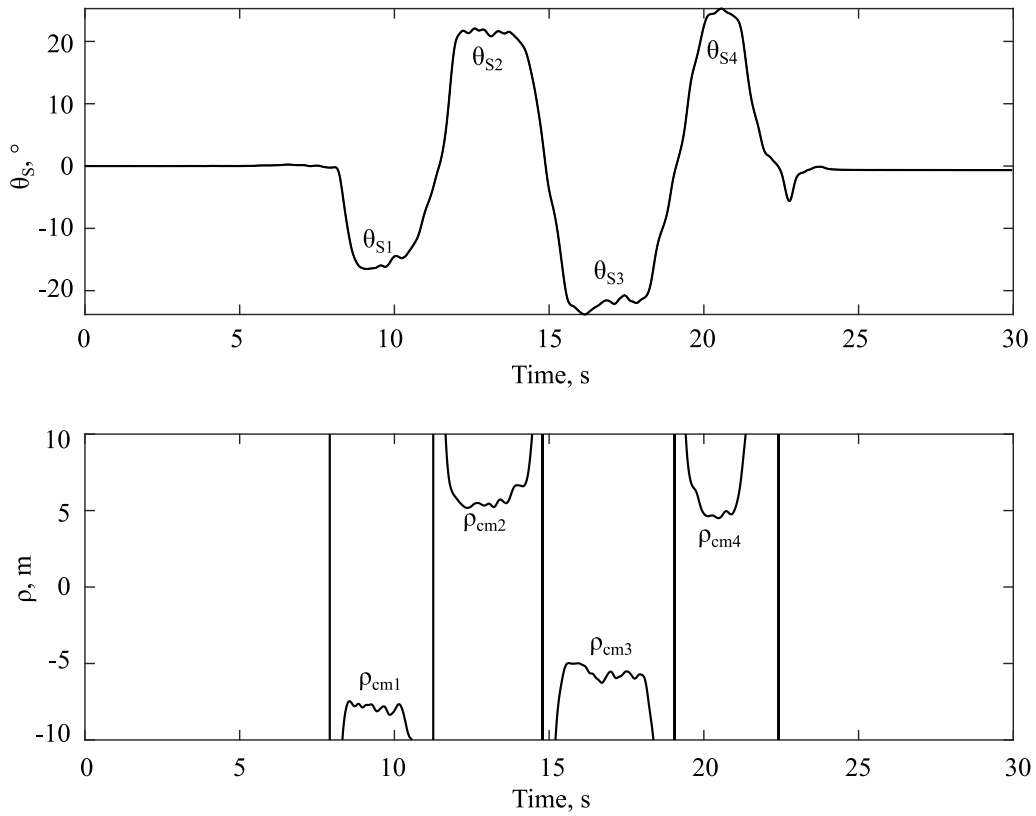

Figure 3.36: Steering angle, top, and curvature radius, below.

3.6.3 Conclusion

This is a preliminary test about the Handwheelchair.q racing. In this test, the minimum curvature radius has been identified and then a zig zag course has been travelled in order to verify the functioning of the prototype.

In the future, the prototype has to be test for sport applications: track and road races, sprint, middle and long distances. The transmission ratio can be modified based on the distance and in the future a variable transmission ratio can be implemented. In addition, the Handhweelchair.q racing can be used to practice light physical activity on a cycle path or in a park safely.

Chapter 4

Conclusion

In this work, the innovative manual wheelchairs with an alternative system of propulsion are presented. In particular, the evolution from the concept, the functional and executive design to the prototype and then the experimental campaign are presented in detail.

The first prototype of Handhweeelchair.q for everyday use is based on a standard wheelchair in which an independent and complete subsystem can be added on the standard wheelchair, by replacing the rear wheels, in order to perform the innovative system of propulsion inspired by the rowing gesture. The innovative gesture is performed by a pulley-cable system to limit the weight and the visual impact of the prototype. The prototype has been equipped with an efficiency brake system that enables to travel safely. In addition, different commercial devices of front wheel can be replaced at the standard front wheels in order to improve the maneuverability, the stability and the comfort of the prototype.

The second prototype, named Handhweelchair.q racing, is a prototype for sport use based on a racing wheelchair that has been modified in order to perform the innovative gesture. In addition, the system to steer the vehicle has been modified with a new system. With the new system is possible to control the steer continuously, not only in the recovery phase and the preliminary test has verified the control of the trajectory and the minimum curvature radius.

The experimental campaign has been strongly limited by the pandemic situation, especially the experimental test with real user. Despite this, the equipment, the experimental data conditioning methodology and data analysis methodology have been defined and described.

In the future, the experimental campaign about the Handhweelchair.q for everyday use has to be expanded involving real users with the main goal to optimize the prototype from a mechanical and biomechanical, point of view. The main parameters that has to be optimize for each user and depending on the external load

concerns: the transmission ratio, the cadence of the gesture, the position of the return pulley, the stability of the wheelchair, the maneuverability and the comfort. The transmission ratio, the cadence, the position of the return pulley have an effect on the force applied by the user, the efficiency of the vehicle and the gesture, on the direction of the force on the shoulder joint and on the muscular activity. The different solutions of the front wheels have an effect on the maneuverability, the comfort and on the stability of the wheelchair. The prototype, the equipment, the post processing of the data, the new index POF and the indices found in literature presented in this work define the solid foundation for a wide experimental campaign. Then, Handwheelchair.q has to be compared with different system of propulsion: handrim, lever and handbike from a mechanical, biomechanical and maneuverability point of view. In addition, it will be fundamental to evaluate the shoulder pain when the Handwheelchair.q will be used as mainly or alternative system of propulsion for a long time

The same speech can be done for the prototype Handwheelchai.q racing that has to be optimized from a mechanical and biomechanical point of view. In addition, the Handwheelchair.q racing has to be compared with the wheelchair racing with the handrim system in the different races: sprint, middle and long distance.

Reference

[1] United Nations and Department of Economic and Social Affairs, *Disability and development report: realizing the sustainable development goals by, for and with persons with disabilities : 2018*. 2019.

[2] F. O. Medola, V. M. C. Elui, C. da S. Santana, and C. A. Fortulan, 'Aspects of manual wheelchair configuration affecting mobility: a review', *J Phys Ther Sci*, vol. 26, no. 2, pp. 313–318, Feb. 2014, doi: 10.1589/jpts.26.313.

[3] J. Leaman and H. M. La, 'A Comprehensive Review of Smart Wheelchairs: Past, Present, and Future', *IEEE Transactions on Human-Machine Systems*, vol. 47, no. 4, pp. 486–499, Aug. 2017, doi: 10.1109/THMS.2017.2706727.

[4] N. A. Silva, N. Sousa, R. L. Reis, and A. J. Salgado, 'From basics to clinical: A comprehensive review on spinal cord injury', *Progress in Neurobiology*, vol. 114, pp. 25–57, Mar. 2014, doi: 10.1016/j.pneurobio.2013.11.002.

[5] M. A. Iqbal, M. Z. Chaudhary, M. W. Abbas, F. Maqsood, F. Fatima, and M. N. Iqbal, 'SPINA BIFIDA; THE BASIC AND CLINICAL REVIEW', *undefined*, 2016, Accessed: Mar. 11, 2022. [Online]. Available: https://www.semanticscholar.org/paper/SPINA-BIFIDA%3B-THE-BASIC-AND-CLINICAL-REVIEW-Iqbal-Chaudhary/165563950bdfb7fdb6ed5b9b8b701346e69391f0

[6] A. I. R. Maas *et al.*, 'Traumatic brain injury: integrated approaches to improve prevention, clinical care, and research', *Lancet Neurol*, vol. 16, no. 12, pp. 987–1048, Dec. 2017, doi: 10.1016/S1474-4422(17)30371-X.

[7] G. M. Rommers, L. D. Vos, J. W. Groothoff, and W. H. Eisma, 'Mobility of people with lower limb amputations: scales and questionnaires: a review', *Clin Rehabil*, vol. 15, no. 1, pp. 92–102, Feb. 2001, doi: 10.1191/026921501677990187.

[8] K. Butler *et al.*, 'A systematic review of the key factors affecting tissue viability and rehabilitation outcomes of the residual limb in lower extremity traumatic amputees', *J Tissue Viability*, vol. 23, no. 3, pp. 81–93, Aug. 2014, doi: 10.1016/j.jtv.2014.08.002.

[9] J. Bickenbach, A. Officer, T. Shakespeare, P. von Groote, W. H. Organization, and T. I. S. C. Society, *International perspectives on spinal cord injury*. World Health Organization, 2013. Accessed: Mar. 11, 2022. [Online]. Available: https://apps.who.int/iris/handle/10665/94190

[10] *The Economic Cost of Spinal Cord Injury and Traumatic Brain Injury in Australia*. Victorian Neurotrauma Initiative, 2009.

[11] GBD 2016 Traumatic Brain Injury and Spinal Cord Injury Collaborators, 'Global, regional, and national burden of traumatic brain injury and spinal cord injury, 1990-2016: a systematic analysis for the Global Burden of Disease Study 2016', *Lancet Neurol*, vol. 18, no. 1, pp. 56–87, Jan. 2019, doi: 10.1016/S1474-4422(18)30415-0.

[12] J. J. Laskin *et al.*, 'Electrical stimulation-assisted rowing exercise in spinal cord injured people. A pilot study', *Spinal Cord*, vol. 31, no. 8, Art. no. 8, Aug. 1993, doi: 10.1038/sc.1993.87.

[13] M. Kjaer, 'Why exercise in paraplegia?', *British Journal of Sports Medicine*, vol. 34, no. 5, pp. 322–323, Oct. 2000, doi: 10.1136/bjsm.34.5.322.

[14] C. Migliorini, B. Tonge, and G. Taleporos, 'Spinal Cord Injury and Mental Health', *The Australian and New Zealand journal of psychiatry*, vol. 42, pp. 309–14, May 2008, doi: 10.1080/00048670801886080.

[15] International Health Conference, 'Constitution of the World Health Organization. 1946', *Bull World Health Organ*, vol. 80, no. 12, pp. 983–984, 2002.

[16] 'World report on disability'. https://www.who.int/publications-detail-redirect/9789241564182 (accessed Mar. 11, 2022).

[17] D.-I. Kim, J. Lee, H. Park, and J. Y. Jeon, 'The Relationship between Physical Activity Levels and Mental Health in Individuals with Spinal Cord Injury in South Korea', *Int J Environ Res Public Health*, vol. 17, no. 12, p. E4423, Jun. 2020, doi: 10.3390/ijerph17124423.

[18] S. de Groot *et al.*, 'Wheelchair-specific fitness of persons with a long-term spinal cord injury: cross-sectional study on effects of time since injury and physical activity level', *Disabil Rehabil*, vol. 38, no. 12, pp. 1180–1186, 2016, doi: 10.3109/09638288.2015.1076072.

[19] T. W. J. Janssen, C. a. J. M. van Oers, H. E. J. Veeger, A. P. Hollander, L. H. V. van der Woude, and R. H. Rozendal, 'Relationship between physical strain during standardised ADL tasks and physical capacity in men with spinal cord injuries', *Spinal Cord*, vol. 32, no. 12, Art. no. 12, Dec. 1994, doi: 10.1038/sc.1994.131.

[20] J. H. Rimmer, W. Schiller, and M.-D. Chen, 'Effects of disability-associated low energy expenditure deconditioning syndrome', *Exerc Sport Sci Rev*, vol. 40, no. 1, pp. 22–29, Jan. 2012, doi: 10.1097/JES.0b013e31823b8b82.

[21] A. C. Buchholz and P. B. Pencharz, 'Energy expenditure in chronic spinal cord injury', *Curr Opin Clin Nutr Metab Care*, vol. 7, no. 6, pp. 635–639, Nov. 2004, doi: 10.1097/00075197-200411000-00008.

[22] W. T. Phillips *et al.*, 'Effect of spinal cord injury on the heart and cardiovascular fitness', *Curr Probl Cardiol*, vol. 23, no. 11, pp. 641–716, Nov. 1998, doi: 10.1016/s0146-2806(98)80003-0.

[23] R. Neshovski, 'Home', *United Nations Sustainable Development*. https://www.un.org/sustainabledevelopment/ (accessed Mar. 11, 2022).

[24] M. P. LaPlante and H. S. Kaye, 'Demographics and trends in wheeled mobility equipment use and accessibility in the community', *Assist Technol*, vol. 22, no. 1, pp. 3–17; quiz 19, 2010, doi: 10.1080/10400430903501413.

[25] C. Jayaraman, Y. Moon, and J. J. Sosnoff, 'Shoulder pain and time dependent structure in wheelchair propulsion variability', *Med Eng Phys*, vol. 38, no. 7, pp. 648–655, Jul. 2016, doi: 10.1016/j.medengphy.2016.04.005.

[26] A. E. Engin and S. M. Chen, 'Statistical data base for the biomechanical properties of the human shoulder complex--I: Kinematics of the shoulder complex', *J Biomech Eng*, vol. 108, no. 3, pp. 215–221, Aug. 1986, doi: 10.1115/1.3138605.

[27] H. E. J. Veeger and F. C. T. van der Helm, 'Shoulder function: The perfect compromise between mobility and stability', *Journal of Biomechanics*, vol. 40, no. 10, pp. 2119–2129, Jan. 2007, doi: 10.1016/j.jbiomech.2006.10.016.

[28] J. D. Mozingo *et al.*, 'Shoulder Mechanical Impingement Risk Associated with Manual Wheelchair Tasks in Individuals with Spinal Cord Injury', *Clin Biomech (Bristol, Avon)*, vol. 71, pp. 221–229, Jan. 2020, doi: 10.1016/j.clinbiomech.2019.10.017.

[29] K. A. Curtis *et al.*, 'Reliability and validity of the Wheelchair User's Shoulder Pain Index (WUSPI)', *Paraplegia*, vol. 33, no. 10, pp. 595–601, Oct. 1995, doi: 10.1038/sc.1995.126.

[30] R. Cooper, M. L. Boninger, and R. Robertson, 'Heavy Handed: Repetitive strain injury among manual wheelchair users', *Team Rehab Report*, vol. 9, no. 2, Art. no. 2, 1998.

[31] C. Jayaraman, C. L. Beck, and J. J. Sosnoff, 'Shoulder pain and jerk during recovery phase of manual wheelchair propulsion', *J Biomech*, vol. 48, no. 14, pp. 3937–3944, Nov. 2015, doi: 10.1016/j.jbiomech.2015.09.018.

[32] D. Rincón, S. Ye, M. Rodriguez, and S. Nasser, 'Electromyographic Activities of Shoulder Muscles during Forward and Reverse Manual Wheelchair Propulsion', *undefined*, 2005, Accessed: Mar. 11, 2022. [Online]. Available: https://www.semanticscholar.org/paper/Electromyographic-Activities-of-Shoulder-Muscles-Rinc%C3%B3n-Ye/4307a737376e23df0286491debe80a25bc8652f3

[33] P. S. Requejo *et al.*, 'Shoulder muscular demand during lever-activated vs pushrim wheelchair propulsion in persons with spinal cord injury', *J Spinal*

Cord Med, vol. 31, no. 5, pp. 568–577, 2008, doi: 10.1080/10790268.2008.11754604.

[34] K. Fagher and J. Lexell, 'Sports-related injuries in athletes with disabilities', *Scand J Med Sci Sports*, vol. 24, no. 5, pp. e320-331, Oct. 2014, doi: 10.1111/sms.12175.

[35] O. W. Heyward, R. J. K. Vegter, S. de Groot, and L. H. V. van der Woude, 'Shoulder complaints in wheelchair athletes: A systematic review', *PLoS One*, vol. 12, no. 11, p. e0188410, 2017, doi: 10.1371/journal.pone.0188410.

[36] B. Mason, M. Warner, S. Briley, V. Goosey-Tolfrey, and R. Vegter, 'Managing shoulder pain in manual wheelchair users: a scoping review of conservative treatment interventions', *Clin Rehabil*, vol. 34, no. 6, pp. 741–753, Jun. 2020, doi: 10.1177/0269215520917437.

[37] Bigant and Allais, *Battle of Kadesh*.

[38] Makron, *The departure of Triptolemus*. 490AD.

[39] 'History of the Wheelchair', *HISTORY.PHYSIO*, Jan. 24, 2019. https://history.physio/history-of-the-wheelchair/ (accessed Mar. 11, 2022).

[40] Blunt and Smith, 'Invalid-chair', 86899, Feb. 16, 1869

[41] R. A. Cooper, 'Wheelchair racing sports science: a review', *J Rehabil Res Dev*, vol. 27, no. 3, pp. 295–312, 1990, doi: 10.1682/jrrd.1990.07.0297.

[42] J. R. Silver, 'History of the treatment of spinal injuries', *Postgraduate Medical Journal*, vol. 81, no. 952, pp. 108–114, Feb. 2005, doi: 10.1136/pgmj.2004.019992.

[43] R. Reismüller and J. Parry, 'The Kladruby Games, the Paralympics, and the pre-history of disability sport', 2017. doi: 10.14712/23366052.2017.6.

[44] 'Paralympic Sport TV - Latest Videos & Highlights of IPC Sports', *International Paralympic Committee*. https://www.paralympic.org/archives (accessed Mar. 11, 2022).

[45] 'History | Boston Athletic Association'. https://www.baa.org/races/boston-marathon/history (accessed Mar. 11, 2022).

[46] 'Bob Hall. Racing Wheelchair. 1986 | MoMA', *The Museum of Modern Art*. https://www.moma.org/collection/works/2533 (accessed Mar. 11, 2022).

[47] R. A. Cooper, 'Racing wheelchair crown compensation', *J Rehabil Res Dev*, vol. 26, no. 1, pp. 25–32, 1989.

[48] 'Paul Cartwright', *National Paralympic Heritage Trust*. https://www.paralympicheritage.org.uk/paul-cartwright (accessed Mar. 11, 2022).

[49] 'Chris Hallam', *National Paralympic Heritage Trust*. https://www.paralympicheritage.org.uk/chris-hallam (accessed Mar. 11, 2022).

[50] S. E. Rodrigo and C. V. Herrera, 'Chapter 11 - Wheelchairs: history, characteristics, and technical specifications', in *Smart Wheelchairs and Brain-Computer Interfaces*, P. Diez, Ed. Academic Press, 2008, pp. 257–290. doi: 10.1016/B978-0-12-812892-3.00011-X.

[51] M. Sasaki, D. Stefanov, Y. Ota, H. Miura, and A. Nakayama, 'Shoulder joint contact force during lever-propelled wheelchair propulsion', *ROBOMECH Journal*, vol. 2, no. 1, p. 13, Oct. 2015, doi: 10.1186/s40648-015-0037-8.

[52] K. Fiok and A. Mróz, 'How does lever length and the position of its axis of rotation influence human performance during lever wheelchair propulsion?', *J Electromyogr Kinesiol*, vol. 25, no. 5, pp. 824–832, Oct. 2015, doi: 10.1016/j.jelekin.2015.06.007.

[53] A. R. Sarraj and R. Massarelli, 'Design History and Advantages of a New Lever-Propelled Wheelchair Prototype', *International Journal of Advanced Robotic Systems*, vol. 8, no. 3, p. 26, Aug. 2011, doi: 10.5772/10669.

[54] U. Arnet, S. van Drongelen, D. H. E. J. Veeger, and L. H. V. van der Woude, 'Are the force characteristics of synchronous handcycling affected by speed and the method to impose power?', *Med Eng Phys*, vol. 34, no. 1, pp. 78–84, Jan. 2012, doi: 10.1016/j.medengphy.2011.07.001.

[55] M. Siebert, 'Adjustable handbike-chassis for offroad-use ("Mountain handbike")', *Procedia Engineering*, vol. 2, no. 2, pp. 3157–3162, Jun. 2010, doi: 10.1016/j.proeng.2010.04.126.

[56] S. van Drongelen, J. van den Berg, U. Arnet, D. (H. E. J.) Veeger, and L. H. V. van der Woude, 'Development and validity of an instrumented handbike: Initial results of propulsion kinetics', *Medical Engineering & Physics*, vol. 33, no. 9, pp. 1167–1173, Nov. 2011, doi: 10.1016/j.medengphy.2011.04.018.

[57] B. Stone, B. S. Mason, A. Bundon, and V. L. Goosey-Tolfrey, 'Elite handcycling: a qualitative analysis of recumbent handbike configuration for optimal sports performance', *Ergonomics*, vol. 62, no. 3, pp. 449–458, Mar. 2019, doi: 10.1080/00140139.2018.1531149.

[58] M. Belloli, F. Cheli, I. Bayati, S. Giappino, and F. Robustelli, 'Handbike Aerodynamics: Wind Tunnel Versus Track Tests', *Procedia Engineering*, vol. 72, pp. 750–755, Jan. 2014, doi: 10.1016/j.proeng.2014.06.127.

[59] J. C. Druvert and F. Rusakievick, 'Wheelchair racing: chair set-up, conventional seating position, kneeling position, para backhand technique, injury prevention', *Annals of Physical and Rehabilitation Medicine*, vol. 55, p. e250, Oct. 2012, doi: 10.1016/j.rehab.2012.07.635.

[60] J. Schipman *et al.*, 'Age-Related Changes in Para and Wheelchair Racing Athlete's Performances', *Hyper Article en Ligne - Sciences de l'Homme et de la Société*, 2019, doi: 10.3389/fphys.2019.00256.

[61] R. A. Cooper and M. MacLeish, 'Racing wheelchair roll stability while turning: a simple model', *J Rehabil Res Dev*, vol. 29, no. 2, pp. 23–30, 1992, doi: 10.1682/jrrd.1992.04.0023.

[62] A. Bundon, B. S. Mason, and V. L. Goosey-Tolfrey, 'Expert Users' Perceptions of Racing Wheelchair Design and Setup: The Knowns, Unknowns, and Next Steps', *Adapt Phys Activ Q*, vol. 34, no. 2, pp. 141–161, Apr. 2017, doi: 10.1123/apaq.2016-0073.

[63] M. S. MacLeish, R. A. Cooper, J. Harralson, and J. F. Ster, 'Design of a composite monocoque frame racing wheelchair', *J Rehabil Res Dev*, vol. 30, no. 2, pp. 233–249, 1993.

[64] R. A. Cooper, 'Racing wheelchair rear wheel alignment', *J Rehabil Res Dev*, vol. 26, no. 1, pp. 47–50, 1989.

[65] R. M. A. van der Slikke, M. A. M. Berger, D. J. J. Bregman, and D. H. E. J. Veeger, 'Wearable Wheelchair Mobility Performance Measurement in Basketball, Rugby, and Tennis: Lessons for Classification and Training', *Sensors*, vol. 20, no. 12, Art. no. 12, Jan. 2020, doi: 10.3390/s20123518.

[66] T. Rietveld, R. J. K. Vegter, R. M. A. van der Slikke, A. E. Hoekstra, L. H. V. van der Woude, and S. de Groot, 'Wheelchair mobility performance of elite wheelchair tennis players during four field tests: Inter-trial reliability and construct validity', *PLoS One*, vol. 14, no. 6, p. e0217514, Jun. 2019, doi: 10.1371/journal.pone.0217514.

[67] University of Nis, Faculty of Sports and Physical Education, Nis, Serbia, N. Prvulovic, M. Hadzovic, University of Nis, Faculty of Sports and Physical Education, Nis, Serbia, A. Lilic, and University of Nis, Faculty of Sports and Physical Education, Nis, Serbia, 'A Biomechanical Analysis of the Free Throw Shooting Technique in Wheelchair Basketball: A Pilot Study', *J. Anthr. Sport Phis. Educ.*, vol. 6, no. 1, pp. 3–6, Jan. 2022, doi: 10.26773/jaspe.220101.

[68] F. Hintzy-Cloutier, N. Tordi, J.-D. Rouillon, and A. Belli, 'The influence of within-cycle pattern characteristics on mechanical parameters developed during wheelchair sprinting?', *Science & Sports*, vol. 17, no. 3, pp. 128–131, May 2002, doi: 10.1016/S0765-1597(02)00130-2.

[69] O. J. Quittmann, T. Abel, K. Albracht, and H. K. Strüder, 'Biomechanics of all-out handcycling exercise: kinetics, kinematics and muscular activity of a 15-s sprint test in able-bodied participants', *Sports Biomechanics*, vol. 0, no. 0, pp. 1–24, May 2020, doi: 10.1080/14763141.2020.1745266.

[70] P. Cavallone, A. Botta, E. Bonisoli, and G. Quaglia, 'Preliminary Experimental Test of a Cable-Driven Wheelchair in Different Configurations', 2022, pp. 166–173. doi: 10.1007/978-3-030-87383-7_18.

[71] P. Cavallone, E. Bonisoli, and G. Quaglia, 'Handwheelchair.q: New Prototype of Manual Wheelchair for Everyday Life', 2021, pp. 111–119. doi: 10.1007/978-3-030-55807-9_13.

[72] P. Cavallone, E. Bonisoli, and G. Quaglia, 'Prototyping of manual wheelchair with alternative propulsion system', *Disabil Rehabil Assist Technol*, vol. 15, no. 8, pp. 945–951, Nov. 2020, doi: 10.1080/17483107.2019.1629185.

[73] G. Quaglia, E. Bonisoli, and P. Cavallone, 'The Design of a New Manual Wheelchair for Sport', *Machines*, vol. 7, p. 31, May 2019, doi: 10.3390/machines7020031.

[74] G. Quaglia, E. Bonisoli, and P. Cavallone, 'Handwheelchair.q: Innovative Manual Wheelchair for Sport: Proceedings of the Second International Conference of IFToMM Italy', in *Mechanisms and Machine Science*, 2019, pp. 370–378. doi: 10.1007/978-3-030-03320-0_40.

[75] G. Quaglia, E. Bonisoli, and P. Cavallone, 'A proposal of alternative propulsion system for manual wheelchair', *International Journal of Mechanics and Control*, vol. 19, pp. 33–38, Jan. 2018.

[76] K. A. Curtis *et al.*, 'Development of the Wheelchair User's Shoulder Pain Index (WUSPI)', *Spinal Cord*, vol. 33, no. 5, Art. no. 5, May 1995, doi: 10.1038/sc.1995.65.

[77] L. A. Harvey and J. V. Glinsky, 'Clinimetrics: The Wheelchair User's Shoulder Pain Index (WUSPI)', *J Physiother*, vol. 65, no. 1, p. 55, Jan. 2019, doi: 10.1016/j.jphys.2018.07.001.

[78] K. E. Roach, E. Budiman-Mak, N. Songsiridej, and Y. Lertratanakul, 'Development of a shoulder pain and disability index', *Arthritis Care Res*, vol. 4, no. 4, pp. 143–149, Dec. 1991.

[79] G. Tian-min, H. Bin, L. Lei, and Q. Mei-chao, 'A study on wheelchair weighted integrated comfort index', in *2011 International Conference on Electronics, Communications and Control (ICECC)*, Sep. 2011, pp. 1289–1292. doi: 10.1109/ICECC.2011.6067851.

[80] M. Cognolato, N. Petrone, and G. Marcolin, 'Quantification of the User-wheelchair System Stability based on the CoP Trajectory within the Base of Support', *Procedia Engineering*, vol. 72, pp. 368–373, 2014, doi: 10.1016/j.proeng.2014.06.102.

[81] C. Sauret, P. Vaslin, J. Bascou, H. Pillet, and F. Lavaste, 'Proposal of an index for evaluating pitch instability during actual locomotion with a manual wheelchair', *Computer Methods in Biomechanics and Biomedical*

Engineering, vol. 16, no. sup1, pp. 130–131, Jul. 2013, doi: 10.1080/10255842.2013.815952.

[82] C. Sauret, P. Vaslin, J. Bascou, H. Pillet, and F. Lavaste, 'Rolling resistance index of manual wheelchairs', *Computer Methods in Biomechanics and Biomedical Engineering*, vol. 14, no. sup1, pp. 65–66, Aug. 2011, doi: 10.1080/10255842.2011.592365.

[83] Y. Vanlandewijck, D. Theisen, and D. Daly, 'Wheelchair propulsion biomechanics: implications for wheelchair sports', *Sports Med*, vol. 31, no. 5, pp. 339–367, 2001, doi: 10.2165/00007256-200131050-00005.

[84] H. E. J. Veeger, L. H. V. van der Woude, and R. H. Rozendal, 'Load on the upper extremity in manual wheelchair propulsion', *Journal of Electromyography and Kinesiology*, vol. 1, no. 4, pp. 270–280, Dec. 1991, doi: 10.1016/1050-6411(91)90014-V.

[85] V. Hernandez, P. Gorce, and N. Rezzoug, 'Evaluation and validation of musculoskeletal force feasible set indices: Application to manual wheelchair propulsion', *J Biomech*, vol. 68, pp. 70–77, Feb. 2018, doi: 10.1016/j.jbiomech.2017.12.012.

[86] H. Pacejka and H. Pacejka, *Tire and Vehicle Dynamics*. Jordan Hill, UNITED KINGDOM: Elsevier Science & Technology, 2006. Accessed: Mar. 14, 2022. [Online]. Available: http://ebookcentral.proquest.com/lib/polito-ebooks/detail.action?docID=311410

[87] A. Dressel and J. Sadauckas, 'Characterization and Modelling of Various Sized Mountain Bike Tires and the Effects of Tire Tread Knobs and Inflation Pressure', *Applied Sciences*, vol. 10, no. 9, Art. no. 9, Jan. 2020, doi: 10.3390/app10093156.

[88] Y. Moon, C. Jayaraman, I. M. K. Hsu, I. M. Rice, E. T. Hsiao-Wecksler, and J. J. Sosnoff, 'Variability of peak shoulder force during wheelchair propulsion in manual wheelchair users with and without shoulder pain', *Clinical Biomechanics*, vol. 28, no. 9, pp. 967–972, Nov. 2013, doi: 10.1016/j.clinbiomech.2013.10.004.

[89] M. M. Morrow, J. W. Rankin, R. R. Neptune, and K. R. Kaufman, 'A comparison of static and dynamic optimization muscle force predictions during wheelchair propulsion', *J Biomech*, vol. 47, no. 14, pp. 3459–3465, Nov. 2014, doi: 10.1016/j.jbiomech.2014.09.013.

[90] C.-J. Lin, P.-C. Lin, F.-C. Su, and K.-N. An, 'Biomechanics of wheelchair propulsion', *J. Mech. Med. Biol.*, vol. 09, no. 02, pp. 229–242, Jun. 2009, doi: 10.1142/S0219519409002948.

[91] M. Blouin, M. Lalumière, D. H. Gagnon, F. Chénier, and R. Aissaoui, 'Characterization of the immediate effect of a training session on a manual

wheelchair simulator with haptic biofeedback: towards more effective propulsion', *IEEE Trans Neural Syst Rehabil Eng*, vol. 23, no. 1, pp. 104–115, Jan. 2015, doi: 10.1109/TNSRE.2014.2330837.

[92] C. Kraaijenbrink, R. J. K. Vegter, A. H. R. Hensen, H. Wagner, and L. H. V. van der Woude, 'Different cadences and resistances in sub-maximal synchronous handcycling in able-bodied men: Effects on efficiency and force application', *PLOS ONE*, vol. 12, no. 8, p. e0183502, Aug. 2017, doi: 10.1371/journal.pone.0183502.

[93] J. W. Rankin, A. M. Kwarciak, W. M. Richter, and R. R. Neptune, 'The Influence of Altering Push Force Effectiveness on Upper Extremity Demand during Wheelchair Propulsion', *J Biomech*, vol. 43, no. 14, pp. 2771–2779, Oct. 2010, doi: 10.1016/j.jbiomech.2010.06.020.

[94] B. S. Mason, J. P. Lenton, and V. L. Goosey-Tolfrey, 'The physiological and biomechanical effects of forwards and reverse sports wheelchair propulsion', *J Spinal Cord Med*, vol. 38, no. 4, pp. 476–484, Jul. 2015, doi: 10.1179/2045772314Y.0000000197.

[95] H. J. Hermens, B. Freriks, C. Disselhorst-Klug, and G. Rau, 'Development of recommendations for SEMG sensors and sensor placement procedures', *J Electromyogr Kinesiol*, vol. 10, no. 5, pp. 361–374, Oct. 2000, doi: 10.1016/s1050-6411(00)00027-4.

[96] T. R. Allen, R. L. Brookham, A. C. Cudlip, and C. R. Dickerson, 'Comparing surface and indwelling electromyographic signals of the supraspinatus and infraspinatus muscles during submaximal axial humeral rotation', *J Electromyogr Kinesiol*, vol. 23, no. 6, pp. 1343–1349, Dec. 2013, doi: 10.1016/j.jelekin.2013.08.002.

[97] T. M. Vieira and A. Botter, 'The Accurate Assessment of Muscle Excitation Requires the Detection of Multiple Surface Electromyograms', *Exerc Sport Sci Rev*, vol. 49, no. 1, pp. 23–34, Jan. 2021, doi: 10.1249/JES.0000000000000240.

[98] J. H. Abbink, A. van der Bilt, and H. W. van der Glas, 'Detection of onset and termination of muscle activity in surface electromyograms', *J Oral Rehabil*, vol. 25, no. 5, pp. 365–369, May 1998, doi: 10.1046/j.1365-2842.1998.00242.x.